

https://dspace.org/

# Langmuir probe diagnostics of the exhaust plume of a miniature DC-discharge plasma-thruster

**Cwele, Mahlomola Daniel**

**2020**

https://hdl.handle.net/10539/30197

Cwele, Mahlomola Daniel. (2020). Langmuir probe diagnostics of the exhaust plume of a miniature DC-discharge plasma-thruster, University of the Witwatersrand, https://hdl.handle.net/10539/30197

Downloaded from a DSpace repository. https://dspace.org/

# Langmuir probe diagnostics of the exhaust plume of a miniature DC-discharge plasma-thruster

Mahlomola Daniel Cwele
School of Physics,
University of the Witwatersrand,
1 Jan Smuts Avenue, Braamfontein, Johannesburg, 2000




UNIVERSITY OF THE
WITWATERSRAND,
JOHANNESBURG

Dissertation submitted for
the degree of
Master of Science

Student number : 472212
Academic Supervisor : Dr. P. Ferrer

**Abstract**

This study is concerned with the design and construction of a computerised measurement acquisition system to be applied to the problem of diagnosing the exhaust plume of a U-shaped miniature DC-discharge micro-thruster. The system includes the design and construction of Langmuir probes in various sizes and the design and construction of a positioning bench for the Langmuir probes which can be used inside of the vacuum chamber of the plasma propulsion laboratory wherein the probe measurements will take place. The collective measurement acquisition system is designed to automatically conduct a survey or collection of probe measurements whilst producing data reports and computationally applying the Langmuir method to each IV curve found and for each specified point in the exhaust plume. Profile plots are produced for each measurement parameter. The system and its components were also tested with a contained plasma using specially constructed discharge tubes. The associated software and robotics collectively aim to eliminate any need for tedious and time consuming manual measurements and seek to reduce human error. These tools will be used by the plasma propulsion laboratory to aid in future studies and designs of DC-discharge micro-thrusters. Due to a relocation of the laboratory, time constraints prevented tests of the probe mechanism on actual micro-thruster systems.

## Acknowledgements

The author herewith acknowledges the assistance and guidance of Dr. William Wright, whose support was instrumental in arranging and conceptualising the experimental work herein, and the supervision and instruction of Dr. Philippe Ferrer, whose tutelage made this project possible.

The author further wishes to acknowledge the aid of the Dosimetry Laboratories of the National Metrology Institute of South Africa (NMISA), where many basic understandings of the fundamental problem(s) of plasmas were acquired and from whom a sponsorship for a full Labview training was attained.

# Contents


**1 Introduction** **1**
1.1 The thruster . . . . . 6

**2 The Langmuir probe** **13**

**3 Design of Langmuir probe and positioning bench** **19**
3.1 probe mechanism . . . . . 19
3.2 The Langmuir probe . . . . . 19
3.2.1 Design Parameters and Restrictions . . . . . 19
3.2.2 Proposed probe design . . . . . 23
3.3 The positioning bench . . . . . 25
3.3.1 Frame . . . . . 26
3.3.2 Actuators . . . . . 28

**4 Discharge tube tests of the Langmuir probes** **30**
4.1 Aims of the test . . . . . 30
4.2 Discharge tube tests with enclosed Plasmas . . . . . 31
4.2.1 Experimental apparatus . . . . . 31
4.3 Arrangement and procedure . . . . . 34
4.3.1 Arrangement of test components . . . . . 34
4.3.2 Potential sources of measurement noise . . . . . 36
4.3.3 IV-curve acquisition . . . . . 37
4.3.4 Control protocols . . . . . 38
4.4 Test Results . . . . . 39
4.4.1 IV plots . . . . . 39
4.4.2 Analysis protocol . . . . . 40
4.4.3 Data fitting and extraction of parameters . . . . . 41
4.4.4 Extracted plasma parameters . . . . . 43

**5 Discharge tube tests with porous electrodes** **45**
5.1 Experimental objectives . . . . . 45
5.2 Experimental apparatus . . . . . 45
5.2.1 Discharge Tubes . . . . . 45
5.2.2 Langmuir probe . . . . . 47
5.3 Experimental procedure for internal measurements . . . . . 48
5.4 Experimental procedure for external measurements . . . . . 50
5.5 Experimental results . . . . . 51
5.5.1 IV plot for internal measurements . . . . . 51
5.5.2 IV plot for external measurements . . . . . 53

**6 Probe test in free air** **57**
6.1 Probe plot . . . . . 59

**7 Control system** **60**
7.1 Survey acquisition protocol . . . . . 61

**8 Conclusions** **62**

**9 A : Current-Voltage data of teletherapy NMS** **64**

**10 B : Current-Voltage data of Langmuir probe in air at 45 Torr** **69**

**11 C : Current-Voltage data of Langmuir probe in Argon at 45 Torr** **70**

**12 D : Mathematica code used for curve fitting of Langmuir model** **71**

**13 E : LabView codes** **73**
13.1 E1 : LV code used to serially control power source . . . . . 74
13.2 E2 : LV code used to build IV plots . . . . . 79
13.3 E3 : LV code used to build excel reports . . . . . 81
13.4 E4 : LV front panel for the GUI . . . . . 83

**14 F : Current-Voltage data of Langmuir probe in flowing Argon at 45 to 145 Torr** **86**

**15 G : High sheath expansion current-Voltage data of Langmuir probe in Argon at 160 Torr** **87**

**16 H : Current-Voltage data of Langmuir probe in internal flowing Argon at 45 to 145 Torr** **88**

**17 I : Current-Voltage data of Langmuir probe in external flowing Argon at 45 to 145 Torr** **89**

**18 J : Voltage source calibration** **90**

# List of Figures


1 Basic schematic of an ionisation chamber exposed to a radiation field. . . . 2
2 Ionisation chambers positioned for dose measurements of a teletherapy gamma radiation source at the National Metrology Institute of South Africa (NMISA) . . . 3
3 A high volume ionisation chamber positioned for low level dose measurements at the NMISA . . . 3
4 U-shaped miniature DC-discharge microthruster . . . 6
5 The characteristic IV curve of a two species quasi-neutral plasma, exemplified by an Argon plasma . . . 7
6 A current-Voltage plot conducted with the South African teletherapy national dosimetry standard in air at 45.7%RH, $22^0C$ and 0.861 bar, using a Co-60 gamma source. . . . 8
7 A U-shaped plasma micro-thruster intended for short measurement tests by the space propulsion research laboratory at University of the Witwatersrand. . . . 9
8 PTW eletrometer used for standard dosimeter calibrations at the NMISA. . . . 10
9 The graphical user interface of a measurement automation software designed for calibration measurements at the NMISA. . . . 11
10 Vacuum chamber of the plasma propulsion laboratory at the University of the Witwatersrand . . . 11
11 Plasma induction by magnetic field . . . 13
12 Asymmetric Langmuir IV plot[2] . . . 15
13 Langmuir probe Inside a vacuum chamber . . . 16
14 Langmuir probe shapes typically used in dc discharge enclosed plasmas, (a) spherical (b) cylindrical, (c) flat [2] . . . 19
15 A blunt cylindrical obstruction in a uniform 1-D fluid flow . . . 20
16 zx-plane. . . . 21
17 xy-plane. . . . 21
18 Glass-insulated cylindrical probe. . . . 23
19 Glass-insulated probes in various sizes. . . . 24
20 Schematic of the positioning bench. . . . 25
21 Frame dimensions of the positioning bench. . . . 26
22 Bench frame inside vacuum chamber. . . . 27
23 Schematic of the arrangement of the bench, probe and thruster inside the vacuum chamber and the circuitry of the probe IV-curve acquisition system. . . . 28
24 Probe mount. . . . 29
25 Schematic of the discharge tube experiment. . . . 34
26 DC discharge of Argon gas in a plastic discharge tube. . . . 35
27 DC discharge of Argon gas in a plastic discharge tube with external discharge. . . . 36
28 IV Plot acquisition algorithm. . . . 37

29 Current Voltage curve conducted on an enclosed discharge containing Argon gas at 145 Torr. . . . . 39
30 IV curve conducted in Air at 45 Torr. . . . . 40
31 A Labview/Mathematica Langmuir Curve fitting of a IV curve conducted in Air at 45 torr with a fit quality of $R^2 = 0,995315$. 41
32 A Labview/Mathematica Langmuir Curve fitting of a IV curve conducted in Argon with a fit quality of $R^2 = 0,993726$. . . . . 42
33 Discharge tube with porous electrodes. . . . . 46
34 Discharge tube with porous electrodes (side view). . . . . 46
35 Plasma discharge of a flowing Argon gas through a porous iron electrode. . . . . 48
36 Schematic of the experimental setup designed for probe measurements with porous electrodes in Argon. . . . . 49
37 Schematic of the experimental setup designed for external probe measurements in Argon. . . . . 50
38 IV plot of flowing Argon. . . . . 51
39 Curve fitting of IV plot of flowing Argon with a fit quality of $R^2 = 0,984799$. . . . . 51
40 External IV plot of flowing Argon plasma. . . . . 53
41 Curve fitting of IV plot of flowing Argon with a fit quality of $R^2 = 0,996678$. . . . . 54
42 Non-linear Sheath expansion. . . . . 56
43 High Mearement noise in a IV plot. . . . . 56
44 Schematic of a free air experiment with probe exposed to a field of Gamma radiation using a Cobalt-60 source. . . . . 57
45 IV plot obtained with the National Measurement Standard (NMS) ionisation chamber in free air . . . . . 58
46 Langmuir probe positioned for IV plot measurements in free air 58
47 IV plot obtained in free air using a Langmuir probe in a 10 cm X 10 cm $^{60}$Co radiation field. . . . . 59
48 State progression of the data acquisition system. . . . . 60
49 Selection of region wherein to conduct Survey (GUI). . . . . 61

# List of Tables


1 Best fit parameters of air at 45 Torr . . . . . 41
2 Best fit parameters of Argon at 145 Torr . . . . . 42
3 Best fit parameters of flowing Argon between 45 Torr and 150 Torr 52
4 Best fit parameters of flowing Argon between 45 Torr and 150 Torr 54
5 Raw current-Voltage data of teletherapy NMS at 45,7%RH,$22^0C$ and 0.861 bar . . . . . 64
6 Raw current-Voltage data of teletherapy NMS at 45,7%RH,$22^0C$ and 0.861 bar continued . . . . . 65
7 Raw current-Voltage data of teletherapy NMS at 45,7%RH,$22^0C$ and 0.861 bar continued . . . . . 66
8 Raw current-Voltage data of teletherapy NMS at 45,7%RH,$22^0C$ and 0.861 bar continued . . . . . 67
9 Raw current-Voltage data of teletherapy NMS at 45,7%RH,$22^0C$ and 0.861 bar continued . . . . . 68
10 Raw current-Voltage data of Langmuir probe in air at 45 Torr . . 69
11 Raw current-Voltage data of Langmuir probe in Argon at 45 Torr 70
12 The roles and functions of Labview Block Diagrams . . . . . 73
13 Raw noisy current-Voltage data of Langmuir probe in flowing Argon between 45 and 145 Torr . . . . . 86
14 Raw high sheath expansion current-Voltage data of Langmuir probe in Argon at 160 Torr . . . . . 87
15 Raw current-Voltage data of Langmuir probe in Internal Flowing Argon . . . . . 88
16 Raw current-Voltage data of Langmuir probe in external flowing Argon . . . . . 89
17 Calibration data for the hivolt.de Voltage Power source . . . . . 90

# 1 Introduction

A *quasi-neutral plasma* is a gaseous state of matter formed when a gas is thermally or electrically ionised to such an extent that there results an electrically neutral mixture of free ions and electrons. In a typical quasi-neutral plasma, the mixture also includes a series of electrically neutral particles, such as gas atoms which have yet to be ionised.

In a high vacuum *plasma-propulsion engine* or *thruster*, a low temperature quasi-neutral plasma is produced by electrically ionising a gas mixture immersed in a region of high potential difference. The engine produces thrust by ejecting a quasi-neutral plasma for its exhaust plume[1]. A similar method is used in a typical fluorescent tube, wherein a known gas is enclosed and subjected to a high potential difference. The resulting ionised gas typically releases this electrical energy by glowing. Contained therein is thus a basic example of a quasi-neutral plasma.

When the potential difference is removed, the quasi-neutral plasma contained in the fluorescent tube undertakes a process known as *plasma recombination* during which the gas loses its ionised state, regains its atomic state and thus causes the tube to slowly lose its familiar glow. The same process takes place in the wake of the plume a plasma propulsion engine, whereat the plasma plume is no longer exposed to an external potential difference as it would be inside the thruster and the same conditions as in the fluorescent tube are reproduced.

Before its release as light, or other forms of electromagnetic radiation, the electrical energy is possessed *thermally* by the host gas(es). An independent *electron gas*, for instance, may exist within the plasma and may thermally posses energy proportional to its *electron temperature*, $T_e$. In essence, when the free electrons which constitute the electron gas are recaptured by the surrounding *ion gas*,and hence surrender their thermal energy to the resulting neutral gas, the process of plasma recombination will have concluded. Plasma recombination is therefore an *exothermic process* and will tend to result in a higher temperature for the resulting neutral gas.

Unlike a typical gas mixture, which often seeks to reach thermodynamic equilibrium among its constituent gases, the component species of a plasma have the unusual property that they can sustain a state of thermodynamic non-equilibrium for as long as the plasma state is sustained by an external energy source, such as an external electric or magnetic field. Of course, the removal of the source voltage and the subsequent commencement of recombination ultimately and collectively lead to thermodynamic equilibrium. In a plasma composed only of two species, for instance, it is possible for the two charged species to behave as independent gases with unequal thermodynamic properties, key among which is temperature. As these properties will certainly include electric charge, the plasma may thus sustain an electric potential, known as the *plasma potential*, between its various constituent gases[1].

For the purpose of this discussion, a gas will be defined as *a collection of free particles of which all members have the same electric charge and mass, have a single collective temperature and pressure and collectively occupy the same region*

*in space*. Thus, the *electron gas*, the *ion gas(es)* and the neutral gas, as so appropriately named, all constitute independent gases within the quasi-neutral plasma.

When a single neutral gas is used to produce the plasma, a typical result contains a single ion gas, an electron gas and a neutral gas, thus resulting in a *two species plasma*. When a more complex gas mixture such as air is used, the resulting quasi neutral plasma may contain more than a single ion gas. The ion gases would be distinguishable from one another as their constituent particles may have different mass and/or electric charge, this would establish them as independent gases.

A connection may exist between the types of species which make up the plasma in a plasma engine and the amount of thermal energy necessary for plasma recombination to occur. Unfortunately, without being able to identify the species which are produced in the plasma, along with their associated thermodynamic properties, it may be difficult to design the process by which the plasma is created and sustained in such a way as to optimise the mechanical efficiency, among other desired traits, of the engine.

In the studies of dosimetry and ionising radiation, an *ionisation chamber* is used to measure one such property of a quasi-neutral plasma. A quasi-neutral plasma is produced by exposing a known volume of gas to a stream of ionising radiation.

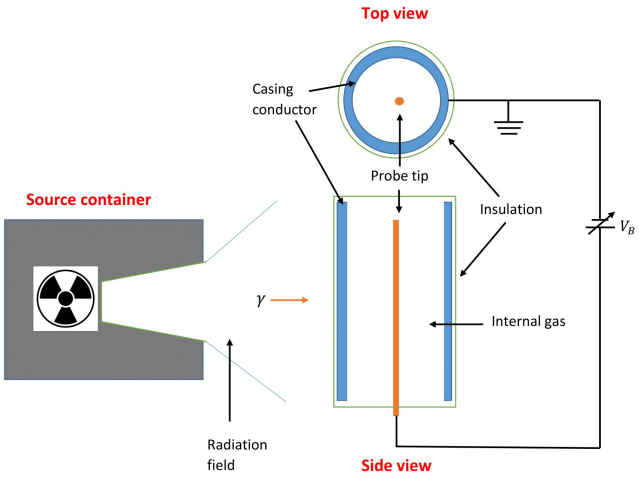


Figure 1: Basic schematic of an ionisation chamber exposed to a radiation field.

The plasma is formed as the radiation ionises the various atoms of the contained volume of gas(es). The primary purpose of the chamber is to measure the *dose* of radiation energy which is delivered to a particular point in space[27,28]. This is done by positioning an electrically biased conducting wire in the midst of the ionised volume of gas and collecting electric current from this conducting wire whilst the volume is exposed to the radiation beam.

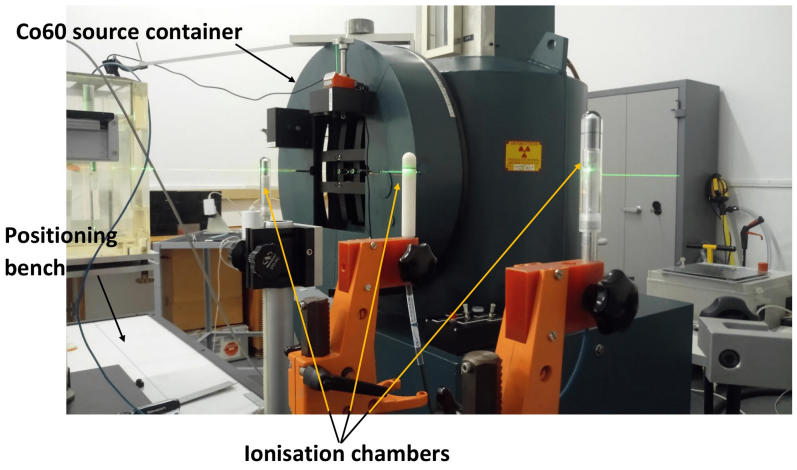


Figure 2: Ionisation chambers positioned for dose measurements of a teletherapy gamma radiation source at the National Metrology Institute of South Africa (NMISA)

The chamber is typically positioned precisely relative to the beam axis with the help of a *positioning bench*. In Figure (2), the positioning bench is used to move the 0.6 cubic centimetre ionisation chambers to precise positions in the cross-section of the beam. In so doing, a precise profile can be produced which shows the dose at each position in the entire region in the neighbourhood of the radiation beam.

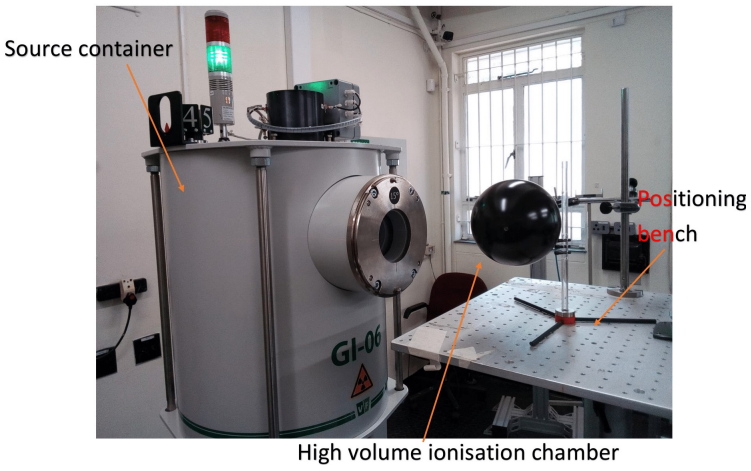


Figure 3: A high volume ionisation chamber positioned for low level dose measurements at the NMISA

A similar device known as a *Langmuir probe* can be used to diagnose the exhaust plume of a plasma-propelled engine precisely for the purpose of gaining insight into the molecular and thermodynamic properties of the resulting low-temperature quasi-neutral plasma. A Langmuir probe is an electrically biased conductor which is exposed to the plasma at a desired position. The probe is used to measure the response of the plasma by *collecting* an electric current into, or out of, the probe. By precisely observing the dependence of the probe current on the bias voltage imposed on the probe, and using statistical mechanics and thermodynamics, it is possible to infer many of the basic thermal and mechanical properties of the plasma, such as the temperature(s) of the species and their respective *average thermal speeds*[2]. In this way, a Langmuir probe is similar to an *ionisation chamber*.

Although most gasses electrically behave as *insulators* even when exposed to relatively low voltages, it is possible to establish a continuous current across a gas or gas mixture by exposing it to a very high potential difference [40,41]. In particular, a high potential difference applied across a volume of gas or gas mixture has the effect of causing gas electrons to be freed from their bound atoms and to travel in the general direction of the potential difference. While some electrons may enter the volume at the point of high potential, others will exit the volume at the point of low potential, thus establishing a continuous current across the volume of gas or gas mixture. Due to this potential difference, the resulting electrons may interact with other neutral atoms resulting in high energy collisions which may result in further ionisations, and may increase the temperature of the gas or gas mixture [40].

As the electrons are freed from their bound gas atoms, the resulting substance is a type of plasma known as a *discharge plasma*, in which a mobile electron gas flows amidst a comparatively static mixture of ions and neutrals. The external voltage is usually required in order to sustain the plasma state, since most of the energy input in the gas is also lost due to particle interactions that result in increased temperatures and some which cause the plasma to glow and release the energy as electromagnetic radiation. As a result, discharge plasmas typically *glow* in response to the exerted potential difference. A *steady state* is established when the energy is lost at precisely the same rate at which it is acquired [41].

Since it generally takes different amounts of energy to successfully ionise different types of gasses, plasma discharges in gas mixtures such as air usually occur to different extents among the various gasses which make up the mixture. The *ionisation* energies , the energy required for ionization, of Carbon dioxide and Dioxygen, for instance, differ from each other. The former being approximately 14 eV while the latter is 12.5 eV. In a mixture like air, therefore, which contains both these gasses, it will be easier to ionise the Dioxygen molecules than to ionise the Carbon dioxide molecules. This may result in a plasma containing more $O_2^+$ ions than $CO_2^+$ ions [40].

Although discharge plasmas are known to be less stable than many other types of plasma, many studies have successfully applied the Langmuir probe method to a variety of discharge plasmas both at low pressures and at or near

atmospheric pressure [46,47,48,49]. When the conditions used to generate and sustain a discharge plasma are kept steady, the plasma therein generally retains steady plasma properties which do not change erratically. Several models which describe many types of plasmas, such as the *Maxwellian model*, can be expected to apply to discharge plasmas under ideal or near ideal conditions.

## 1.1 The thruster

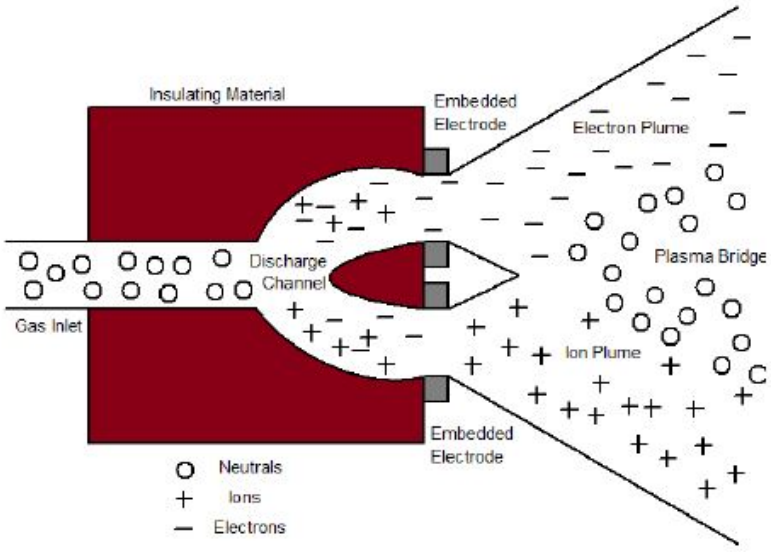


Figure 4: U-shaped miniature DC-discharge microthruster

A *DC-discharge* plasma propulsion engine/thruster uses a direct current electrode arrangement in order to sustain the plasma. Some such engines, as in the case shown in Figure (4), are special in that the bulk of the negative species of the plasma are known to be ejected into the plume at or near the cathode while the positive species are known to be ejected at or near the anode. The two sets of species nevertheless form a quasi-neutral plasma as they mix thereafter[4].

The plasma plume is therefore an amalgam of two charged jets of ions, which take place at different positions in space. The result is a plasma plume which has different properties at different positions in the wake of the thruster.

As far as the Langmuir probe is concerned, the thruster as shown in Figure (4) is analogous to the radiation source containers in Figures (2) and (3). Whereas the source container ejects a beam of high energy gamma radiation which then ionises the air down-source thereby producing a quasi-neutral plasma which has different plasma conditions at different positions, the thruster is similar in that it ejects an already ionised quasi-neutral plasma which is anticipated to have different plasma conditions at differing positions in space as a result of different plasma species having been ejected from different exhaust points.

A Langmuir probe is traditionally kept static inside a closed volume containing a fairly static and uniform plasma, wherein the precise location of the probe

is of little or no consequence[1]. However, the non-uniform nature of the plume in the case of the thruster means a *mobile Langmuir probe* will be required such that a much more complete survey of the region in the wake of the thruster can be performed.

This study focusses on a type of miniature DC-discharge microthruster known as a *U-shaped Microthruster*[4]. As Figure (4) demonstrates, the device generates thrust by first ionising a neutral gas. This process results in at least two different species of charged particles. One set of these species is attracted to and ejected from the cathode, while the oppositely charged set is attracted to and ejected from the anode. The result is a plume in the wake of the thruster which is formed when the two sets of species form a quasi-neutral mixture.

Along a region in the wake of the thruster called the *plasma bridge*, the plume is expected to form a complete mixture of both or all plasma species. As the source voltage will no longer exist in the plume, it is also in this region that the process of plasma recombination is expected to begin.

Micro-thrusters of this type could be used to propel small spacecraft or artificial satellites in a low-pressure and low-gravity environment. The plasma plume is also expected to expand in space as it exists the thruster, thereby creating variations in space of both the pressure and temperatures of the plasma. These properties also form part of the thermodynamics of the plasma plume, and may therefore be important in providing a complete diagnosis of the plume. The low-pressure environment can be recreated in a vacuum chamber under laboratory conditions.

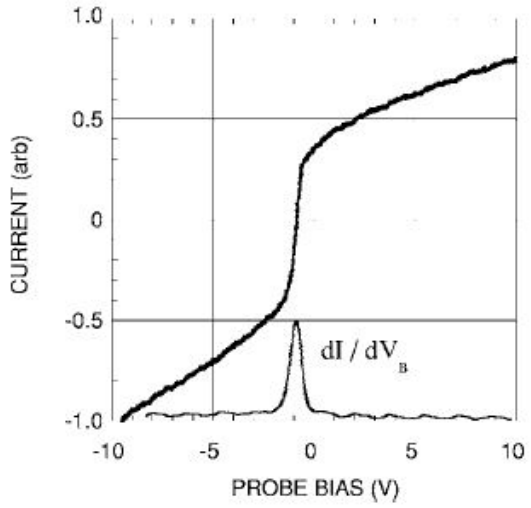


Figure 5: The characteristic IV curve of a two species quasi-neutral plasma, exemplified by an Argon plasma

.

In a two species plasma, where the mixture includes neutral gas particles,it is possible to characterise the relationship between the current collected by the Langmuir probe and the bias voltage imposed on the probe. This relationship is demonstrated by a current-Voltage (IV) curve, such as in the case shown in Figure (5)[1]. This would be typical of the IV curve conducted on a single point in the plume. In order to produce an IV curve o this type, as few at ten measurements and as many as one hundred individual current measurements may be required. Figure (6) shows an example of a IV plot which was conducted using the South African teletherapy National Measurement Standard (NMS) which is used to maintain the basic SI unit of radiation dose, the Grey, and to disseminate it to various industries in South Africa. Although the NMS is an ionisation chamber, it is easy to observe similarities between the IV plot in Figure (6) and the characteristic IV plot of Langmuir probes shown in Figure (5). The plot in Figure (6) was produced at the NMISA using a Keithley 6517B electrometer, which is capable of reading electric currents as low as $10^{-25}A$. The raw experimental data for the plot is shown in Appendix A.

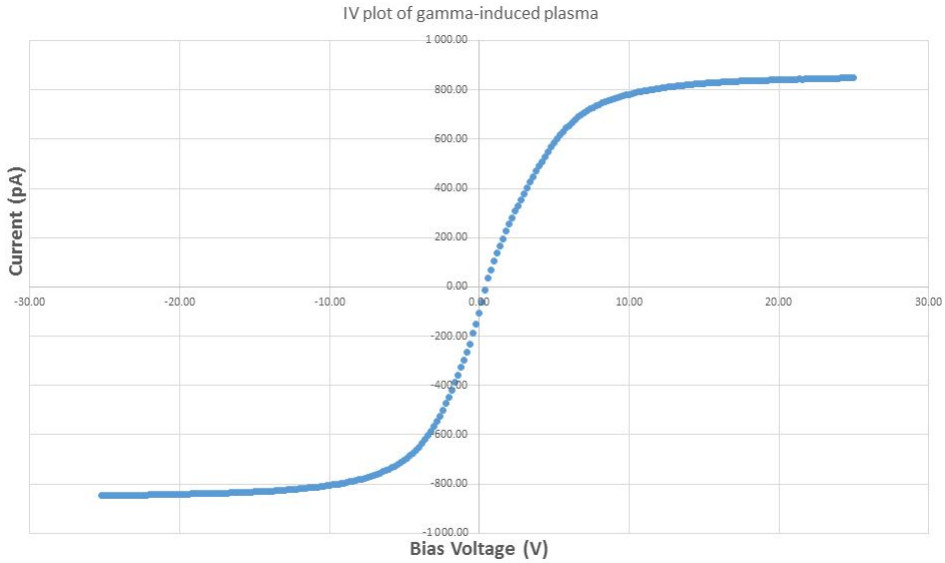


Figure 6: A current-Voltage plot conducted with the South African teletherapy national dosimetry standard in air at 45.7%RH, $22^0C$ and 0.861 bar, using a Co-60 gamma source.

In order to conduct a full survey of the plume, a series of IV plots of this type corresponding to a variety of well-defined coordinates in the exhaust plume is required. The process of producing all these IV curves would be extremely tedious and time consuming if conducted manually. Moreover, the plasma micro-thrusters which have thus far been produced in the space propulsion research laboratory of the school of physics at the University of the Witwatersrand, shown in Figure (7), which have initially been modelled from plastic materials and can only be sustained for a short period of time[4]. This generally implies that the process of producing the IV curves must be completed within the lifetime of each thruster and must be conducted for as many points in the plume which cover as large a range as is possible.

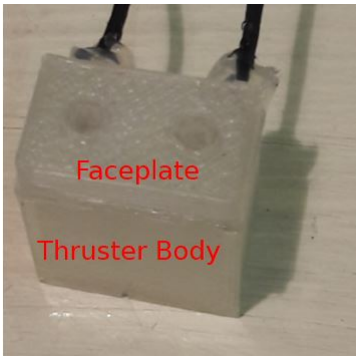


Figure 7: A U-shaped plasma micro-thruster intended for short measurement tests by the space propulsion research laboratory at University of the Witwatersrand.

The best way to conduct this kind of measurement in a way that is both efficient and accurate is with the use of a computerised measurement system which is designed effectively to automate the measurement acquisition process, thereby eliminating any tediousness that may be involved in a manual acquisition and reducing the risk of human error. Such a system would be used to control and direct a series of unmanned instruments, including those which collect and record the data from the measurements, position the probe and run the thruster and collect information regarding environmental conditions in the laboratory.

Similar such measurement acquisition systems were created in parallel with this project for the NMISA, where a series of long-range and long-duration measurements, some lasting as long as sixteen hours, are regularly conducted using mobile ionisation chambers of the types shown in Figures (2) and (3). Similar or related automation projects in other dosimetry and radiation laboratories have also been previously undertaken[6]. These automated measurement systems typically include software components in addition to electronic and mechanical components.

Additionally, the system may interface with some standard instruments

which are capable of *serial communication* with a computing system. Instruments of this type are able to receive coded text strings called *serial commands* as instructed by a computer and accordingly make changes or corrections to their operational settings and protocols.




Figure 8: PTW eletrometer used for standard dosimeter calibrations at the NMISA.

Depicted in Figure (8) is an example of an instrument which can be used to set and control the bias voltage of a plasma probe, be it an ionisation chamber or a Langmuir probe. The instrument voltage can be set serially from a remote computer which may itself be unmanned. Information from the instrument, such as the current collected as a result of the set voltage can also be received, logged and analysed by the remote computer.

The computer can in turn be directed by a specially designed software which can concurrently send and receive data and instructions to and from a multitude of similar instruments. In this way, the process of collecting the measurement data can be fully automated. A software of this type is shown by the graphical user interface shown in Figure (9), where a *beam profile* of a Co-60 radioactive source is displayed. The beam profile is similar to a survey of the plume of a thruster in that it represents the magnitude of a parameter on the y axis, which is current in this case, measured at a particular position or coordinate represented by the x axis. The bell shape seen in Figure (9) is a characteristic feature of the Co-60 unit shown in Figure (2).

A direct current plasma discharge can be induced in a variety of different gases, such as Argon, and in some gas mixtures, such as air. Among many properties which can affect the extent, quality and ease with which such discharge can be induced is the pressure at which the gas or gas mixture in question is kept during the discharge.

One way to achieve a DC discharge at a non-atmospheric pressure is to use a contained gas in a vacuum-sealed *discharge tube*. This type of arrangement will be known as a *closed discharge*.

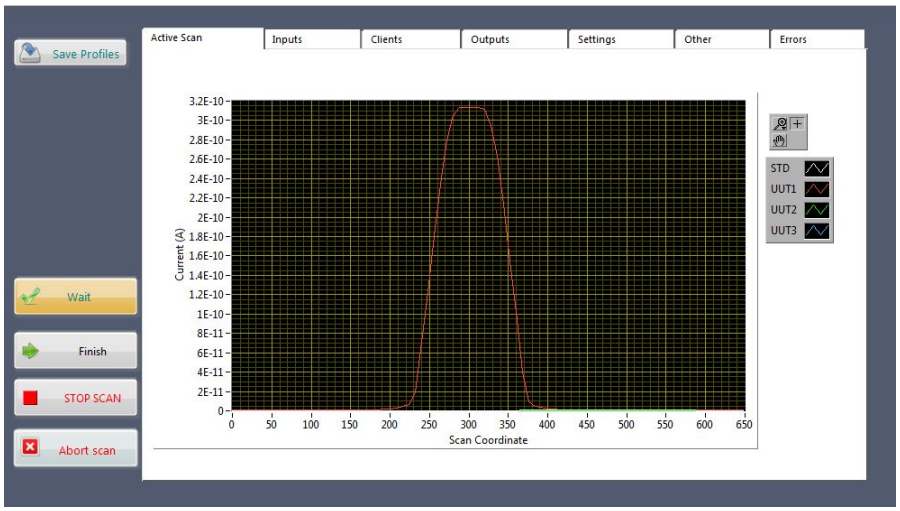


Figure 9: The graphical user interface of a measurement automation software designed for calibration measurements at the NMISA.

An *open discharge* will occur when the gas in discharge is not vacuum sealed from its immediate environment. Rather, the local environment may itself be kept at a desired non-atmospheric pressure. In the plasma propulsion laboratory at University of the Witwatersrand, this is accomplished by making use of *vacuum chamber* as shown in Figure(10).

A non-vacuum-sealed discharge tube can be placed inside the vacuum chamber and allowed to freely exchange gas molecules with what gas is contained by the remainder of the chamber.

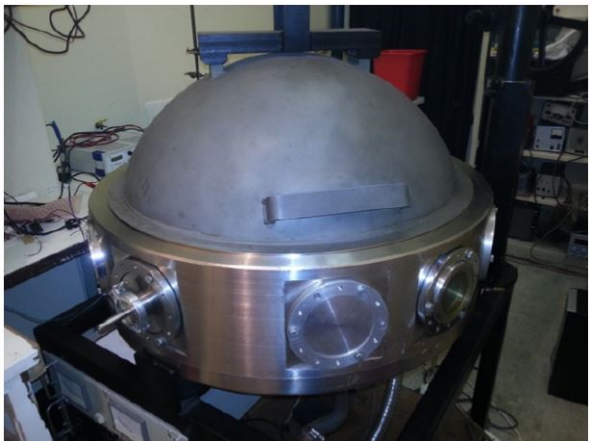

Figure 10: Vacuum chamber of the plasma propulsion laboratory at the University of the Witwatersrand

The remainder of the dissertation is structured as follows: Chapter 2 will discuss the theory of the Langmuir probes and how it is applied for diagnostics, while chapter 3 will consider some design considerations related to the probe structure in the measurement context. A mobile bench for moving the probe will also be discussed. Chapters 4 and 5 describe the experimental set up and data acquired from a closed and open discharge channel, and chapter 6 will discuss the structure of the software used to control the mobile bench for conducting surveys in the plume. Chapter 7 draws conclusions, which are followed by the appendices.

# 2 The Langmuir probe

The Langmuir method employs a systematic approach to the problem of acquiring data on and characterising the main properties of a plasma. As with all measurements, collecting data from an ionised plasma requires that the experiment interacts directly with the system, which may result in a quantifiable disturbance.

The Langmuir method interacts with the plasma by introducing a biased conducting wire known as a *Langmuir probe* at a desired position within the plasma. Typically this type of measurement is done on an enclosed plasma, which will have been produced by one of three main methods. A *hot plasma*, for example, occurs when the parent gas is ionised by having its temperature increased to a high extent such that its bound electrons are freed from their host atoms or molecules.

A contained plasma can also be produced and maintained by *magnetic confinement* by exposing the neutral parent gas to a high magnetic field in the vicinity of a biased electron source/sink, such as a tungsten filament.

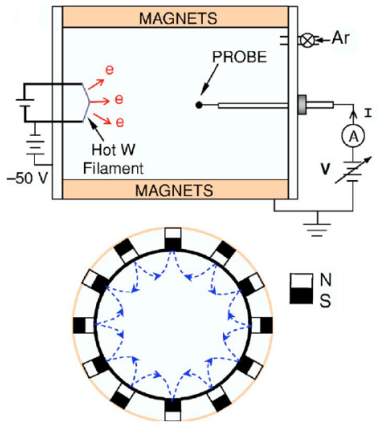


Figure 11: Plasma induction by magnetic field

Some of the typical properties of a magnetised plasma which has been produced as Figure (11) shows can be found in [1]. Typical such enclosed plasmas have the convenient property that their plasma parameters such as the *electron temperature*, a property of the plasma related to the average speed of the electrons of the plasma, are known to have a constant value across the enclosure.

This *uniformity* of the plasma has the added convenience that the precise location of the probe inside the enclosure is of little or no consequence. In Figure (11) for example, the probe is shown as being securely and perpetually positioned at a single point in the enclosure. This type of probe will be known as a *static probe*.

Typically, the enclosure of the induced plasma is composed of a conducting material which is kept at standard local voltage (or ground) and forms part of

the circuitry of the probe. That is, as Figure (11) implies, what electrons are collected from the plasma by the probe at its given location are automatically replaced back into the plasma by the grounded enclosure. Thus, the plasma remains quasi-neutral despite the presence of the biased probe[1].

In such a dc discharge plasma, the probe is known to result in the formation of a *sheath region* in the immediate vicinity of the of the *collecting surface* of the probe. The sheath region forms when the plasma is locally over-saturated with or extensively drained of electrons as a result of the bias voltage of the probe[2].

The effect of the bias voltage of the probe on the plasma is typically limited by the sheath region in the vicinity of the probe, which can be several *Debye lengths* wide, which is primarily determined by properties of the local electron gas. The Debye length $\lambda_D$ is known to be given by

$$\lambda_D = \left( \frac{\epsilon_0 k T_e}{e^2 n_e} \right)^{1/2} , \tag{1}$$

for some local electron density $n_e$ and electron temperature $T_e$, where the elementary charge, the Boltzmann constant and the permeability of free space are respectively denoted as $e$,$k$ and $\epsilon_0$[1]. Thus, as the magnitude $\lambda_D$ increases so too does the local disturbance produced by the presence of the probe.

In a plasma produced by a *direct current (DC) discharge*, and when the size of sheath regions becomes large enough, the probe can begin to behave as an electrode. In this case, the probe would have disturbed the local plasma properties to such an extent that its presence has resulted in a different kind of plasma of a different set of plasma properties.

Fortunately, the Langmuir probe method will typically have produced the measurements of the local plasma properties for relatively low bias voltages compared to that voltage which will have resulted in the plasma discharge.

The local electron temperature $T_e$ and plasma potential $V_p$ are related to the electron contribution of the probe current by the following expression,

$$I_e = \begin{cases} I_{es} \exp\left( -\dfrac{e\,(V_b - V_p)}{k T_e} \right) & , V_b \leq V_p \\ I_{es} & , V_b > V_p \end{cases} , \tag{2}$$

for some probe bias voltage $V_b$, where the *electron saturation current* is denoted as $I_{es}$ [2,3]. A similar expression embodies the ion contribution to the probe current as described by

$$I_i = \begin{cases} -I_{is} \exp\left( \dfrac{e\,(V_b - V_p)}{k T_i} \right) & , V_b \geq V_p \\ -I_{is} & , V_b < V_p \end{cases} , \tag{3}$$

where the *ion saturation current* is denoted as $I_{is}$. The relationship between the probe current and the probe bias voltage is thus a piecewise function embodied by the total of the electron and ion contributions as explicitly given by the following expression,

$$I = \begin{cases} I_{es} \exp\left(-\dfrac{e\,(V_b - V_p)}{kT_e}\right) - I_{is} & , V_b \leq V_p \\ I_{es} - I_{is} \exp\left(\dfrac{e\,(V_b - V_p)}{kT_i}\right) & , V_b > V_p \end{cases} . \tag{4}$$

Relationships of this type follow from known properties of the very ideal *Maxwellian* gases [12]. The fundamental gas *velocity distributions* which serve as the basis for the derivations of Equation (4) are explored by F. Mandl [12]. A typical plot of this Langmuir relationship is shown by Figure (5)[1,2,3].

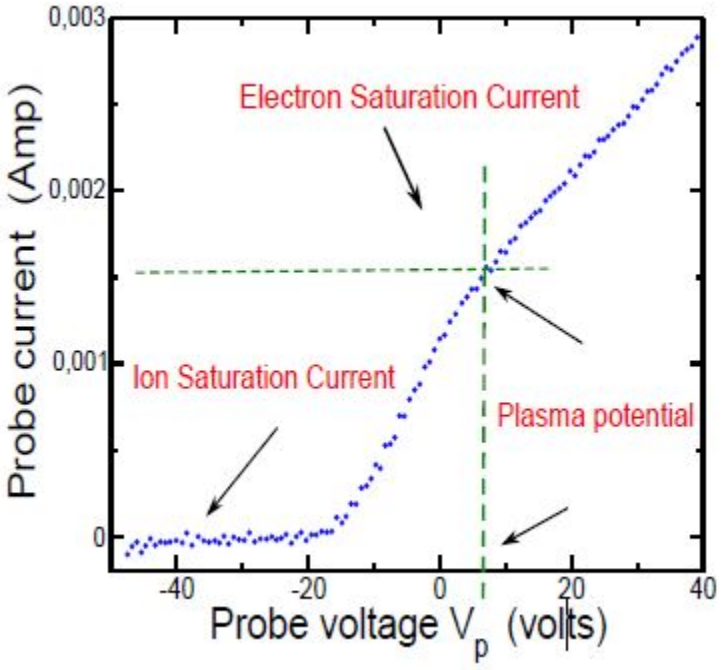


Figure 12: Asymmetric Langmuir IV plot[2]

Figure (5) shows the IV plot of which the local plasma properties are relatively symmetric with respect to the ion and electron gases. A more typical scenario can be seen in Figure (12), where the two gases may have unequal saturation currents, $I_{es} >> I_{is}$, and the local particle temperatures may also differ significantly, $T_e >> T_i$[1,2].

The Langmuir technique is favoured by the unique property that, the structure of Equation(4) does not change regardless of the type, shape or size of the probe being used. As such, a variety of probe shapes and sizes, as later shown by Figure (14), are typically used when measuring the properties of enclosed plasmas.

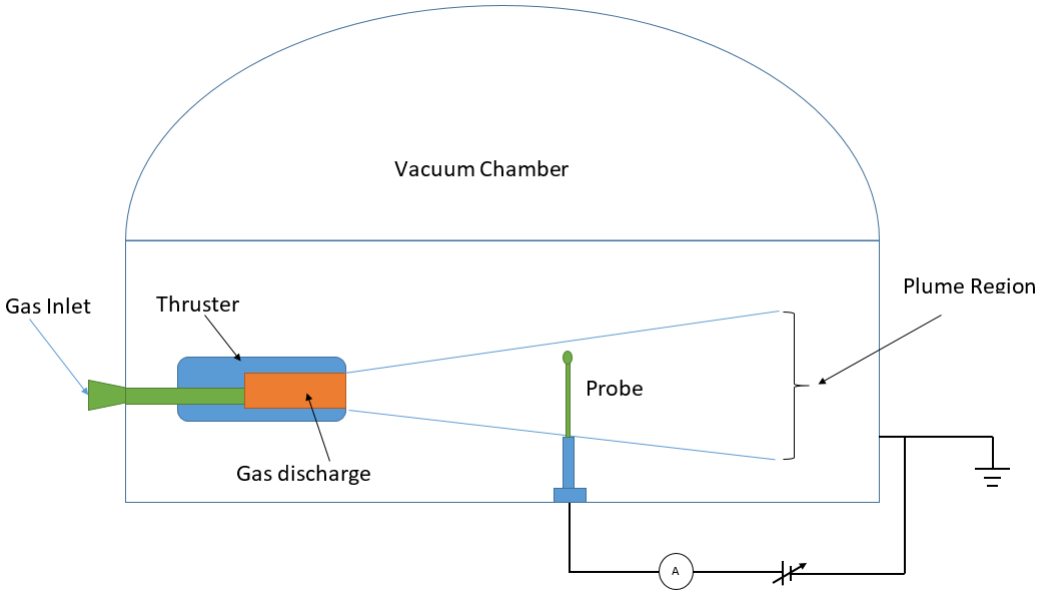


Figure 13: Langmuir probe Inside a vacuum chamber

The scenario of the enclosed plasma is reproduced when a DC-discharge microthruster produces a plasma plume inside of an evacuated chamber of the type shown by Figure (10)[4]. A static Langmuir probe, in this case, can be installed as demonstrated by Figure (13) inside the plasma plume of the thruster, where the plume is enclosed inside of a grounded vacuum chamber.

Should the plasma in the vicinity of the probe be uniform, Equation(4) should be able to describe the current there collected by the probe.

Unlike the scenario shown in Figure (11), however, the U-shaped DC-discharge micro thruster of Figure (4) should produce a plasma plume which is generally non-uniform in space. This non-uniformity is expected to be present predominantly in the 2D plane as shown by Figure (4)[4].

Thus, the expectation should then be that the plasma properties of the this plume should also vary as a function of the position of the probe inside the plume.

Static Langmuir probes are usually used to diagnose these types of enclosed plasmas, as the non-uniformity in space of the plasma parameters is an extremely rare scenario. As such, a *mobile langmuir probe* will be used to assess the properties of the plasma at a variety of positions inside of the enclosure and which can be used to track how the various plasma properties change from one such position to another.

When the electron Temperature $T_e$ is not significant compared to the ion temperature $T_i$ of the uniform quasi-neutral plasma, the two are known to be related to the average electron and ion speeds as per the respective expressions

$$v_e = \left(\sqrt{\frac{8k}{\pi}}\right)\left(\frac{T_e}{m_e}\right)^{1/2}, \tag{5}$$

and

$$v_i = \left(\sqrt{\frac{8k}{\pi}}\right)\left(\frac{T_i}{m_i}\right)^{1/2}, \tag{6}$$

where the mass of the electron and the mass of the ion are respectively denoted as $m_e$ and $m_i$ [1,2,3]. The implication is thus that the ratio of the two average speeds is related to the ratio of the masses of the two species,

$$m_i = \left(\frac{v_e}{v_i}\right)^2 \left(\frac{T_i}{T_e}\right) m_e. \tag{7}$$

Thus, when the ratio of the average speeds of the two species and the ratio of their respective temperatures are known, and given the known mass of the electron, the mass of the ions therein can be calculated by Equation(7) and a likely candidate species can be suggested based on the calculated mass.

When a gas discharge takes place in a gas mixture containing a variety of different gases wherein the discharged gas is unknown, Equation(7) can help to identify the gas in discharge. One such gas mixture is air, which is known to predominantly consist of nitrogen, oxygen and carbon dioxide, all of which are gases capable of a voltage discharge.

The *Bohm current* is a special case of the ion saturation current of a quasi-neutral plasma of which the ion temperature is insignificant compared to the electron temperature, $T_e >> T_i$. The ion saturation current takes the form

$$I_{is} \approx I_{Bohm} = 0.6 e n_i \sqrt{\frac{kT_e}{m_i}}, \tag{8}$$

in which the ion saturation current, and thus the average ion speed, explicitly depends on the local electron temperature, a direct result of the development of a sheath region in the neighbourhood of the probe[1,2,3].

The drastic effect of a phenomenon known as *Sheath expansion* is directly and easily observable in Figure (12), wherein the probe current tends to behave linearly as a function of the probe bias beyond the local plasma potential[1]. Sheath expansion occurs when the size and surface of the sheath region increases when the probe bias is far from the local plasma potential $V_p$ [1,2]. In the neighbourhood of $V_p$, the effect of sheath expansion is to increase the *effective collecting surface* of the probe in such a way as to linearly affect the local saturation currents[1,2].

When the probe bias is significantly greater than the local plasma potential in a small-volume plasma discharge, for instance, the sheath region around the probe will have increased to a large fraction of the volume of the gas in the discharge, such that the probe begins to behave as an independent electrode contributing to the discharge of the propellant gas, thereby nullifying the Langmuir method.

For this reason, the probe bias should ideally be kept insignificant compared to the discharging voltage and in the neighbourhood of the local plasma potential.

The presence or relative absence of the sheath expansion effect directly affect the extent to which and effectiveness with which the plasma properties of the plume/plasma can be measured, and knowledge of its presence can greatly improve the quality of the measurement.

It is thus befitting that a realistic characterisation of the probe current as demanded by Equation(4), and assuming measurements close to $V_p$, requires that current saturations vary linearly with the probe bias. This requires a modification of the form

$$I = \begin{cases} \left(I_{es} + C_{pe}\left(V_b - V_p\right)\right) \exp\left(-\dfrac{e\left(V_b - V_p\right)}{kT_e}\right) - \left(I_{is} + C_{pi}\left(V_b - V_p\right)\right) & , V_b \leq V_p \\ \left(I_{es} + C_{pe}\left(V_b - V_p\right)\right) - \left(I_{is} + C_{pi}\left(V_b - V_p\right)\right) \exp\left(\dfrac{e\left(V_b - V_p\right)}{kT_i}\right) & , V_b > V_p \end{cases}, \tag{9}$$

where $C_{pe}$ and $C_{pi}$ will be known as *coefficients of sheath expansion* which are insignificant in an ideal *Maxwallian* quasi-neutral plasma.The two constants hence serve as a measure of the local *plasticity* of the sheath region in the neighbourhood of the probe. As the effect of sheath expansion is expected to be very low or limited, the constants served as a *first approximation* of the phenomenon. This helps to keep the model simple.

The task of measuring the average speed(s) of any of the species in the plasma is necessarily complicated by the arrangement of the experiment in question. In a non-uniform plasma, for instance, the speed may vary as a function of position and so too might the particle temperature(s)[4].

Automated measurements of the Langmuir type have been previously explored in the study of instrument calibrations of dosimeters in the field of teletherapy metrology[6,10]. Specific applications of automation and control of Langmuir probes have scarcely been explored in the area of plasma propulsion.

The problem of producing a mobile Langmuir probe which can be used to diagnose a spatially distributed plasma can thus be fundamentally divided into two separate problems. The first being the task of *designing* a candidate mechanical/electrical solution and its associated software, which requires interaction with works of electromechanical engineering. The second is to experimentally or empirically demonstrate both the structural and electrical functionality of the designed solution, along with a validation of its associated software.

# 3 Design of Langmuir probe and positioning bench

## 3.1 probe mechanism

The design of the probe mechanism consists of two separate problems, the first of which is the design and construction of an appropriate Langmuir probe. The mechanism must, of course, also include the design and construction of a positioning bench for the probe.

## 3.2 The Langmuir probe

### 3.2.1 Design Parameters and Restrictions

Langmuir probe measurements conducted in an enclosed plasma are typically done with a probe having a spherical, cylindrical or flat geometry, as in Figure (14). The various geometries differ mainly in their respective arrangement of the *collecting surface*(i.e. the surface region of the probe,$A_p$, along which the local voltage is exactly equal to the probe bias voltage and which is entirely exposed to the plasma being measured.

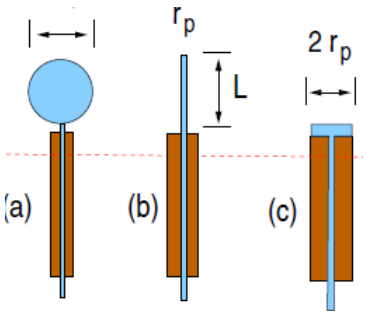


Figure 14: Langmuir probe shapes typically used in dc discharge enclosed plasmas, (a) spherical (b) cylindrical, (c) flat [2]

The probe surface area is important in that it is known to be directly proportional to the *saturation current(s)* of the various species of the plasma. In a plasma of which the ion temperature $T_i$ is significant compared to the electron temperature $T_e$, the ion saturation current, is known to be given by the expression

$$I_{is} = \frac{e}{4} n_i v_i A_p, \tag{10}$$

wherein the elementary charge, ion density and the average ion thermal speed are respectively denoted as $e$, $n_i$ and $v_i$[1]. By definition, the ion saturation current is the the contribution to the probe current at a bias voltage below the plasma potential. In a fairly uniform plasma, the ion saturation current is independent of the probe bias voltage. The direct proportionality between the ion saturation current and the probe collecting surface means that an ideal Langmuir probe has a large collecting surface. This would be to ensure that

the measurement instrumentation auxiliary to the probe can detect the current signal as provided by the probe. A small collecting surface would risk the current measurements being smaller than necessary for them to be detectable by the laboratory instruments.

The electron saturation current, which is known to be given by the expression

$$I_{es} = \frac{e}{4} n_e v_e A_p, \tag{11}$$

is also easier to detect with a large probe collecting surface.

The size and shape of the probe are, however, restricted by a variety of other factors, not least among which is the fact that the plasma properties of the exhaust plume in discussion vary as a function of position as shown by Figure (4). The size and shape of the probe therefore directly affect the resolution of the probe survey in the exhaust plume. A probe which is very broad, such as a flat probe deployed in the 2-D region as seen in Figure (4) would have the undesired consequence of covering a potentially non-uniform region in space. Reducing the size of such a probe would improve the resolution, but would worsen the detectability of the current measurements as argued by Equations (10) and (11).

If the 2-D plane view shown in Figure (4) is the xy-plane, then plasma properties of the plume are expected to vary little, if at all, along the z-direction [4], which is out of the page. The main source of the non-uniformity in the xy-plane is the fact that the two exhaust points eject different types of particles, which then leads to a non-uniform charge distribution along with other plasma properties.

Along the z-direction such disparities may occur to a lesser extent for any given point in the xy-plane. Therefore, along any such direction and for any such point, the plasma can be approximately uniform. An ideal probe should take advantage of this fact.

Another important restriction on the shape of the probe is imposed by the possibility that the plasma plume may be essentially a dynamic fluid and its fluid dynamic properties, including $n_i$ and $n_e$, may vary in space from their true values with the introduction of the probe. To this end, the probe represents a blunt obstruction amidst a flowing fluid, as shown by Figure (15).

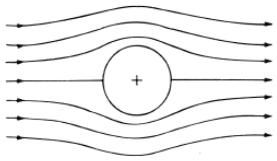

Figure 15: A blunt cylindrical obstruction in a uniform 1-D fluid flow

.

An obstructed uniform laminar flow of this type approaches its unobstructed form as the radius of the obstruction is reduced [7]. An ideal probe would have a minimised obstructive effect on the plume.

A cylindrical Langmuir probe has a number of advantages over most possible geometries, not least among which is its ability to have both a small radius and a fairly large collecting surface in the plume. The collecting surface of the probe would be given by

$$A_p = 2\pi r L + \pi r^2, \tag{12}$$

for some radius $r$ and some length $L$. The second term in Equation(12) would ideally be negligible compared to the first term. The objective is thus to maximise the first term and minimise the second term, thereby benefiting from a large collecting surface with minimal obstruction to the flow of the plume. If one expects to take survey measurements in steps of between 1.5 mm and 2 mm, for example, then it is advisable that the probe radius be between 0.3 mm and 0.5 mm and the approximate length of the probe be of the order of 1 cm to 1.5 cm. Under these conditions, the first term in Equation (12) would be at least ten times higher that the second term. The 1 cm to 1.5 cm range is also the approximate expected hight of the plume region[4].

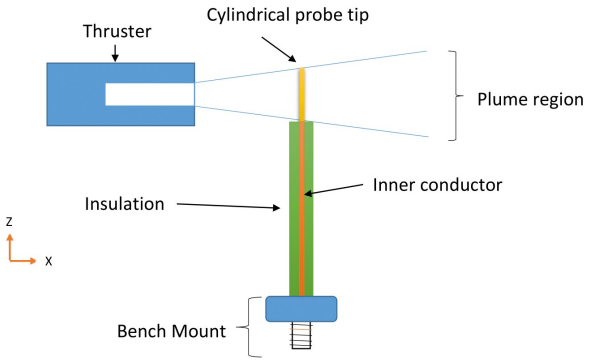


Figure 16: zx-plane.

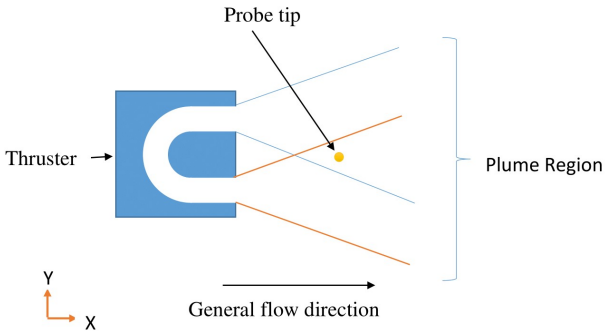


Figure 17: xy-plane.

Seen from the xy-plane, such a probe would have a relatively insignificant presence. The reported plasma parameters would also represent a unique point in the xy-plane, although not in the other two planes. The resolution, and thus the uniqueness, of the position of the probe in the xy-plane is therefore limited by the radius of probe. That is, the smaller the radius, the more the probe measurements represent a unique point in the plume.

The collecting surface at any given point in the xy-plane would also be relatively large as the entire available length of the plume along the z-direction at the given xy-point will be exposed to the probe bias. This will especially be the case close to the exhaust points of the thruster.

What remains of the probe must be both thermally and electrically insulated from the plasma and vacuum sealed from the plume. This follows from the knowledge that the plume near the exhausts of the thruster is expected to experience variations in temperature, density and pressure. These thermodynamic variables explicitly affect parameters included in Equation (10), such as the local particle density. Moreover, they may also affect the electrical properties of any exposed regions of the probe.

The easiest way to thermally and electrically insulate the probe is with a ceramic material which is mouldable enough to allow the probe conductors to be vacuum sealed from the surrounding plasma plume.

### 3.2.2 Proposed probe design

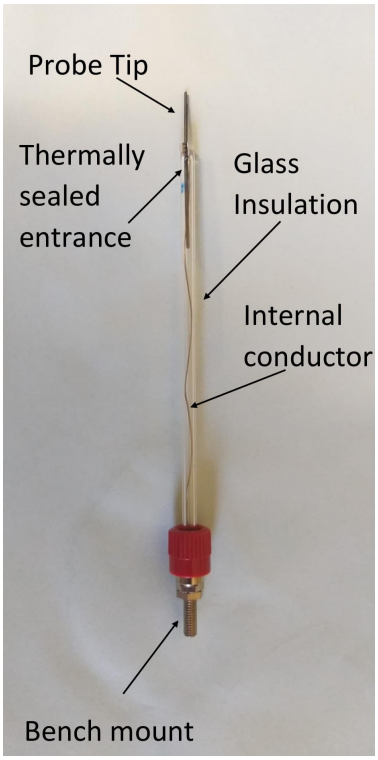


Figure 18: Glass-insulated cylindrical probe.

The expected thermodynamic conditions of the plasma inevitably place a series of strict requirements on the probe design. High among these requirements is the probe's ability to withstand sudden changes in local environmental temperatures ranging from $20^oC$ to $70^oC$ [4]. A fairly inexpensive conducting material which can be used for this purpose is tungsten wire. The material is known to have a coefficient of thermal expansion of $4.5 \times 10^{-6} K^{-1}$ which implies a maximum thermal expansion of 0.0225 % in the temperature range from $20^oC$ to $70^oC$[8]. This helps to minimise the positioning uncertainty of the bench as the size and shape of the probe will remain relatively unchanged. Likewise, the current collected by the probe will not vary significantly as far as the size and shape of the probe are concerned.

The probe tip, which is to be exposed both to the plasma plume and to the high vacuum environment, is made of tungsten wire.

The rest of the Lungmiur probe is insulated from both the thermal and vacuum effects of the environment by means of glass insulation. Like most ceramic materials, most glasses are good electrical and thermal insulators. No particular glass variant is specified here.

The more important property of glass is its ability to be moulded and thus vacuum sealed. In Figure (18) the probe is shown with its probe tip securely sealed by having melted the glass and allowed it to cool with the probe tip securely positioned.

A typical copper or zinc conductor is used to carry the current within the glass tubing thermally insulated from the surrounding plasma.

The probe also has the additional requirement that it must be compatible with a positioning bench, the primary task of which is to move the probe from one location in the plume to another . As such, it must be possible to securely mount the probe on the positioning bench whereupon it may be connected to the source of its bias potential.

This is accomplished by a threaded *bench mount* which is used to screw the probe to its point of contact with the positioning bench.

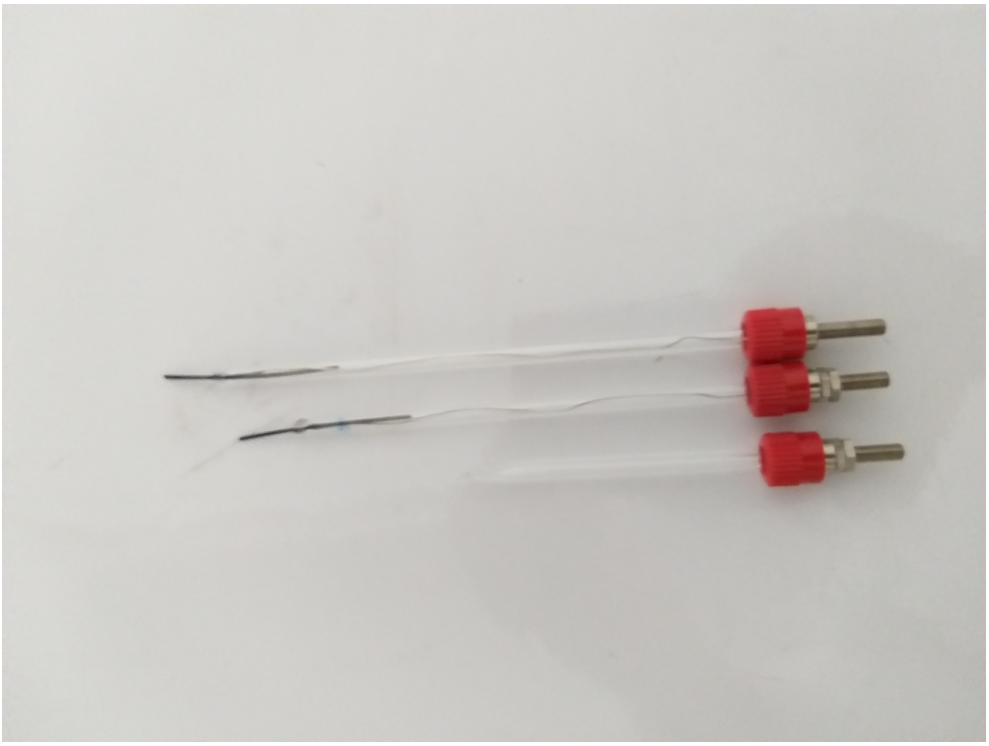

Figure 19: Glass-insulated probes in various sizes.

The probes are created in a variety of sizes to serve the purpose of handling different experimental arrangements. The probes are fragile and brittle and can easily be damaged if dropped.

## 3.3 The positioning bench

The probe is made mobile by the use of a *positioning bench*, the main purpose of which is to help remotely position the probe within the plasma plume while the probe, plume and thruster are all enclosed inside a vacuum chamber where they would otherwise be impossible to reach or to interact with. The bench thus has the same purpose as the ionisation chamber positioning bench(es) as depicted in Figures .(2) and (3), where the precise position of the instrument is central to the measurement effort.

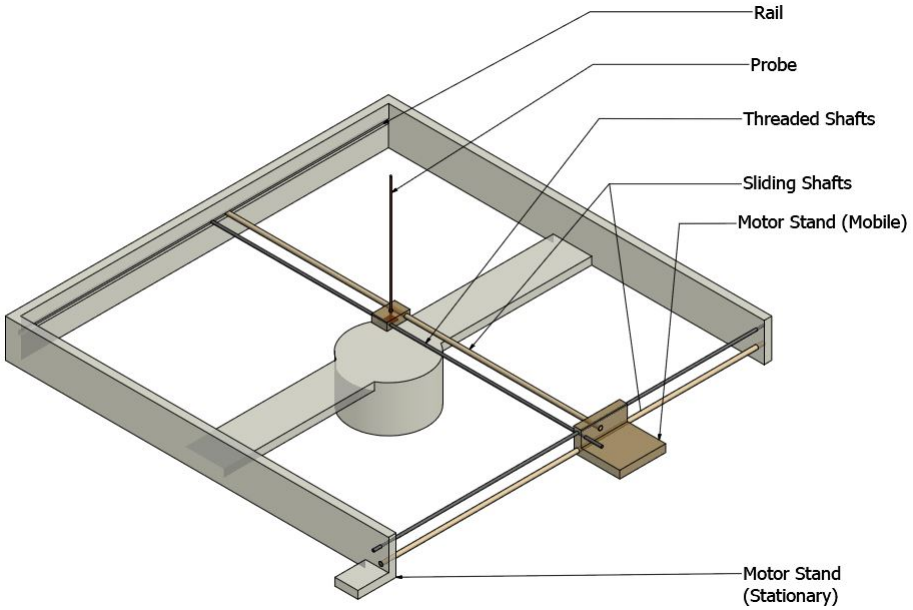


Figure 20: Schematic of the positioning bench.

In this way, the positioning bench is central to the effort of conducting Langmuir probe surveys of the plume region as it would allow for the probe to be moved to a variety of positions/coordinates in the plume region each of which can then be associated with a probe IV curve from which all necessarily desired plasma characteristics can be extracted and thus associated with said position or set of coordinates.

The bench must thus be capable of securely and safely moving and positioning the probe shown in Figure (18) to and from all points/coordinates in the plasma plume. As the thrusters and the extent of their exhausts may vary in size, the plume region may be a relatively small or large fraction of the floor area of the vacuum chamber wherein the experiments are expected to occur.

For this reason, and despite the current designs of the DC-discharge microthrusters being very small compared to the vacuum chamber, the positioning bench should ideally be designed to allow the probe to reach a relatively large

fraction of the floor area of the vacuum chamber, thereby accommodating possible future designs of the thrusters.

The actuators of the positioning bench, lest they be affected negatively by the plasma plume being measured, ideally should be kept at a sizeable distance from the plume region. This follows from the expectation that such actuators would be electrical in nature.

### 3.3.1 Frame

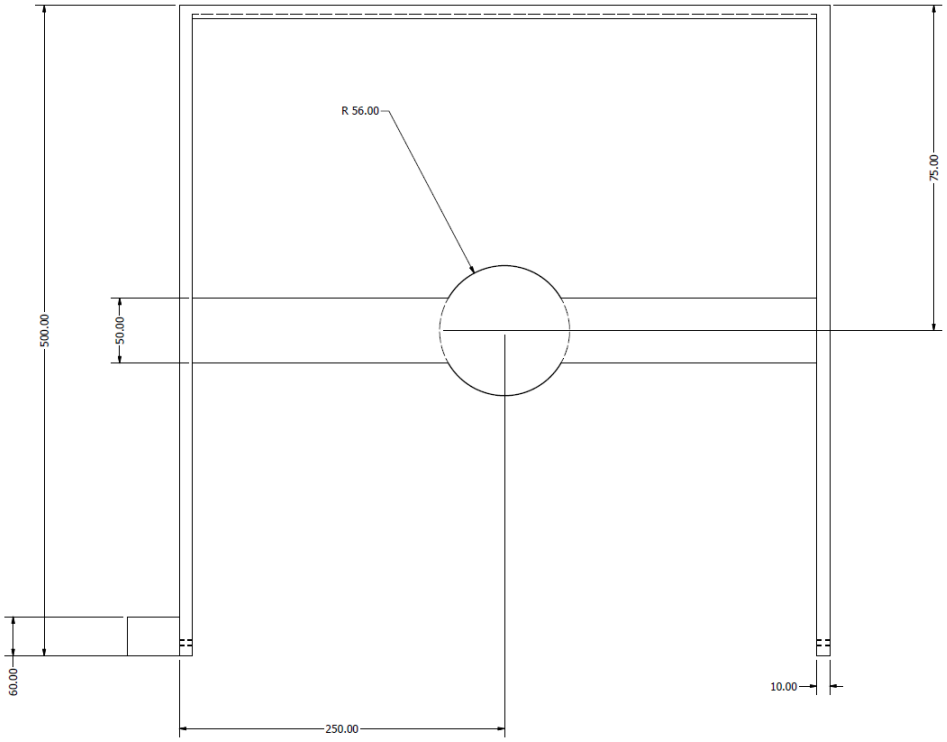


Figure 21: Frame dimensions of the positioning bench.

The 500 mm × 500 mm frame of the positioning bench as depicted by Figure (21) is designed to give the probe access to a 470 mm × 480 mm region inside the vacuum chamber covering a maximum floor area of 225600 $mm^2$. The probe can thus reach upto 49.7% of the roughly 380 mm radius floor space of the vacuum chamber.

As depicted in Figures (21) and (22), the frame is fitted with a 500 mm long rail along one edge of the frame, which is to be used to help stabilise the movement of the probe during positioning. Two mounts are also built and fitted to the frame for the purpose of securely holding in place two servo motors,

shown in Figure (22), which will be used as the main actuators when moving the probe.

The frame takes advantage of two features of the inside of the chamber in order to ensure that no unforeseen movement occurs which may lead to greater uncertainty in the position/coordinates of the probe. The first such feature is the chamber's existing screw-inlets, which can be used to ensure that the frame is rigid. The chamber also has a large closed cylindrical depression which is about 112 mm in diameter, which is used to keep the frame centralised while still be able to rotate.This is a feature which will be useful when a variety of different thruster positions and arrangements inside the chamber are desired as it will help orient the bench ideally relative to the thruster .

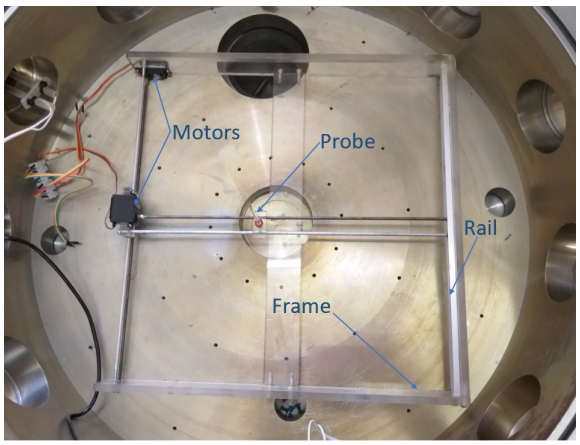


Figure 22: Bench frame inside vacuum chamber.

While the plume is expected to experience variations in temperature across the plume region, the remainder of the chamber is expected to have a relatively stable temperature , of approximately 20 $^oC$ to 25 $^oC$. The main body of the frame is therefore made of perspex plastic material, which functions well under these conditions.

In an effort to minimise the extent to which the frame and its various components can electrically interact with the plasma plume. The perspex material was chosen for its capacity as an effective insulator and was used in all but one of the main structural components of the positioning bench, that being the threaded bars of the probe mount/stand and the mobile motor stand.

The material is likely to fail structurally, however, should the average temperature of the interior of the vacuum chamber reach as high as 100 $^oC$. This is understood to be an extreme case which is unlikely to happen.

### 3.3.2 Actuators

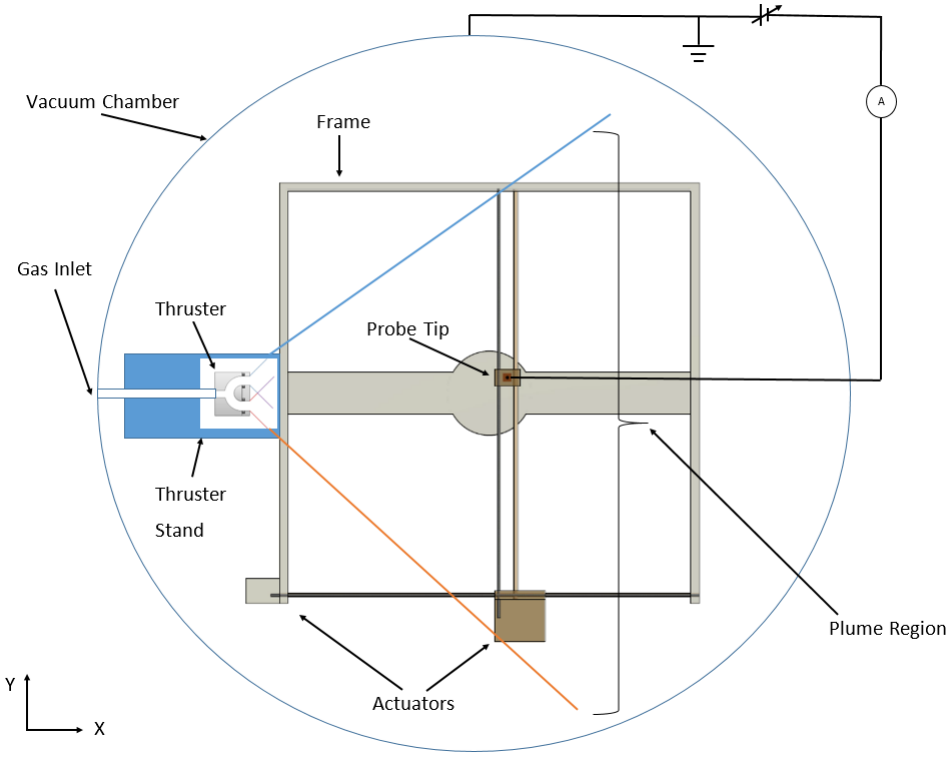


Figure 23: Schematic of the arrangement of the bench, probe and thruster inside the vacuum chamber and the circuitry of the probe IV-curve acquisition system.

The overall system is actuated by a system of motors, screwed/threaded bars and a variety of integrated circuit (IC) micro controllers, which have their instructions from a computerised control system.

The electrical actuators of choice are two unbounded servo motors which turn two 500 mm long threaded bars that each gear a probe stand or a motor stand. The motors are chosen for their ability to move the probe within the plume as the desired low average speed of 3 mm/s, when paired with threaded bars using the M8 $\times$ 5 standard threads.

As shown in Figure (23), the actuators move the probe by gearing one motor (the mobile motor) along the x-axis, which then gears the probe mount along the y-axis. Non-threaded rods are also used to help keep the two stands upright and stable during movement.

The probe mount, with one inlet for the threaded rod and one for the non-threaded rod is illustrated in Figure (24) with the probe mounted in an upright position.

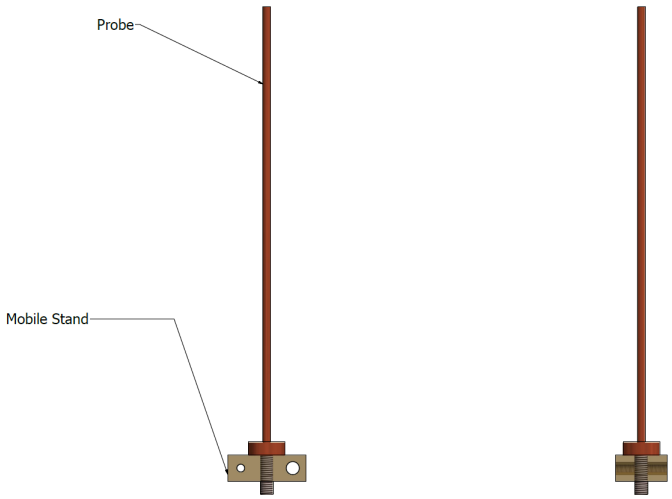


Figure 24: Probe mount.

The probe moves along with a conductor, as shown in Figure (23) which is connected to variable power source which is used to set the probe bias voltage. A control protocol on the central computer controls both the actuation system and the power supply and acquires current data from the ammeter in order to conduct a survey of the plume. The power supply is then also used to ground the vacuum chamber, thereby completing the circuit.

Figure (24) shows the assembly of the probe, the probe mount and the mobile stand. The configuration of the threads by which the probe is positioned can also be seen in Figure (24).

# 4 Discharge tube tests of the Langmuir probes

In order to test the functionality of the probes, two basic systems were constructed and run simultaneously and a series of data was then collected. The experimental setup consisted of the design and construction of a variety of discharge tubes in the interior of which a high voltage power supply could induce a DC discharge plasma from which the probe's ability to acquire and collect the plasma properties could be tested.

The probes also require the design and creation of a computerised data acquisition protocol which can be used to remotely build the IV curves independently and, in so doing, help to minimise measurement noise whilst maximising the precision with which each probe bias can be set.

A test of the probes is thus a test of both the probe design and of the computer acquisition system in a DC discharge plasma.

## 4.1 Aims of the test

The tests of the probe mechanism thus have a variety of basic aims.

Namely,

1. **To establish the suitability of the designed probe(s) for the problem of diagnosing a low temperature discharge plasma.**

   This will be achieved demonstratively by acquiring a characteristic IV plot of a two species quasi-neutral plasma and by making use of the probe amidst a DC discharge plasma.

2. **To verify the system's ability to reliably build a current-Voltage plot.** This will be achieved by having the characteristic IV plot of a two species quasi-neutral plasma be produced by an unmanned computerised IV acquisition system.

3. **To verify the suitability of the designed Langmuir probe(s) for acquiring IV data in a DC discharge plasma.**

4. **To verify the suitability of the designed Langmuir probe(s) for acquiring IV data in a globally non-uniform,but locally uniform plasma.** This will be achieved by having the characteristic IV plot of a two species quasi-neutral plasma be conducted inside of a small discharge tube of fixed volume containing an immobile quasi-neutral plasma.

5. **To establish the probe's capability to measure reliable IV data in a moving plasma.**

6. **To demonstrate the system's ability to conduct unmanned Langmuir probe analysis.** This will be accomplished by having the computing system use an algorithmic and unconventional method to apply the Langmuir probe model to the collected IV data and report the appropriate plasma parameters.

These aims are accomplished by employing a variety of rudimentary *discharge tubes* which can broadly be grouped into two classes, the first of which produce *enclosed* plasmas, while the other produce flowing and globally non-uniform plasmas. The discharge tubes are hence used to produce test cases for the types of plasmas which will be typical of the plumes of DC discharge micro-thrusters.

## 4.2 Discharge tube tests with enclosed Plasmas

An *enclosed plasma* will henceforth be known as a quasi-neutral plasma which is, for all practical purposes, static inside of a fixed volume. Such a plasma will be further known to be *uniform* when its plasma properties are constant throughout the fixed volume.

### 4.2.1 Experimental apparatus

#### Discharge tubes

The plasma discharge tubes are made for inducing a DC discharge plasma amidst a relatively small volume inside of an evacuated chamber. The tube is a 1 cm diameter by 2 cm length plastic tube which has two circular copper extremities which act as discharge electrodes. As the discharge takes place at relatively low temperatures, the tubes are expected to remain intact during the plasma discharge despite being made of plastic materials. The tubes are not reused after each discharge test. The copper electrodes are used to produce two circular regions of different potentials roughly 1 cm - 1.5 cm apart. The resulting potential difference between the two electrodes thus serves as a source of plasma discharge within the cylindrical volume therein.

A *gas-inlet* in the form of a smaller plastic tube is fitted to the discharge tube in order to ensure that the pressure inside of the discharge tube is always equal to the pressure in the immediate neighbourhood of the tube, thereby guaranteeing that, except for a short period of time during which the propellant gas seeks to reach equilibrium, the volume of gas within the discharge tube is effectively static, as there will be no large pressure or temperature gradients in space.

#### Langmuir probe

The tests were performed on the Langmuir probes shown in Figures .(18) and (19), of which the tungsten *probe tip* is exposed to the interior of the plastic discharge tube where it was used to expose the plasma to a local bias voltage and thus produce a Langmuir IV plot.

The Langmuir probes thus need not be mobile for this test, as the test volume in discussion is supposed to be static.

### Vacuum chamber

A stable and sustained plasma discharge is easier to achieve and to maintain at lower and stabilised pressures. The task of producing a volume of low pressure is designated to the vacuum chamber of Figure (10). The propellant gas inside of the discharge tube, and thus the pressure at which the discharge occurs, is given by the pressure inside of the vacuum chamber. The plasma test thus takes place in isolation in the volumetric interior of the chamber.

The chamber also serves as a way to isolate Argon gas from air in order to guarantee that the gas in discharge is known.

### Electrical Pressure probe

The vacuum chamber is fitted with a vacuum sealed electrical pressure probe which is used to measure the pressure the interior of the vacuum chamber. The DC discharge tubes are all placed inside of the chamber and are always allowed to exchange gas particles with the rest of the chamber and are thus are always kept at the same pressure as the vacuum chamber.

### Digital voltage power source

The accuracy, precision and effectiveness with which the bias voltage of the probe can be set and controlled requires the use of a computer-compatible voltage power source which can be used by an unmanned computer programme to conduct or build an IV plot. The THQ hivolt.de Voltage source is designated for this purpose.

The Power supply makes use of a USB and/or a RS232 serial interface in order to send and receive information and instruction to and from a computer.

### Vacuum pump

In order to evacuate the vacuum chamber, a single Alcatel 2012A roughing pump is used to remove any existing gas inside of the vacuum chamber. The gas is then replaced with the test gas which is maintained at a specified pressure by periodically employing the pump.

### Discharge power supply

A high voltage, low current, analogue voltage power supply is used to produce a plasma discharge across the volumetric interior of the discharge tube.

### Data acquisition

The data acquisition is performed by a Labview computer programme aboard a standard windows PC in the Laboratory.

### Gas container

A pressurised gas cylinder is used to fill the interior of the vacuum chamber with the test gas. The gas travels from the cylinder to the vacuum chamber due to a pressure difference between the interior of the cylinder and the interior of the vacuum chamber.

## 4.3 Arrangement and procedure

### 4.3.1 Arrangement of test components

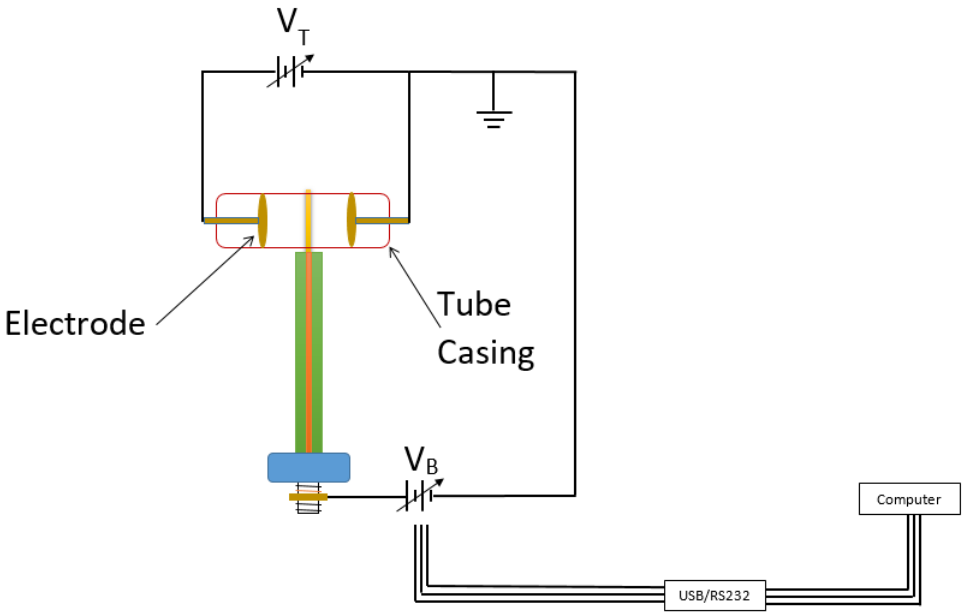


Figure 25: Schematic of the discharge tube experiment.

As illustrated by Figure (25), the tubes are fitted with a set of flat copper electrodes which are placed a small distance apart on either side of the probe tip.

The discharge voltage power source is employed to supply a constant high discharge voltage $V_T$, which tends to produce a dc discharge plasma inside of the discharge tube. To ensure consistency, the probe tip is positioned equidistant from both electrodes.

When the electrodes are placed at some potential difference $V_T$, which may depend on the gas in the tube and the pressure, the gas is set to experience a discharge thereby producing a dc discharge quasi-neutral plasma in the vicinity of the probe tip.

The resulting energetic particles, as is typical, will tend to give up their energy in the form of visible light, by which it is then possible to confirm the occurrence of the plasma discharge.

The entirety of the electrical arrangement as illustrated by Figure (25), less the two power supplies, is positioned inside of the vacuum chamber, which is evacuated to a specified pressure using the vacuum pump. The chamber is evacuated periodically to maintain the pressure as required.

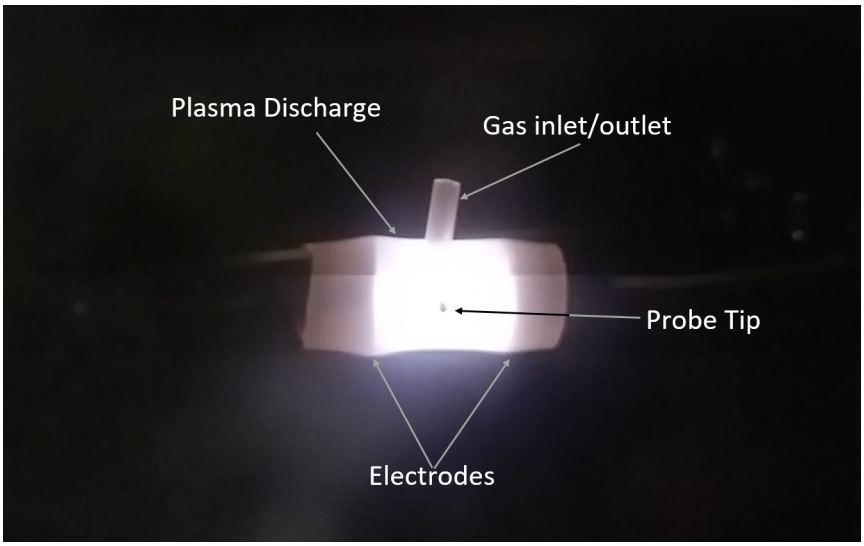


Figure 26: DC discharge of Argon gas in a plastic discharge tube.

Figure (26) shows one such tube during a sustained plasma discharge where the vacuum chamber, and thus the discharge tube, has been filled with Argon gas. As the Figures hows, the tubes have a gas outlet which helps to ensure that there is never a large pressure difference between the inside of the tube and the rest of the vacuum chamber as this would generally have a tendency to reduce the structural integrity of the tube and its fitted electrodes. This also helps to guarantee that the gas being discharged is the same gas by which the vacuum chamber has been filled.

The gas inside of the tube is also *static* precisely due to the lack of pressure and temperature gradients between the interior of the tube and its exterior. When the discharge gas is air, which contains oxygen, a slow process of oxidization can occur at the electrodes and can cause the electrodes to slowly heat up. The rate at which the electrodes gain temperature, even in that case, remains so low as to negligibly affect the motion of the gas.

This sustained discharge of Figure (26) is an example a typical Argon discharge at a pressure of 45 torr and an operating voltage $V_T$ of 5 kV and above.

Since the plasma in the discharge tube is not expected to come into contact with the walls of the vacuum chamber, the chamber is not grounded. However, both the voltage source of $V_T$ and of the probe bias voltage $V_B$ are set to a common ground terminal in order to ensure that both the discharge circuit and the probe circuit are closed. The two two circuits also need a common ground in order to guarantee that measured local plasma potential $V_p$, as demanded by Equation (4), is measured with respect to the same ground by both circuits.

### 4.3.2 Potential sources of measurement noise

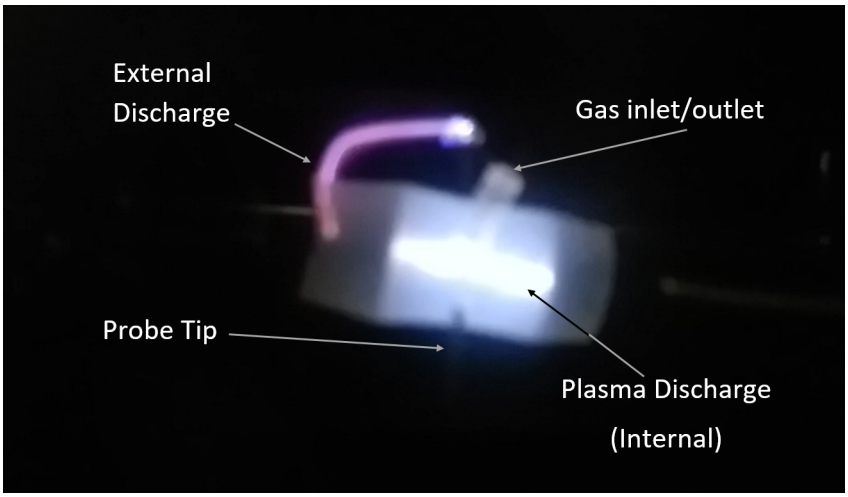


Figure 27: DC discharge of Argon gas in a plastic discharge tube with external discharge.

The probe is typically placed at a high bias voltage relative to ground and this bias may be incremented by small amounts in order to ensure a high quality data set. The bias voltage, although high, will usually be only a small fraction of the operating voltage $V_T$, such that the inside of the discharge tube largely dominated by $V_T$.

Those parts of the probe which are external to the inside of the tube must thus be electrically insulated from the surrounding gas, lest they lead to the occasional phenomenon of external discharge depicted in Figure (27). This is when a discharge between the probe and one of the electrodes of the tube in a region not dominated by $V_T$ occurs. When this kind of discharge occurs, it can frequently induce a significant amount of measurement noise which may result in a large uncertainty on the measured plasma parameters. This is especially the case given that the probe will typically collect current of the order of 10 $\mu$A to 40 $\mu$A.

The external discharge is prevented by ensuring that the diameter of the tube is of similar magnitude to the length of the probe tip and that the remainder of the probe is insulated at all exposed regions. Despite this, however, small amounts of external discharges may still occur randomly throughout the measurement period. As the measurements will show, however, this effect is minimised.

Similar such discharges may occur between the probe and the vacuum chamber, if the probe is not securely insulated.

### 4.3.3 IV-curve acquisition

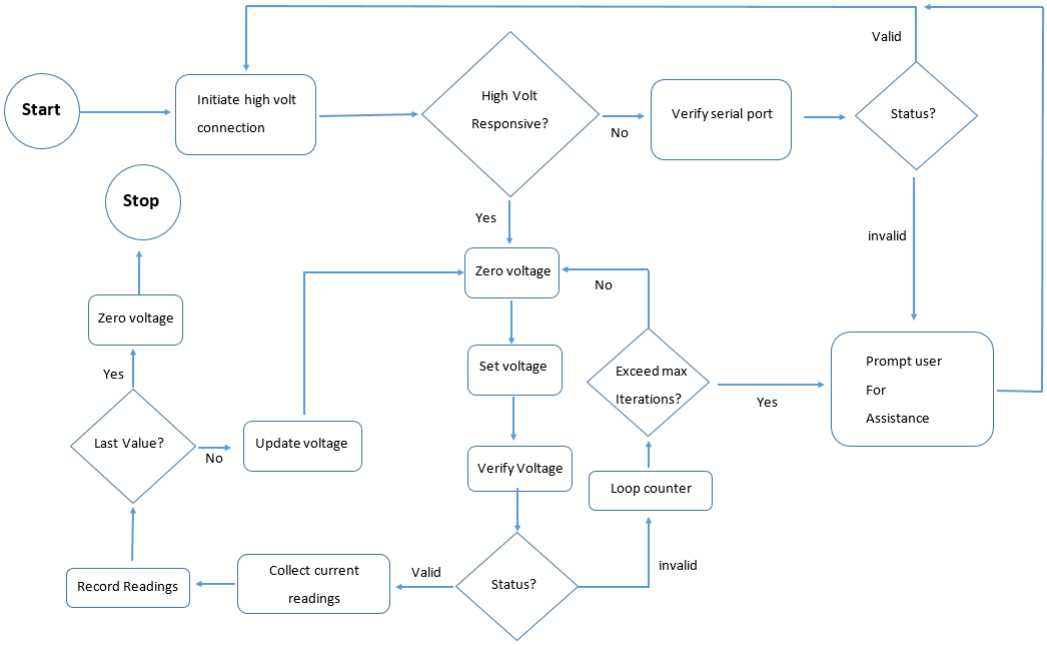


Figure 28: IV Plot acquisition algorithm.

The IV curves are acquired from the experiment using an automated algorithmic acquisition system, the primary purpose of which is to remotely control the external power sources and collect appropriate data from the experiment regarding all variables which potentially affect the results.

The central instrument in this data acquisition process is a variable power source which is equipped with the ability to serially interface with a computing system. The computer can thus send and receive information to and from the serial instrument, which then sets the bias voltage of the probe inside of the closed vacuum chamber as instructed by the computer. As Figure (25) illustrates, the computer interfaces with the voltage source which sets $V_B$ with either a USB or a RS232 interface.

The system follows the acquisition algorithm illustrated by Figure (28), where the main instrument being controlled is the serial power source.

Analogue power sources can also be used provided their signals are first digitised and the voltage is set using an external IC controller such as an ARDUINO.

The digital power source of choice for this system is the THQ Hi-volt power source.

### 4.3.4 Control protocols

In order to acquire the IV plot, the chamber pressure is first set by controlling a vacuum pump. The pump is periodically turned on and off in order to keep the pressure constant. The voltage $V_T$ is then slowly increased until the discharge tube is illuminated, at which point the algorithm illustrated in Figure (28) is initiated.

A valid range of possible values for $V_B$ is imposed on the measurement. This is usually

$$\mid V_B \mid \leq 0.1 \mid V_T \mid .$$

The bias voltage is then slowly increased in small predetermined increments within the defined range. In order to minimise the possible effect of corona ionisations, the voltage is zeroed in-between each voltage setting. These tasks are all hard coded into the computer programme and little or no assistance is required from the user.

The plasma potential is not expected to be of the same order of magnitude as the local operating voltage because, in that rage, the probe will be gin to be have as a separate electrode and may itself cause additional gas discharge inside the tube. The computer searches the range of possible plasma potentials starting on the low end of the voltage settings and ending close to the high end. The computer typically finds the correct range of possible plasma potential before the bias is set too high. The search criteria is enforced by continually applying the Langmuir model to the data obtained until the lowest error is found by the least square method.

One hundred or more readings may be necessary before a distinctive langmuir IV curve is observed. Since the system is meant to complete the task unmanned, a minimum of 150 readings are usually taken so that an unmanned analytical protocol can also be possible. However, the system allows for a smaller range to be predetermined.

## 4.4 Test Results

### 4.4.1 IV plots

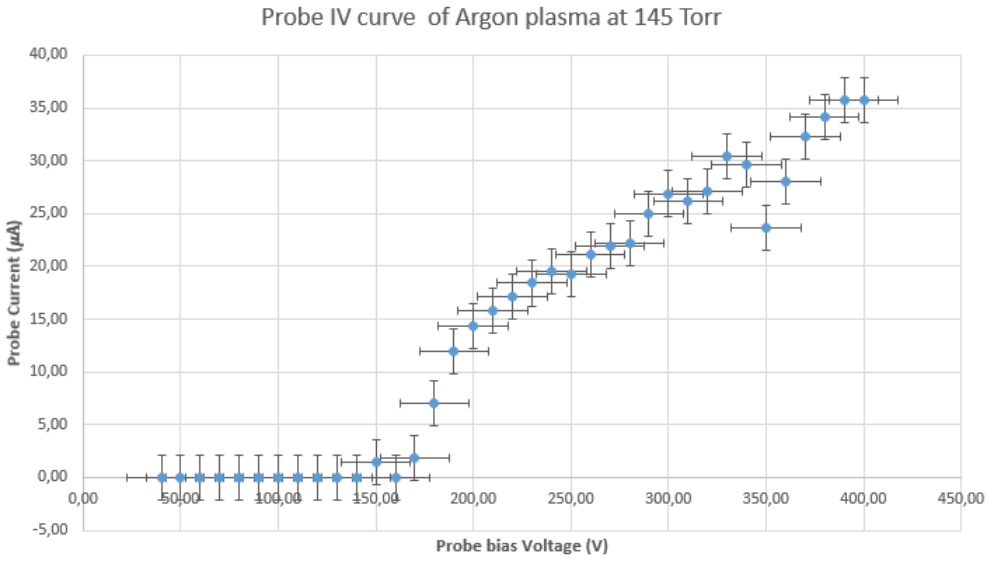


Figure 29: Current Voltage curve conducted on an enclosed discharge containing Argon gas at 145 Torr.

Shown in Figure (29) is a current-Voltage plot conducted with a 1.5 cm long discharge tube at a pressure of 145 ± 5 Torr when the chamber was filled with Argon gas.

Comparing Figure (29) with Figure (5) confirms that the interior of the discharge tube contains a dc discharge two species quasi-neutral plasma. According to
Equation(4), the lack of symmetry about the point of inflection on the curve in Figure (29) is evidence that the electron and ion saturation currents, as calculable by Equations(10) and (11), do not have equal magnitudes,

$$\mid I_{es} \mid \neq \mid -I_{is} \mid .$$

In fact, the electron saturation current is many orders of magnitude greater than the ion saturation current. The local particle densities $n_e$ and $n_i$ should be approximately equal, of course, given that the plasma is quasi-neutral. The ratio, therefore, of the two saturation currents should be approximately equal to the ratio of the respective average particle speeds, provided the two particle temperatures are of the same order of magnitude.

$$\left(\frac{I_{es}}{I_{is}}\right)^2 \approx \left(\frac{v_e}{v_i}\right)^2 . \tag{13}$$

The first experimental objective is thus met.

### 4.4.2 Analysis protocol

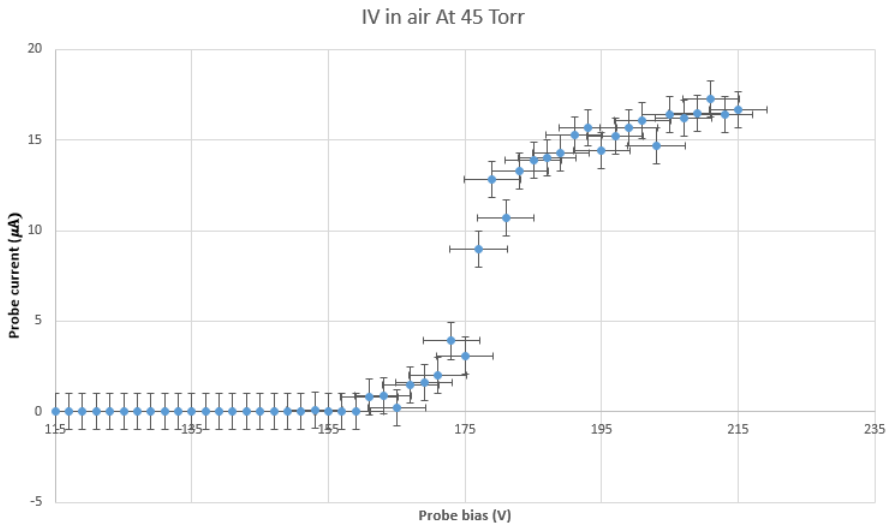


Figure 30: IV curve conducted in Air at 45 Torr.

The behaviour seen in Figure (29) regarding the local saturation currents is relatively typical of IV plots found using the same 1.5 mm long discharge tube. Figure (30), for instance, shows a current voltage curve conducted in air at a pressure of 45 torr. The process of extracting the plasma parameters of such a plot with an unmanned computerised system requires a piecewise curve fitting protocol which can fit the model demanded by Equation (4) to the data set seen in Figure (30).

The system accomplishes this task by iteratively running through all of the voltage values in the range of $V_B$, setting each one equal to $V_P$ and performing two numerical exponential model fittings, one to the left of $V_P$ and one to the right as demanded by Equation (4). Each voltage in the domain of $V_B$ is then assigned a coefficient of determination $R^2$ which speaks to the quality of the fit mirrored at that value. The voltage associated with the highest coefficient of determination is then reported as the local plasma potential and the exponential fit parameters associated with that voltage are reported as the local plasma properties.

A sample Mathematica code, which is used by the Labview system, is provided in Appendix C.

The quality of the fit is limited by the amount of measurement noise present in the data set. When the data set has a high level of noise, the maximum possible value of $R^2$ may be a relatively low number and, in some cases, it may

lead to a failure of the unmanned method. For a data set which has low noise level, such as is the case in Figures (29) and (30), a relatively high $R^2$ can be expected along with a relatively low uncertainty of measurement.

### 4.4.3 Data fitting and extraction of parameters

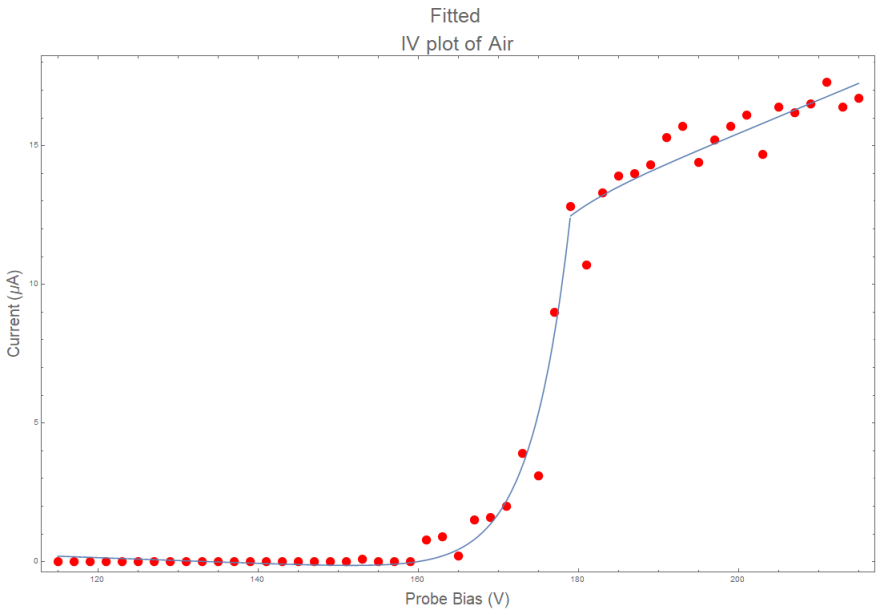


Figure 31: A Labview/Mathematica Langmuir Curve fitting of a IV curve conducted in Air at 45 torr with a fit quality of $R^2 = 0,995315$.

Table 1: Best fit parameters of air at 45 Torr

| Fit Parameter | Notation | Magnitude | Uncertainty | Confidence Level (%) |
|---|---|---|---|---|
| Ion Sat Current ( $\mu$A ) | $Iis$ | -0,5 | 0,9 | 95,45 |
| Elec Sat Current ( $\mu$A ) | $Ies$ | 12,9 | 1,5 | 95,45 |
| Electron Temp (eV/e) | $kT_e/q$ | 5,2 | 1,9 | 95,45 |
| Ion Temp (eV/e) | $kT_i/q$ | 4,2 | 0,6 | 95,45 |
| Plasma Potential(V) | $V_p$ | 179,0 | 1,3 | 95,45 |
| Ion Co. Exp ($\mu$A/V) | $C_{pi}$ | -0,01 | 0,0 | 95,45 |
| El Co. Exp ( $\mu$A/V) | $C_{pe}$ | 0,1 | 0,0 | 95,45 |

The development environment of choice for the analysis system is Labview, and has been used to apply the Langmuir method to the data shown in Figure (30). The resulting curve of best fit is shown in Figure (31) and has a coefficient of determination of $R^2 = 0,995315$.

A comparison between the experimentally obtained IV plot of Figure (31) and the characteristic IV plot of a asymmetric plasma shown in Figure (12), demonstrates the consistency of the probe in use with the expected type of data outputs.

A demonstrative test was also conducted for the Argon data in Figure (29), as shown in Figure (32).

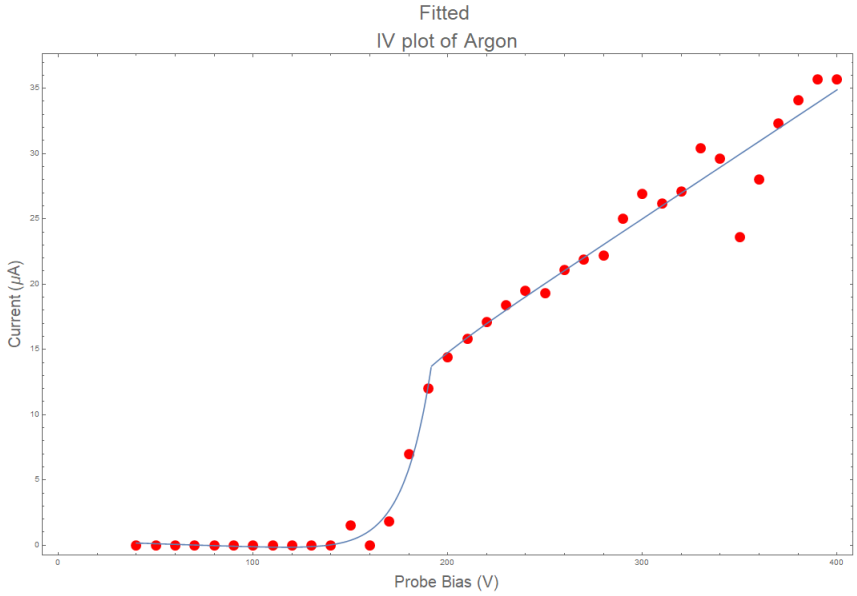


Figure 32: A Labview/Mathematica Langmuir Curve fitting of a IV curve conducted in Argon with a fit quality of $R^2 = 0,993726$.

Table 2: Best fit parameters of Argon at 145 Torr

| Fit Parameter | Notation | Magnitude | Uncertainty | Error | Conf. Lvl(%) |
|---|---|---|---|---|---|
| Ion Sat Current ($\mu$A) | $Iis$ | 0 | 3 | 0,0 | 95,45 |
| Elec Sat Current($\mu$A) | $Ies$ | 14 | 4 | 1,7 | 95,45 |
| Electron Temp (eV/e) | $kT_e/q$ | 16 | 4 | 4,1 | 95,45 |
| Ion Temp (eV/e) | $kT_i/q$ | 16 | 1,0 | 2,0 | 95,45 |
| Plasma Potential (V) | $V_p$ | 192 | 6,3 | 3,0 | 95,45 |
| Ion Co. Exp($\mu$A/V) | $C_{pi}$ | -0,01 | 0,0 | 0,0 | 95,45 |
| El Co. Exp ($\mu$A/V) | $C_{pe}$ | 0,10 | 0,0 | 0,0 | 95,45 |

Appendix A and Appendix B respectively provide the raw experimental data which was used to generate the IV plots in Figures (30) and (29).

Experimental plots of the types in Figures (30) and (29) demonstrate that,

1. The Langmuir probes are suitable for acquiring characteristic Langmuir probe data both in an Argon discharge plasma and in an air discharge plasma.

2. The Langmuir probes are suitable for conducting IV measurements in a dc discharge low temperature discharge plasma.

3. The computer system can reliably build current-Voltage plots.

The numerical data fitting plots of Figures (31) and (32) and the accompanying tables of plasma parameters demonstrate that,

1. The Computer system is capable of analysing a Langmuir IV plot and appropriately extractng plasma parameters.

2. Such data extraction is possible both in an Argon discharge plasma and in an air discharge plasma.

Collectively, these demonstrations meet the second, third and fourth experimental objectives.

#### 4.4.4 Extracted plasma parameters

As one will have expected, the ion saturation current $I_{is}$ in both air,

$$(I_{is})_{Air} = -0,46 \pm 0,883824\mu A, \tag{14}$$

and in Argon,

$$(I_{is})_{Argon} = -0.05 \pm 3,36405\mu A, \tag{15}$$

is much more difficult to measure than its electron counterpart. In fact, effectively, the true measurement of the ion saturation current is the region of confidence represented by the uncertainty statement. The measured magnitudes themselves are not meaningful. Only the uncertainties are at all helpful. It may therefore be more meaningful to say

$$-1,34324\mu A \leq (I_{is})_{Air} \leq 0,42324\mu A \tag{16}$$

$$-3,41405\mu A \leq (I_{is})_{Argon} \leq 3,31405\mu A, \tag{17}$$

This is a direct limitation of the precision with which the THQ Hivolt.de instrument can measure the probe current. A more precise instrument, more capable of measuring even lower current magnitudes would surely fare better.

The size of the collecting surface of the probe is another factor, which limits the accuracy with which the Ion saturation current can be measured. This is a direct consequence of the conflict between the two design interests, one being to maximise the precision of the measurement instrument and the other being to maximum its resolution.

The electron saturation currents, by contrast, display a smaller relative uncertainty.

$$(I_{es})_{Argon} = 14.29 \pm 3,62\mu A. \tag{18}$$

$$(I_{es})_{Air} = 12,93 \pm 3,37\mu A. \tag{19}$$

Although the absolute uncertainty of the measurement(s) is no better, the relative measurement uncertainty is much better. The reported magnitudes are also entirely plausible, because the electron saturation current occurs, when the $I_{is}$ is much lower, at $V_b \approx V_p$. That is, at or near the discontinuity point. This is a value which is thus much simpler to verify as the discontinuity point in a typical IV plot is fairy simple to estimate.

One reaches a similar conclusion regarding the measured temperatures. The claim the measurement makes is that, for an electron gas, the local temperature in air is $kT_e = 5,20 \pm 1,95eV$, where the charge per particle is the elementary charge. This is also an entirely plausible value for the local electron temperature as is simple to compare with other types of plasmas. In [1] and [2], for example, magnetically induced plasmas were observed having $kT_e$ values between 1,5 eV and 5 eV. Even in discharge plasmas used in [48] and [47], for instance, $kT_e$ values between 1 eV and 6 eV were observed.

The same measurement in Argon produces the equally plausible $kT_e = 16,00 \pm 3,93eV$, where a similar relative uncertainty is observed. It is not immediately obvious why an Argon plasma would experience such a noticeably higher temperature.

The results seem to show that the local plasma potentials are computed reasonably, as this is perhaps the more easily computable parameter thanks to the ease with which one can locate the point of discontinuity in a typical Langmuir IV plot.

# 5 Discharge tube tests with porous electrodes

The structural and electrical functionality of the probe as so far shown in a static and enclosed plasma demonstrates the systems ability to conduct and apply the Langmuir method. The problem of the DC discharge thrusters will, however, involve Langmuir probe measurements in a generally *dynamic* plasma plume. A demonstrative experiment has been conducted which aims to show the system's ability to conduct and apply the Langmuir method to a flowing gas both in a constrained discharge tube and in the remainder of the vacuum chamber.

## 5.1 Experimental objectives

The experiment intends to satisfy the following aims of the study.

1. **Establishing the probe's capacity to measure reliable IV data in a moving plasma.**

   This will be accomplished demonstratively by having the system build IV plots in volumetric regions where high pressure gradients in space, which cause the exhaust gas to flow, exist.

2. **Verifying the suitability of the designed Langmuir probe(s) for acquiring IV data in a globally non-uniform, but locally uniform plasma.**

   This will be accomplished demonstratively by having the system build IV plots in *open plasmas* which are not confined to a small volume compared to the probe tip and which are not confined between the discharge electrodes.

## 5.2 Experimental apparatus

In order to accomplish its various objectives, the experimental test of the probe makes use of many of the same laboratory apparatus as in the case of the *Enclosed Plasma Experiment*, with a different discharge tube.

### 5.2.1 Discharge Tubes

The plasma discharge tubes are made for inducing a dc discharge plasma amidst a relatively small volume inside of an evacuated chamber. The tube, shown by Figure (33), is a 2 cm diameter by 2 cm length plastic tube which has two circular *steel net* extremities which act as discharge electrodes. The steel electrodes are porous and see-through and are used to produce two circular regions of different potentials roughly 1 cm - 1.5 cm apart. The resulting potential difference between the two electrodes thus serves as a source of plasma discharge within the cylindrical volume of the tube.

A *gas-inlet* in the form of a plastic pipe is fitted to the discharge tube in order to ensure that the propellant gas only enters the vacuum chamber through the

discharge tube, thereby guaranteeing a pressure gradient between the gas inside of the discharge tube and the remainder of the vacuum chamber. The netted steel electrodes experience minimal drag from the moving gas which enters the chamber via the discharge tube.

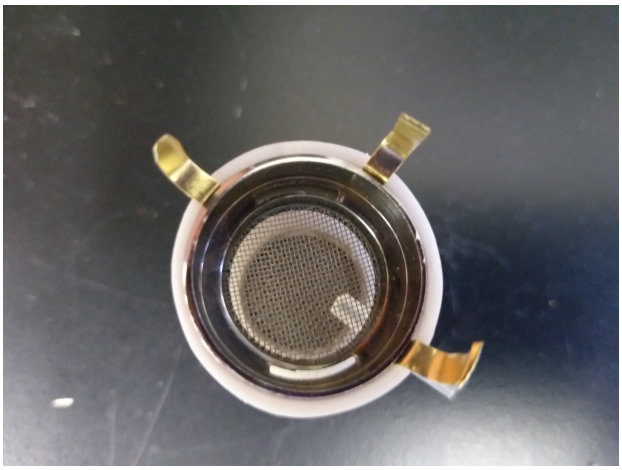

Figure 33: Discharge tube with porous electrodes.

The discharge tube of Figure (33) is chosen for its ability to locally mimic the internal and external plasmas of DC discharge thruster plumes, as the thrusters are where the probes will eventually be applied.

The netted electrodes of the discharge tubes allow that, although the gas which enters the tubes is free to exit the tube with minimal interaction with the electrodes, the discharge nevertheless remains possible and sustainable in the interior of the discharge tube.

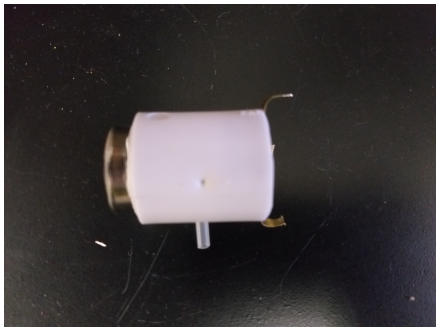

Figure 34: Discharge tube with porous electrodes (side view).

### 5.2.2 Langmuir probe

The Langmuir probes are again used to collect IV data both inside and outside of the discharge tube.

## 5.3 Experimental procedure for internal measurements

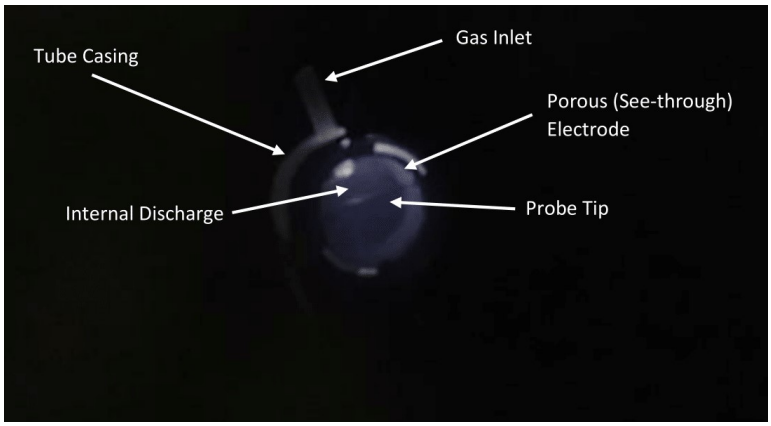


Figure 35: Plasma discharge of a flowing Argon gas through a porous iron electrode.

The u-shaped DC discharge thrusters can produce a plasma plume by allowing the propellant gas to pass through both the electrodes of the thruster. A simple way to achieve this in a discharge tube is to employ a set of *porous electrodes* which have the advantageous property of producing an evenly distributed potential difference across the cross-section of the discharge tube whilst also allowing any gas, and thus any charged particles, which is present inside the tube to escape with little resistance, if any, from the electrode itself.

In Figure (35), a side view of the discharge tube, which demonstrates an even gas discharge produced by a set of two porous and see-through electrodes, is shown. A pressured gas enters the tube through the *gas inlet* whereupon it is exposed to a high potential difference inside of the tube. The gas then subsequently exits the discharge tube due to a pressure difference between the inside of the tube and the rest of the vacuum chamber. The discharge thus occurs in a *flowing gas* which remains in motion so long as the pressure difference is sustained.

The propellant gas is only allowed to enter the vacuum chamber through the discharge tube, thereby ensuring that a sustainable pressure difference can be maintained between the gas inside the tube and the remainder of the chamber. A small fraction of the escaping gas leaves the tube in its plasma form to interact with elements of the remainder of the vacuum chamber where it subsequently encounters a grounded internal surface of the chamber. Thus, a rudimentary plume develops past each of the two electrodes.

A schematic of the experimental arrangement for the probe measurements is demonstrated by Figure (36). The probe measurements can be conducted *internally*, as demonstrated by Figure (36) or *externally* as later demonstrated by Figure (37).

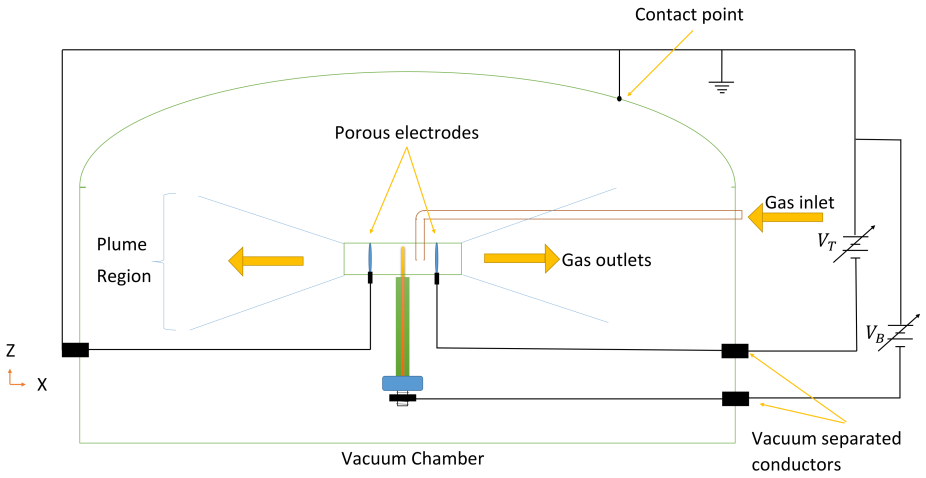


Figure 36: Schematic of the experimental setup designed for probe measurements with porous electrodes in Argon.

The expectation is thus that the characteristic IV plot of a two species plasma as demanded by Figure (5) will be obtained both in the interior and the exterior neighbourhood of the plasma discharge, thereby demonstratively confirming the functionality of the Langmuir probes of Figure (18) in diagnosing the plume types typified by the U-shaped DC discharge micro-thrusters of Figure (4).

The pressure in the vacuum chamber is thus not constant, given that the gas continuously enters the chamber. The pressure in the chamber at the beginning and at the end of the measurements are here used as an indication of the *range* of pressures at which the measurements where conducted.

The discharge voltage $V_T$ for all IV plots was kept between 5 kV and 10 kV depending on the point where the discharge is first observed. It was observed that too high discharge voltages were prone to cause the discharging power source to have electrical failures.

## 5.4 Experimental procedure for external measurements

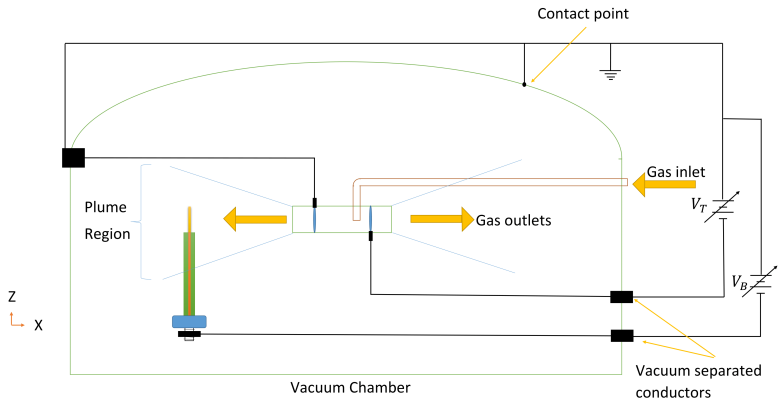


Figure 37: Schematic of the experimental setup designed for external probe measurements in Argon.

The Langmuir probe can subsequently be placed in the external plume region as demonstrated schematically by Figure (37), whereupon the experiment can be repeated.

Langmuir probe measurements in the external region are often susceptible to significant levels of measurement noise, owing the difficulty in maintaining stable plasma conditions outside of the discharge tube. Extreme and proper care normally must be taken to ensure there is no direct electrical interaction, however minute, between the high voltages responsible for the plasma discharge and the grounded vacuum chamber, as this can often lead to a variety of noisy interactions in the chamber which ultimately contaminate the data.

## 5.5 Experimental results

### 5.5.1 IV plot for internal measurements

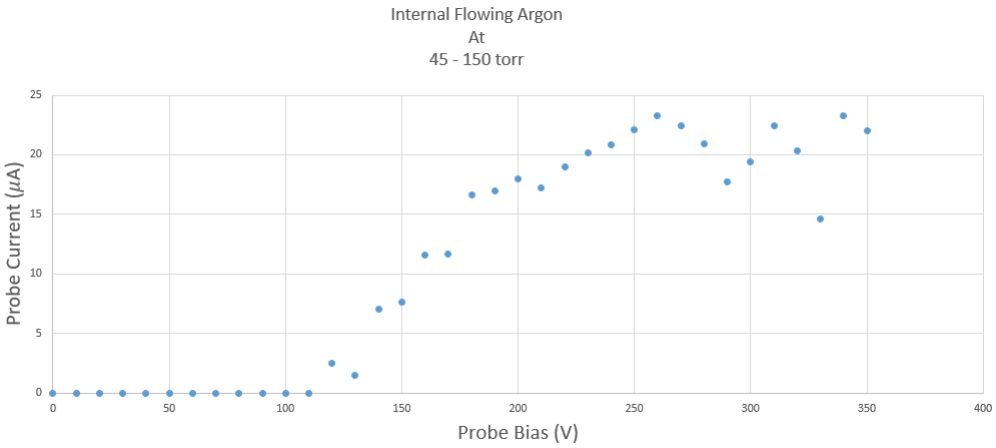


Figure 38: IV plot of flowing Argon.

Figure (38) shows an IV plot conducted in the interior of the discharge tube following the arrangement if Figure(36). The plasma parameters of the IV plot thus be found by applying the Langmuir model as per Figure (39).

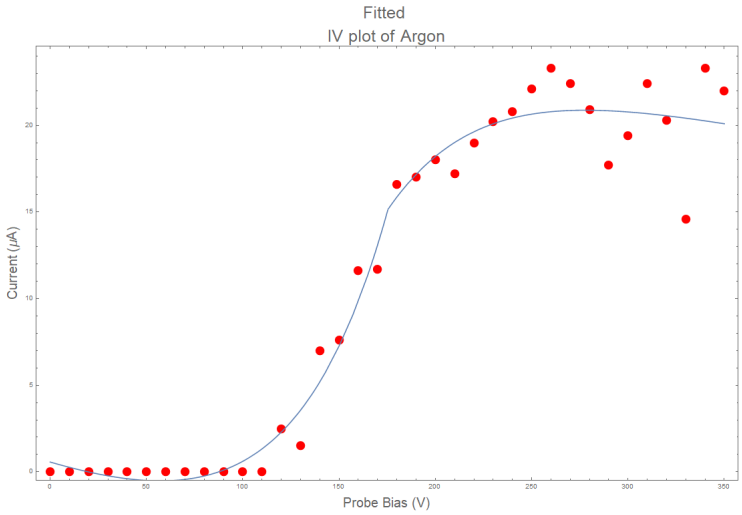


Figure 39: Curve fitting of IV plot of flowing Argon with a fit quality of $R^2 = 0,984799$.

The Langmuir best fit parameters of this measurement are given by the following table.

Table 3: Best fit parameters of flowing Argon between 45 Torr and 150 Torr

| Fit Parameter | Notation | Magnitude | Uncertainty | Conf. Lvl (%) |
|---|---|---|---|---|
| Ion Sat Current( $\mu$A ) | $Iis$ | 0,0 | 1,5 | 95,45 |
| Elec Sat Current( $\mu$A ) | $Ies$ | 24,0 | 18,7 | 95,45 |
| Electron Temp (eV/e) | $kT_e/q$ | 50,7 | 39,6 | 95,45 |
| Ion Temp(eV/e) | $kT_i/q$ | 38,2 | 20,7 | 95,45 |
| Plasma Potential (V) | $V_p$ | 175,4 | 24,8 | 95,45 |
| Ion Co. Exp ($\mu$A/V) | $C_{pi}$ | 0,0 | 0,1 | 95,45 |
| El Co. Exp ($\mu$A/V) | $C_{pe}$ | 0,0 | 0,1 | 95,45 |

Evident in this data extraction is both the extent to which the flow of the Argon gas inside of the discharge tube can lead to higher levels of measurement uncertainty. Although some parameters may appear to be high, they carry very high uncertainties as compared with the measurements done in the enclosed discharge tubes.

It may be worth noting that, although the ion saturation current is usually reported as a negative current, the model in Equation (3) already takes the expected polarity into account and a negative sign is already included in the equation. Thus, the computation usually returns positive values even for the ion saturation currents.

The characteristic IV plot remains observable, as is evident in Figure (38), while the contribution of the measurement noise can more easily be observed in Figure (39).

The IV plot nevertheless shows that *the probe is capable of producing characteristic IV data of a two species plasma in a moving plasma.* Thus, the first experimental objective has been met.

The accuracy of the extracted plasma parameters will depend, as is always the case, on the quality of the IV data obtained.

In some cases, when the measurement data is very poor, it may be necessary that a more manual and manned extraction approach be employed.

### 5.5.2 IV plot for external measurements

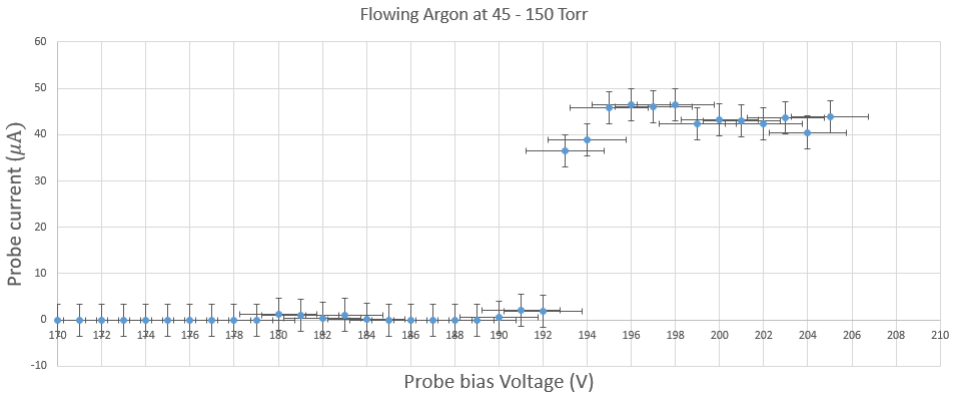


Figure 40: External IV plot of flowing Argon plasma.

Provided that sources of noise are appropriately minimised, a stable external IV plot can be obtained, such as in the case of Figure (40). Appropriately identifying a familiar Langmuir plot in these external plots generally requires changing the bias voltage is smaller steps compared with the internal measurements.

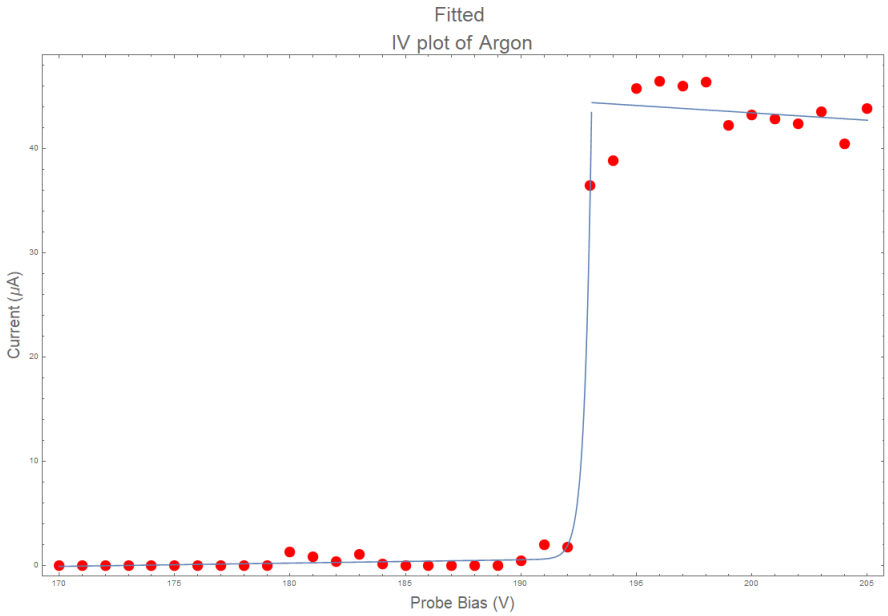


Figure 41: Curve fitting of IV plot of flowing Argon with a fit quality of $R^2 = 0,996678$.

The Langmuir best fit parameters of this measurement are given by the following table.

Table 4: Best fit parameters of flowing Argon between 45 Torr and 150 Torr

| Fit Parameter | Notation | Magnitude | Uncertainty | Conf. Lvl (%) |
|---|---|---|---|---|
| Ion Sat Current($\mu$A) | $Iis$ | 0,0 | 1,5 | 95,45 |
| Elec Sat Current ($\mu$A) | $Ies$ | 44,5 | 1,9 | 95,45 |
| Electron Temp(eV/e) | $kT_e/q$ | 0,3 | 0,7 | 95,45 |
| Ion Temp(eV/e) | $kT_i/q$ | 0,0 | 0,0 | 95,45 |
| Plasma Potential (V) | $V_p$ | 193,1 | 0,1 | 95,45 |
| Ion Co. Exp ($\mu$A/V) | $C_{pi}$ | 0,0 | 0,1 | 95,45 |
| El Co. Exp ($\mu$A/V) | $C_{pe}$ | -0,1 | 0,3 | 95,45 |

The IV plot in the exterior of the tube shows that *The probe is capable of producing IV data of a two species plasma in a moving non-uniform plasma.* Thereby meeting the second experimental objective.

External Measurements are generally susceptible to a variety of challenges, including comparatively high uncertainties.

Namely

1. The plasmas in the exterior of the tubes are generally ionised to a lesser

extent than those in the interior. This can often mean that the instrument being used to measure the current must be capable of reading much lower values of current. As low, in some cases,as 1 $pA$. Instruments which can perform this measurement, such as the PTW Unidos electrometer shown in Figure (8), are very expensive and beyond the scope of this project.

2. The Maxiwellian assumptions which inform the Langmuir probe model may not be valid everywhere in the exterior of the tubes. This can often produce IV curves which are distorted and hard to fit algorithmically to the Langmuir Model. A more Manual and Manned technique may be necessary when face with such plasma IV plots. An example of this behaviour can be seen in Figure (42), where some non-linear sheath expansion behaviour can be seen.

3. Due to often unforeseen external discharge behaviour between the probe, chamber and one or both of the electrodes of the tube, the IV signal can be very susceptible to high levels of measurement noise, shown by Figure (43).

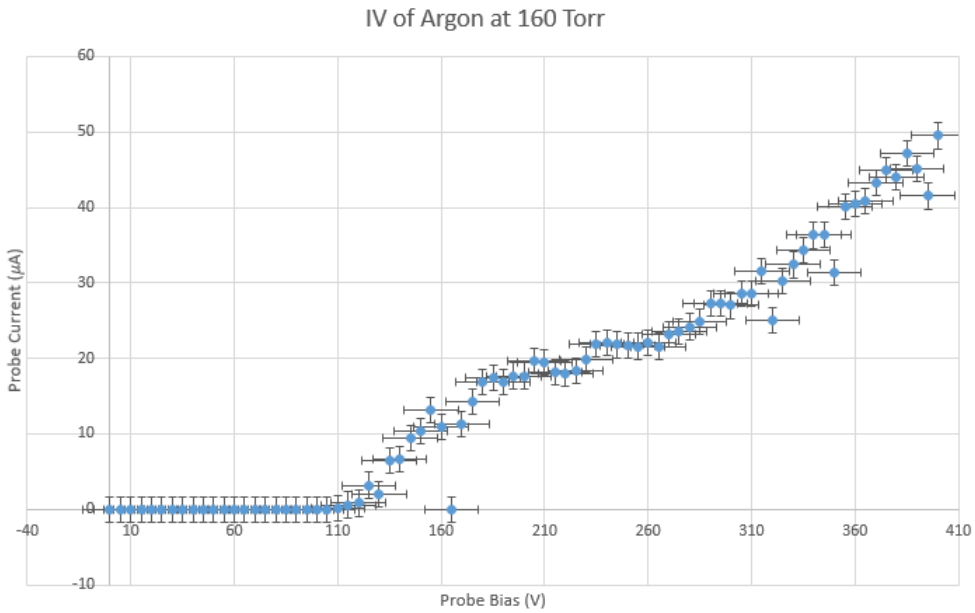


Figure 42: Non-linear Sheath expansion.

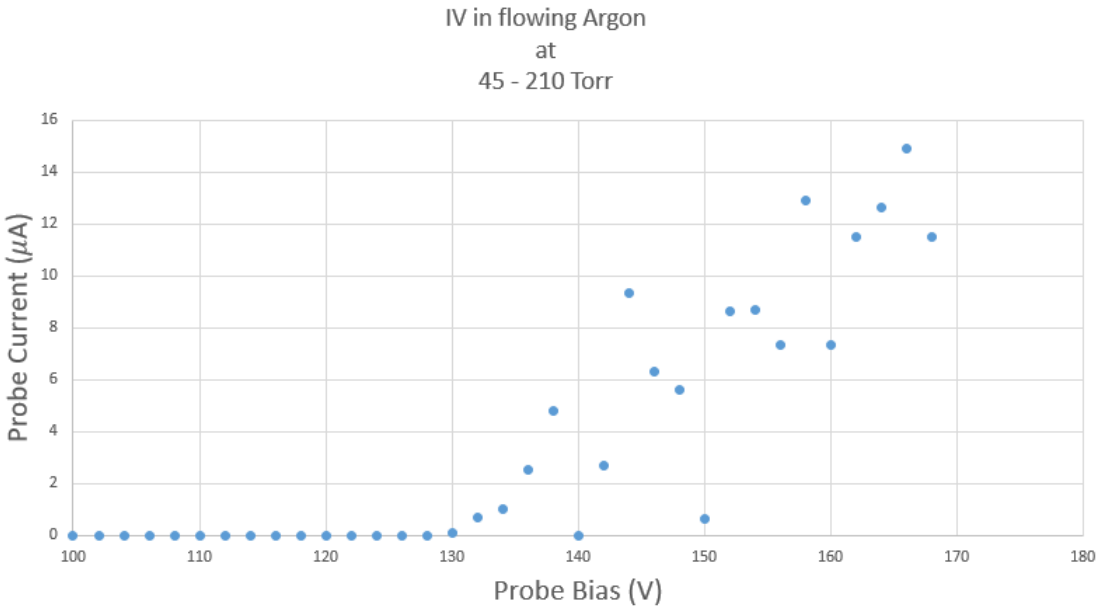


Figure 43: High Mearement noise in a IV plot.

# 6 Probe test in free air

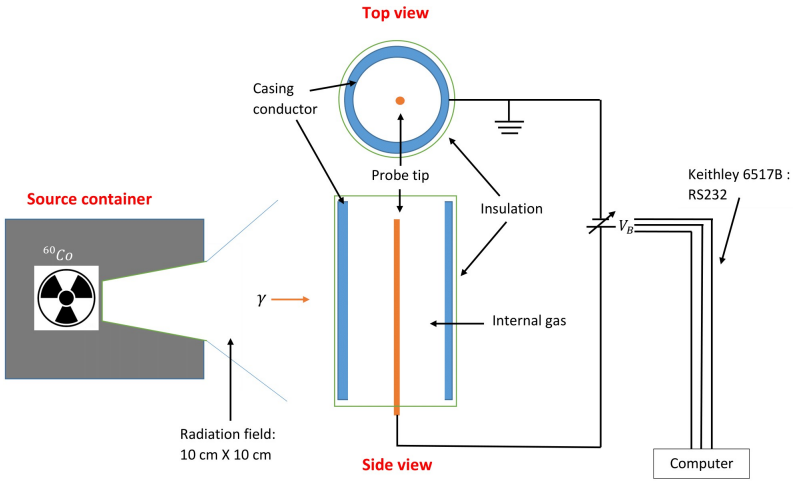


Figure 44: Schematic of a free air experiment with probe exposed to a field of Gamma radiation using a Cobalt-60 source.

Although the study of plasmas produced by means of a radiation field is beyond the scope of the present work, it is possible to conduct a qualitative comparison of probe measurements conducted with the Langmuir probes designed for measurements on the plasma plumes of the microthrusters, as compared to those measurements obtained using standard air kerma ionisation chambers, which are instruments more specialised to taking measurements in free air on plasmas produced by means ionising radiation.

In figure (44), for instance, a schematic is shown of an experiment conducted using an ionisation chamber typically used for standardising the units of radiation dose (i.e. the Gray (Gy) and the Sievert (Sv) ) in South Africa. The chamber was then *substituted* with the Langmuir probe, which was then also used to conduct the same measurements. A qualitative comparison of the two measurements is thus performed and is hereby used as a demonstration of the probe's ability to conduct plasma measurements in free air amidst a plasma produced by exposure to ionising radiation.

The test was conducted at the National Metrology Institute of South Africa (NMISA) using Cobalt-60 as the source of ionising gamma radiation, at the center of a 10cm X 10cm field and with a *source to center distance* (SCD) of 100 cm. As the typical magnitude of currents measurable under these conditions are much lower than those typical of the interior of the discharge tubes, a much more accurate instrument which is capable of measuring current magnitudes as low as 1 pA was required. For this reason, a Keithley 6517B electrometer was used to set the probe bias and the bias on the ionisation chamber and to also read the resulting current value.

A computer programme was then used to automate the data acquisition process as well as to produce the resulting IV plots.

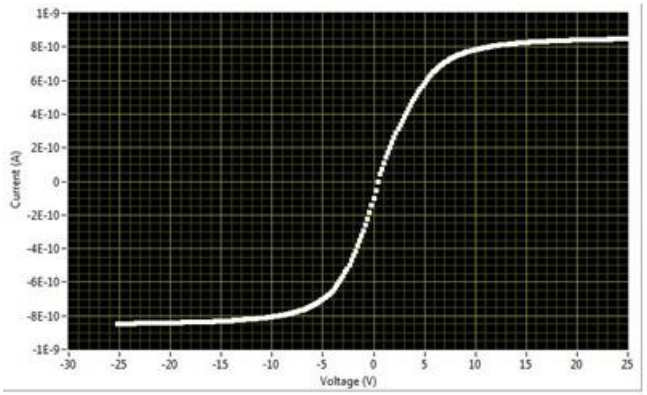


Figure 45: IV plot obtained with the National Measurement Standard (NMS) ionisation chamber in free air

When positioned at the centre of the beam profile, the national measurement standard (NMS) ionization chamber produced the current-voltage plot pattern observed in figure (45), where some plot similarities with the Langmuir IV plots can be observed.

The expectation is therefore that the Langmuir probes, when placed at the same position as the NMS will lead to a similar IV plot, thereby demonstrating that the probes are capable of producing langmuir IV plots in free air in a radiation-induced plasma. The probe positioned for measurements in free air in abreast the source container shown in figure (2) is depicted in figure (46).

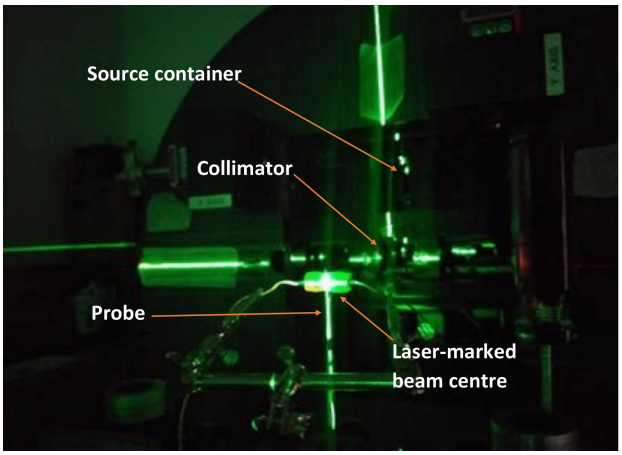


Figure 46: Langmuir probe positioned for IV plot measurements in free air

## 6.1 Probe plot

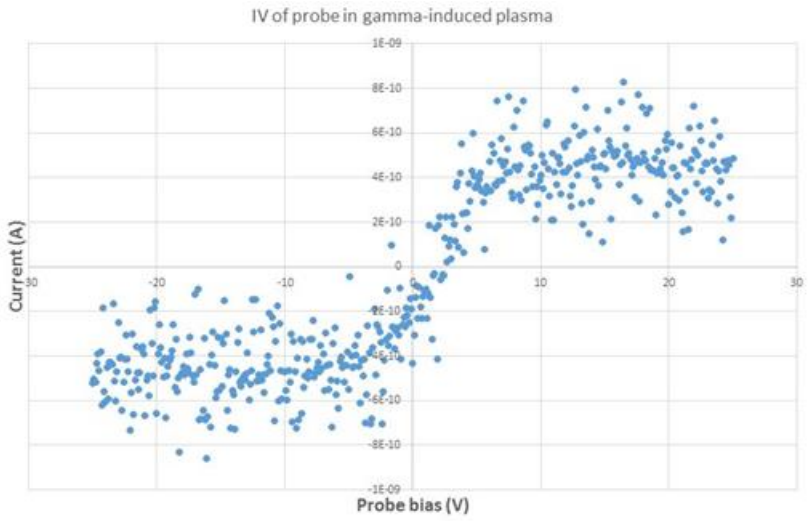


Figure 47: IV plot obtained in free air using a Langmuir probe in a 10 cm X 10 cm $^{60}$Co radiation field.

Figure (47) shows the IV plot which was obtained using the Langmuir probe in free air having been substituted for the NMS from which the plot in figure (45) was obtained. The two plots are qualitatively similar, the main difference being the level and extent of measurement noise experienced by each instrument.

In figure (47), the Langmuir probe can be seen to be much more susceptible to to background level noise. The probes are not designed to reliably collect current in the range 1 pA to 100 nA, as the expected range of the typical currents to be found in the thrusters is greater than 1 $\mu$A.

Compared to the NMS, the probes are also not as well insulated from the immediate environment and, at such low currents, the measurements may be extremely sensitive to small changes in environmental conditions, such as changes in temperature, pressure and humidity.

# 7 Control system

The problem of conducting Langmuir probe surveys of the plume of a DC discharge thruster in the interior of the vacuum chamber requires the design and construction of a complete and unmanned control system for which the primary objective is to keep accurate track of the position of the probe in the plume relative to the thruster.

The system must complete the task by accurately controlling the actuators of the positioning bench in order to send the probe to a desired location in the plume, remotely controlling and setting the bias voltage of the probe, acquiring and reporting probe data from each probe position and applying the Langmuir probe method to each data set.

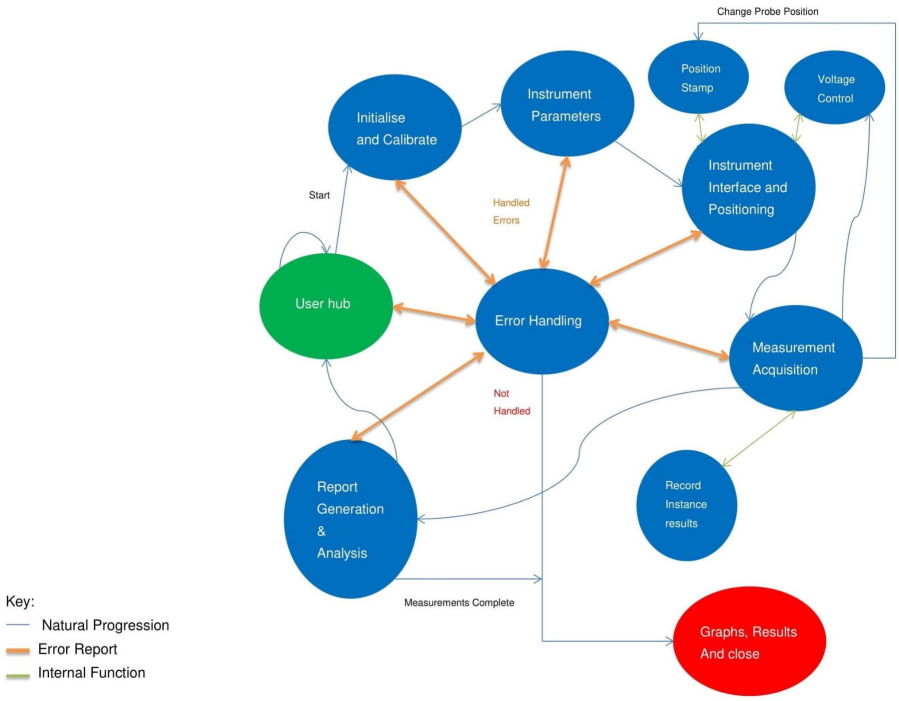


Figure 48: State progression of the data acquisition system.

Each of these sub-tasks is necessarily a unique computational problem which can be addressed separately from the rest. A *State machine*, such as that diagrammatically represented by Figure (48), divides the computer protocols into a series of programmed tasks called *states* which can be called and executed by the computer as and when needed. The data acquisition protocols are initiated, for instance, by the "*Initialise and Calibrate*" state, which also has the responsibility of ensuring that the positioning bench is properly zeroed, and thus calibrating the bench for what probe positioning will occur in a later state,

*Instrument interface and Positioning.*

## 7.1 Survey acquisition protocol

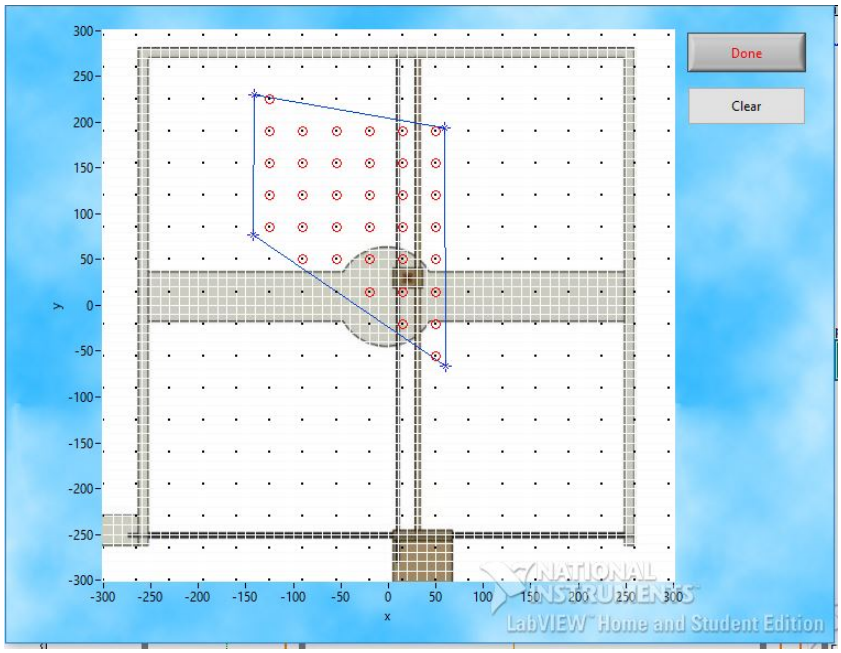


Figure 49: Selection of region wherein to conduct Survey (GUI).

The basic objective of the system is to move the probe to a provided set of positions, or coordinates, in the two dimensional region which spans the plume of the thruster. At each coordinate location, the computer system locally builds an IV plot by means of the algorithm of Figure (28). The result is thus a series of IV plots at each of the coordinates.

The Langmuir probe method is thus applied to each such IV plot, thereby producing a series of plasma properties associated with each such position. In this way, the system conducts a *survey* of the plasma plume.

Figure (49) shows a user control panel from which a select set of coordinates are specified by a user. Effectively, the set of coordinates constitute a *region* inside of the vacuum chamber in which a survey is set to take place.

The control system can thus serve as a tool for future studies of exhaust plumes of DC discharge thrusters.

Unfortunately, due to a relocation of the space propulsion research laboratory, which limited the amount of time available for the survey tests, a full survey on a real micro-thruster was not conducted. The tool can,and will, still be tested when a functional micro-thruster/engine is available for testing.

# 8 Conclusions

The basic objectives of the present work centred on designing a diagnostic tool for understanding the structure of the types of plasmas typical the plume(s) of DC discharge micro-thrusters. Central to this effort was the use of the method of Langmuir probes, which seeks to perform this type of diagnosis by developing and analysing current-Voltage plots which are appropriately modelled after the statistical mechanics of Maxwellian gases.

A Langmuir probe was thus designed and appropriated to the specific conditions which are expected to be faced under the laboratory setting wherein a series of U-shaped DC discharge thrusters will be designed, constructed, and tested.

An important feature of these probes is their ability to apply the method of Langmuir to a variety of positions inside of what is expected to be a spatially non-uniform plasma plume of the micro-thrusters, thereby also presenting as a tool by which models and simulations of these plumes can be tested.

The task of designing and constructing the complete mechanism that informs the probe is fundamentally an engineering design problem. While the task of testing and validating the functionality of the probe and its various components is treated herein as an experimental problem.

The experimental tests further sort to validate the Maxwellian approach to the Langmuir method by seeking to demonstrate that the same results which are typical of Langmuir probes in other more well established Maxwellian plasmas are also observed in the case of discharge plasmas of the sort observed in DC discharge micro-thrusters. These similarities were seen in such results as seen in Figure (28).

To this end, a set of controlled plasmas which are reminiscent of the plasma plumes of DC discharge thrusters were used as test cases representing the plumes. The Plasmas are produced in contained discharge tubes, for which the basic environmental conditions of pressure and temperature can be more carefully controlled than would be the case in more chaotic plumes, where temperature can very more wildly and pressure distributions are less well understood.

The results implicitly show, however, that the discharge plasmas can and sometimes would deviate considerably from the Maxwellian Models, as evident in IV plots which are poorly met or explained by the Langmuir model.

Much more generally, however, the Maxwellian gas assumption is valid, especially when the plasmas in question are globally uniform, as is evident in the consistency of IV plots which were obtained inside of enclosed discharge tubes and where the discharge gas(es) was known to be static, with the model.

Moving or Flowing plasma have proven to result in less certain measurements using these probes. While less certain, the system's ability to produce these IV plots is a positive result.

The Langmuir probes generally serve their intended function of producing clear IV plots which are/can be available for interpretation.

Using the *exposed-tungsten* probes which is insulated from a low temperature

plasma by a glass and plastic casing in a low pressure environment, it was demonstratively possible to conduct and apply a Langmuir probe technique to a plasma produced by a direct current discharge.

Such a probe can thus be used as a diagnostic tool amidst the study of the plume(s) of plasma engines or thrusters which produce their thrust by emitting such low temperature plasma(s). Langmuir probes of this type cannot be used in high temperature plasma plumes lest they experience structural and electrical failure.

It is further possible to reliably construct Langmuir probe current-Voltage (IV) plots in the midst of such plasmas using an unmanned, or semi-manned, computerised system which has the ability to conduct many individual and independent measurements.

The unmanned langmuir analysis of the data has shown that the current instrumentation of the system may not be completely adequate for precisely measuring ion saturation currents which are less than 1,5 $\mu$A, as the overall uncertainty of making these measurements is typically higher than this value. As a result, only a range of confidence can usually be submitted for ion saturation currents.

The electron saturation currents, which are typically higher than the ion saturation currents by a upto three orders of magnitude, are much more readily measurable with the current precision of the system. The results show that the results for both the electron saturation currents and for the local plasma potential are plausible, although they can each have relative measurement uncertainties of up 25% even with the best sample IV plots obtained.

The electron and ion temperatures, which are shown to range between 1,5 ev and 18 ev, are not significantly far from what literature sources have shown for other types of plasmas, including magnetically induced plasmas, for which values between 1 ev and 5 ev have been found. This leads one to conclude that these measured values are also plausible.

The system and its analytical components are however not currently capable of reliably handling any scenario where the probes submit IV plots which are not completely consistent with the Langmuir probe model having either no sheath expansion or having simple linear sheath expansion. In those cases, the Langmuir probe analytical system is likely to produce results that are unreliable or incorrect.

Further future studies of more chaotic types of plasmas may help to produce a more complete understanding of the current-Voltage behaviour of Langmuir probes in these kinds of plasma plumes.

# 9 A : Current-Voltage data of teletherapy NMS

Table 5: Raw current-Voltage data of teletherapy NMS at 45,7%RH,$22^0C$ and 0.861 bar

| Probe bias (V) | Voltage uncertainty | Probe current(A) | Std uncertainty (A) |
|---|---|---|---|
| -25,00 | 0,10 | 7,1018E-10 | 2,0E-14 |
| -24,80 | 0,10 | 7,1034E-10 | 3,7E-14 |
| -24,60 | 0,10 | 7,1029E-10 | 9,1E-14 |
| -24,40 | 0,10 | 7,1068E-10 | 2,1E-25 |
| -24,20 | 0,10 | 7,1034E-10 | 9,2E-14 |
| -24,00 | 0,10 | 7,1044E-10 | 3,9E-14 |
| -23,80 | 0,10 | 7,1063E-10 | 5,5E-14 |
| -23,60 | 0,10 | 7,1050E-10 | 2,0E-14 |
| -23,40 | 0,10 | 7,1089E-10 | 1,1E-13 |
| -23,20 | 0,10 | 7,1082E-10 | 1,8E-13 |
| -23,00 | 0,10 | 7,1114E-10 | 2,0E-14 |
| -22,80 | 0,10 | 7,1089E-10 | 2,1E-25 |
| -22,60 | 0,10 | 7,1032E-10 | 1,3E-13 |
| -22,40 | 0,10 | 7,1071E-10 | 2,0E-14 |
| -22,20 | 0,10 | 7,1060E-10 | 9,2E-15 |
| -22,00 | 0,10 | 7,1077E-10 | 1,3E-13 |
| -21,80 | 0,10 | 7,1092E-10 | 9,9E-14 |
| -21,60 | 0,10 | 7,1076E-10 | 1,0E-13 |
| -21,40 | 0,10 | 7,1042E-10 | 5,9E-14 |
| -21,20 | 0,10 | 7,1042E-10 | 8,2E-14 |
| -21,00 | 0,10 | 7,1063E-10 | 4,9E-14 |
| -20,80 | 0,10 | 7,1048E-10 | 1,5E-13 |
| -20,60 | 0,10 | 7,1010E-10 | 9,2E-14 |
| -20,40 | 0,10 | 7,1055E-10 | 4,9E-14 |
| -20,20 | 0,10 | 7,1010E-10 | 3,3E-14 |
| -20,00 | 0,10 | 7,1009E-10 | 1,2E-13 |
| -19,80 | 0,10 | 7,0995E-10 | 9,8E-14 |
| -19,60 | 0,10 | 7,0938E-10 | 2,5E-14 |
| -19,40 | 0,10 | 7,0949E-10 | 1,8E-13 |
| -19,20 | 0,10 | 7,0974E-10 | 2,7E-14 |
| -19,00 | 0,10 | 7,0946E-10 | 5,8E-14 |
| -18,80 | 0,10 | 7,0931E-10 | 6,6E-14 |
| -18,60 | 0,10 | 7,0892E-10 | 1,1E-13 |
| -18,40 | 0,10 | 7,0881E-10 | 4,6E-14 |
| -18,20 | 0,10 | 7,0808E-10 | 9,8E-15 |
| -18,00 | 0,10 | 7,0879E-10 | 2,5E-14 |
| -17,80 | 0,10 | 7,0837E-10 | 8,3E-14 |
| -17,60 | 0,10 | 7,0798E-10 | 4,6E-14 |
| -17,40 | 0,10 | 7,0829E-10 | 1,8E-14 |
| -17,20 | 0,10 | 7,0777E-10 | 8,2E-14 |
| -17,00 | 0,10 | 7,0748E-10 | 9,8E-14 |
| -16,80 | 0,10 | 7,0750E-10 | 3,3E-14 |
| -16,60 | 0,10 | 7,0680E-10 | 7,3E-14 |
| -16,40 | 0,10 | 7,0729E-10 | 1,0E-13 |
| -16,20 | 0,10 | 7,0652E-10 | 2,7E-14 |
| -16,00 | 0,10 | 7,0682E-10 | 8,2E-14 |
| -15,80 | 0,10 | 7,0673E-10 | 5,5E-14 |
| -15,60 | 0,10 | 7,0631E-10 | 3,7E-14 |
| -15,40 | 0,10 | 7,0600E-10 | 2,2E-14 |
| -15,20 | 0,10 | 7,0571E-10 | 0,0E+00 |
| -15,00 | 0,10 | 7,0512E-10 | 2,1E-25 |
| -14,80 | 0,10 | 7,0455E-10 | 1,7E-13 |

Table 6: Raw current-Voltage data of teletherapy NMS at 45,7%RH,$22^0C$ and 0.861 bar continued

| Probe bias (V) | Voltage uncertainty | Probe current(A) | Std uncertainty (A) |
|---|---|---|---|
| -14,60 | 0,10 | 7,0403E-10 | 7,5E-14 |
| -14,40 | 0,10 | 7,0387E-10 | 9,8E-15 |
| -14,20 | 0,10 | 7,0360E-10 | 1,2E-13 |
| -14,00 | 0,10 | 7,0309E-10 | 1,8E-14 |
| -13,80 | 0,10 | 7,0268E-10 | 9,8E-15 |
| -13,60 | 0,10 | 7,0257E-10 | 1,5E-13 |
| -13,40 | 0,10 | 7,0144E-10 | 3,7E-14 |
| -13,20 | 0,10 | 7,0107E-10 | 2,0E-14 |
| -13,00 | 0,10 | 7,0087E-10 | 3,3E-14 |
| -12,80 | 0,10 | 6,9985E-10 | 9,2E-15 |
| -12,60 | 0,10 | 6,9926E-10 | 4,9E-14 |
| -12,40 | 0,10 | 6,9858E-10 | 1,8E-13 |
| -12,20 | 0,10 | 6,9778E-10 | 5,0E-14 |
| -12,00 | 0,10 | 6,9739E-10 | 7,5E-14 |
| -11,80 | 0,10 | 6,9627E-10 | 8,3E-15 |
| -11,60 | 0,10 | 6,9595E-10 | 6,6E-14 |
| -11,40 | 0,10 | 6,9459E-10 | 8,3E-15 |
| -11,20 | 0,10 | 6,9337E-10 | 9,2E-14 |
| -11,00 | 0,10 | 6,9287E-10 | 2,7E-14 |
| -10,80 | 0,10 | 6,9163E-10 | 0,0E+00 |
| -10,60 | 0,10 | 6,9118E-10 | 1,8E-14 |
| -10,40 | 0,10 | 6,8914E-10 | 3,7E-14 |
| -10,20 | 0,10 | 6,8768E-10 | 9,2E-15 |
| -10,00 | 0,10 | 6,8648E-10 | 1,5E-13 |
| -9,80 | 0,10 | 6,8534E-10 | 9,8E-14 |
| -9,60 | 0,10 | 6,8311E-10 | 1,3E-13 |
| -9,40 | 0,10 | 6,8209E-10 | 5,8E-14 |
| -9,20 | 0,10 | 6,7988E-10 | 1,7E-14 |
| -9,00 | 0,10 | 6,7803E-10 | 3,3E-14 |
| -8,80 | 0,10 | 6,7580E-10 | 1,7E-14 |
| -8,60 | 0,10 | 6,7372E-10 | 5,8E-14 |
| -8,40 | 0,10 | 6,7142E-10 | 2,5E-14 |
| -8,20 | 0,10 | 6,6837E-10 | 5,5E-14 |
| -8,00 | 0,10 | 6,6600E-10 | 1,8E-14 |
| -7,80 | 0,10 | 6,6194E-10 | 5,5E-14 |
| -7,60 | 0,10 | 6,5853E-10 | 2,7E-14 |
| -7,40 | 0,10 | 6,5555E-10 | 0,0E+00 |
| -7,20 | 0,10 | 6,5115E-10 | 2,5E-14 |
| -7,00 | 0,10 | 6,4636E-10 | 1,2E-13 |
| -6,80 | 0,10 | 6,4140E-10 | 4,3E-25 |
| -6,60 | 0,10 | 6,3532E-10 | 9,2E-15 |
| -6,40 | 0,10 | 6,2979E-10 | 7,8E-14 |
| -6,20 | 0,10 | 6,2220E-10 | 4,1E-14 |
| -6,00 | 0,10 | 6,1442E-10 | 5,0E-14 |
| -5,80 | 0,10 | 6,0714E-10 | 7,3E-14 |
| -5,60 | 0,10 | 5,9824E-10 | 3,7E-14 |
| -5,40 | 0,10 | 5,8753E-10 | 5,8E-14 |
| -5,20 | 0,10 | 5,7610E-10 | 9,2E-15 |
| -5,00 | 0,10 | 5,6297E-10 | 4,6E-14 |
| -4,80 | 0,10 | 5,4896E-10 | 4,9E-14 |
| -4,60 | 0,10 | 5,3332E-10 | 8,3E-15 |
| -4,40 | 0,10 | 5,1701E-10 | 2,0E-14 |
| -4,20 | 0,10 | 4,9828E-10 | 2,7E-14 |
| -4,00 | 0,10 | 4,8173E-10 | 9,2E-15 |

Table 7: Raw current-Voltage data of teletherapy NMS at 45,7%RH,$22^0C$ and 0.861 bar continued

| Probe bias (V) | Voltage uncertainty | Probe current(A) | Std uncertainty (A) |
|---|---|---|---|
| -3,80 | 0,10 | 4,6110E-10 | 6,8E-14 |
| -3,60 | 0,10 | 4,3880E-10 | 3,3E-14 |
| -3,40 | 0,10 | 4,1537E-10 | 1,8E-14 |
| -3,20 | 0,10 | 3,9117E-10 | 4,6E-14 |
| -3,00 | 0,10 | 3,6559E-10 | 9,8E-15 |
| -2,80 | 0,10 | 3,3940E-10 | 8,3E-15 |
| -2,60 | 0,10 | 3,1187E-10 | 4,6E-14 |
| -2,40 | 0,10 | 2,8844E-10 | 4,9E-14 |
| -2,20 | 0,10 | 2,5979E-10 | 8,3E-15 |
| -2,00 | 0,10 | 2,2922E-10 | 8,3E-15 |
| -1,80 | 0,10 | 1,9411E-10 | 2,0E-13 |
| -1,60 | 0,10 | 1,6398E-10 | 6,4E-15 |
| -1,40 | 0,10 | 1,2975E-10 | 1,7E-14 |
| -1,20 | 0,10 | 9,2066E-11 | 2,0E-14 |
| -1,00 | 0,10 | 4,9306E-11 | 3,3E-14 |
| -0,80 | 0,10 | -1,4388E-12 | 3,4E-14 |
| -0,60 | 0,10 | -4,5496E-11 | 4,9E-14 |
| -0,40 | 0,10 | -9,5406E-11 | 6,2E-14 |
| -0,20 | 0,10 | -1,4067E-10 | 7,1E-14 |
| 0,00 | 0,10 | -1,8300E-10 | 7,3E-14 |
| 0,20 | 0,10 | -2,2791E-10 | 1,8E-13 |
| 0,40 | 0,10 | -2,6368E-10 | 8,3E-15 |
| 0,60 | 0,10 | -2,9967E-10 | 5,0E-14 |
| 0,80 | 0,10 | -3,3405E-10 | 2,7E-14 |
| 1,00 | 0,10 | -3,6640E-10 | 6,4E-14 |
| 1,20 | 0,10 | -3,9230E-10 | 2,0E-14 |
| 1,40 | 0,10 | -4,2172E-10 | 2,0E-14 |
| 1,60 | 0,10 | -4,4822E-10 | 2,9E-14 |
| 1,80 | 0,10 | -4,7387E-10 | 1,8E-14 |
| 2,00 | 0,10 | -4,9660E-10 | 2,0E-14 |
| 2,20 | 0,10 | -5,1696E-10 | 2,0E-14 |
| 2,40 | 0,10 | -5,3545E-10 | 3,7E-14 |
| 2,60 | 0,10 | -5,5240E-10 | 3,7E-14 |
| 2,80 | 0,10 | -5,6500E-10 | 5,0E-14 |
| 3,00 | 0,10 | -5,7863E-10 | 4,6E-14 |
| 3,20 | 0,10 | -5,9013E-10 | 2,0E-14 |
| 3,40 | 0,10 | -6,0069E-10 | 2,0E-14 |
| 3,60 | 0,10 | -6,1060E-10 | 7,3E-14 |
| 3,80 | 0,10 | -6,1884E-10 | 3,9E-14 |
| 4,00 | 0,10 | -6,2653E-10 | 5,0E-14 |
| 4,20 | 0,10 | -6,3345E-10 | 3,7E-14 |
| 4,40 | 0,10 | -6,3967E-10 | 2,0E-14 |
| 4,60 | 0,10 | -6,4398E-10 | 9,2E-15 |
| 4,80 | 0,10 | -6,4948E-10 | 0,0E+00 |
| 5,00 | 0,10 | -6,5397E-10 | 7,3E-14 |
| 5,20 | 0,10 | -6,5851E-10 | 8,8E-14 |
| 5,40 | 0,10 | -6,6185E-10 | 1,8E-14 |
| 5,60 | 0,10 | -6,6570E-10 | 5,9E-14 |
| 5,80 | 0,10 | -6,6880E-10 | 9,8E-14 |
| 6,00 | 0,10 | -6,7216E-10 | 1,4E-13 |
| 6,20 | 0,10 | -6,7395E-10 | 8,8E-14 |
| 6,40 | 0,10 | -6,7699E-10 | 5,0E-14 |
| 6,60 | 0,10 | -6,7910E-10 | 8,2E-14 |
| 6,80 | 0,10 | -6,8119E-10 | 2,9E-14 |
| 7,00 | 0,10 | -6,8327E-10 | 1,5E-13 |
| 7,20 | 0,10 | -6,8480E-10 | 1,8E-14 |
| 7,40 | 0,10 | -6,8709E-10 | 5,9E-14 |
| 7,60 | 0,10 | -6,8867E-10 | 1,6E-13 |
| 7,80 | 0,10 | -6,9022E-10 | 2,1E-25 |

Table 8: Raw current-Voltage data of teletherapy NMS at 45,7%RH,$22^0C$ and 0.861 bar continued

| Probe bias (V) | Voltage uncertainty | Probe current(A) | Std uncertainty (A) |
|---|---|---|---|
| 8,00 | 0,10 | -6,9144E-10 | 1,7E-14 |
| 8,20 | 0,10 | -6,9292E-10 | 1,7E-14 |
| 8,40 | 0,10 | -6,9434E-10 | 6,6E-14 |
| 8,60 | 0,10 | -6,9514E-10 | 3,7E-14 |
| 8,80 | 0,10 | -6,9615E-10 | 9,2E-14 |
| 9,00 | 0,10 | -6,9760E-10 | 6,6E-14 |
| 9,20 | 0,10 | -6,9822E-10 | 8,3E-15 |
| 9,40 | 0,10 | -6,9904E-10 | 9,8E-14 |
| 9,60 | 0,10 | -7,0007E-10 | 1,6E-13 |
| 9,80 | 0,10 | -7,0105E-10 | 6,6E-14 |
| 10,00 | 0,10 | -7,0187E-10 | 5,0E-14 |
| 10,20 | 0,10 | -7,0165E-10 | 6,5E-14 |
| 10,40 | 0,10 | -7,0276E-10 | 9,2E-15 |
| 10,60 | 0,10 | -7,0344E-10 | 8,2E-14 |
| 10,80 | 0,10 | -7,0445E-10 | 1,8E-14 |
| 11,00 | 0,10 | -7,0539E-10 | 1,1E-13 |
| 11,20 | 0,10 | -7,0601E-10 | 5,5E-14 |
| 11,40 | 0,10 | -7,0621E-10 | 8,2E-14 |
| 11,60 | 0,10 | -7,0666E-10 | 8,2E-14 |
| 11,80 | 0,10 | -7,0683E-10 | 3,7E-14 |
| 12,00 | 0,10 | -7,0784E-10 | 5,9E-14 |
| 12,20 | 0,10 | -7,0799E-10 | 2,5E-14 |
| 12,40 | 0,10 | -7,0902E-10 | 1,7E-14 |
| 12,60 | 0,10 | -7,0919E-10 | 3,7E-14 |
| 12,80 | 0,10 | -7,0956E-10 | 3,9E-14 |
| 13,00 | 0,10 | -7,0980E-10 | 6,4E-14 |
| 13,20 | 0,10 | -7,1064E-10 | 4,9E-14 |
| 13,40 | 0,10 | -7,1059E-10 | 3,7E-14 |
| 13,60 | 0,10 | -7,1060E-10 | 8,1E-14 |
| 13,80 | 0,10 | -7,1142E-10 | 2,0E-14 |
| 14,00 | 0,10 | -7,1126E-10 | 1,8E-14 |
| 14,20 | 0,10 | -7,1147E-10 | 2,0E-14 |
| 14,40 | 0,10 | -7,1131E-10 | 4,6E-14 |
| 14,60 | 0,10 | -7,1231E-10 | 1,1E-13 |
| 14,80 | 0,10 | -7,1291E-10 | 3,3E-14 |
| 15,00 | 0,10 | -7,1290E-10 | 9,9E-14 |
| 15,20 | 0,10 | -7,1253E-10 | 6,4E-14 |
| 15,40 | 0,10 | -7,1350E-10 | 1,7E-14 |
| 15,60 | 0,10 | -7,1378E-10 | 2,5E-14 |
| 15,80 | 0,10 | -7,1367E-10 | 1,7E-14 |
| 16,00 | 0,10 | -7,1440E-10 | 3,3E-14 |
| 16,20 | 0,10 | -7,1400E-10 | 1,0E-13 |
| 16,40 | 0,10 | -7,1452E-10 | 9,2E-15 |
| 16,60 | 0,10 | -7,1457E-10 | 3,7E-14 |
| 16,80 | 0,10 | -7,1477E-10 | 5,5E-14 |

Table 9: Raw current-Voltage data of teletherapy NMS at 45,7%RH,$22^0C$ and 0.861 bar continued

| Probe bias (V) | Voltage uncertainty | Probe current(A) | Std uncertainty (A) |
|---|---|---|---|
| 17,00 | 0,10 | -7,1503E-10 | 1,8E-13 |
| 17,20 | 0,10 | -7,1483E-10 | 7,5E-14 |
| 17,40 | 0,10 | -7,1539E-10 | 8,3E-15 |
| 17,60 | 0,10 | -7,1516E-10 | 1,2E-13 |
| 17,80 | 0,10 | -7,1573E-10 | 1,9E-13 |
| 18,00 | 0,10 | -7,1600E-10 | 4,1E-14 |
| 18,20 | 0,10 | -7,1557E-10 | 2,7E-14 |
| 18,40 | 0,10 | -7,1635E-10 | 9,2E-15 |
| 18,60 | 0,10 | -7,1643E-10 | 3,9E-14 |
| 18,80 | 0,10 | -7,1685E-10 | 1,1E-13 |
| 19,00 | 0,10 | -7,1642E-10 | 1,8E-14 |
| 19,20 | 0,10 | -7,1667E-10 | 8,2E-14 |
| 19,40 | 0,10 | -7,1650E-10 | 9,8E-15 |
| 19,60 | 0,10 | -7,1698E-10 | 2,5E-14 |
| 19,80 | 0,10 | -7,1726E-10 | 8,3E-14 |
| 20,00 | 0,10 | -7,1728E-10 | 5,5E-14 |
| 20,20 | 0,10 | -7,1739E-10 | 9,2E-15 |
| 20,40 | 0,10 | -7,1776E-10 | 6,4E-14 |
| 20,60 | 0,10 | -7,1699E-10 | 2,9E-14 |
| 20,80 | 0,10 | -7,1776E-10 | 1,7E-14 |
| 21,00 | 0,10 | -7,1749E-10 | 9,1E-14 |
| 21,20 | 0,10 | -7,1785E-10 | 6,4E-14 |
| 21,40 | 0,10 | -7,1757E-10 | 1,1E-13 |
| 21,60 | 0,10 | -7,1771E-10 | 1,8E-14 |
| 21,80 | 0,10 | -7,1800E-10 | 3,9E-14 |
| 22,00 | 0,10 | -7,1797E-10 | 9,2E-15 |
| 22,20 | 0,10 | -7,1799E-10 | 5,5E-14 |
| 22,40 | 0,10 | -7,1785E-10 | 9,2E-15 |
| 22,60 | 0,10 | -7,1779E-10 | 5,5E-14 |
| 22,80 | 0,10 | -7,1786E-10 | 2,7E-14 |
| 23,00 | 0,10 | -7,1785E-10 | 9,2E-14 |
| 23,20 | 0,10 | -7,1834E-10 | 8,2E-14 |
| 23,40 | 0,10 | -7,1899E-10 | 2,5E-14 |
| 23,60 | 0,10 | -7,1889E-10 | 3,3E-14 |
| 23,80 | 0,10 | -7,1787E-10 | 7,3E-14 |
| 24,00 | 0,10 | -7,1812E-10 | 7,3E-14 |
| 24,20 | 0,10 | -7,1894E-10 | 8,3E-14 |
| 24,40 | 0,10 | -7,1897E-10 | 9,1E-14 |
| 24,60 | 0,10 | -7,1859E-10 | 2,6E-14 |
| 24,80 | 0,10 | -7,1900E-10 | 4,9E-14 |
| 25,00 | 0,10 | -7,1882E-10 | 8,3E-14 |
| 25,20 | 0,10 | -7,1939E-10 | 1,8E-14 |

# 10 B : Current-Voltage data of Langmuir probe in air at 45 Torr

Table 10: Raw current-Voltage data of Langmuir probe in air at 45 Torr

| probe Bias (V) | probe Current($\mu$A) |
|---|---|
| 115 | 0 |
| 117 | 0 |
| 119 | 0 |
| 121 | 0 |
| 123 | 0 |
| 125 | 0 |
| 127 | 0 |
| 129 | 0 |
| 131 | 0 |
| 133 | 0 |
| 135 | 0 |
| 137 | 0 |
| 139 | 0 |
| 141 | 0 |
| 143 | 0 |
| 145 | 0 |
| 147 | 0 |
| 149 | 0 |
| 151 | 0 |
| 153 | 0,1 |
| 155 | 0 |
| 157 | 0 |
| 159 | 0 |
| 161 | 0,8 |
| 163 | 0,9 |
| 165 | 0,2 |
| 167 | 1,5 |
| 169 | 1,6 |
| 171 | 2 |
| 173 | 3,9 |
| 175 | 3,1 |
| 177 | 9 |
| 179 | 12,8 |
| 181 | 10,7 |
| 183 | 13,3 |
| 185 | 13,9 |
| 187 | 14 |
| 189 | 14,3 |
| 191 | 15,3 |
| 193 | 15,7 |
| 195 | 14,4 |
| 197 | 15,2 |
| 199 | 15,7 |
| 201 | 16,1 |
| 203 | 14,7 |
| 205 | 16,4 |
| 207 | 16,2 |
| 209 | 16,5 |
| 211 | 17,3 |
| 213 | 16,4 |
| 215 | 16,7 |

# 11 C : Current-Voltage data of Langmuir probe in Argon at 45 Torr

Table 11: Raw current-Voltage data of Langmuir probe in Argon at 45 Torr

| probe Bias (V) | probe Current($\mu$A) |
|---|---|
| 40,00 | 0,00 |
| 50,00 | 0,00 |
| 60,00 | 0,00 |
| 70,00 | 0,00 |
| 80,00 | 0,00 |
| 90,00 | 0,00 |
| 100,00 | 0,00 |
| 110,00 | 0,00 |
| 120,00 | 0,00 |
| 130,00 | 0,00 |
| 140,00 | 0,00 |
| 150,00 | 1,50 |
| 160,00 | 0,00 |
| 170,00 | 1,80 |
| 180,00 | 7,00 |
| 190,00 | 12,00 |
| 200,00 | 14,40 |
| 210,00 | 15,80 |
| 220,00 | 17,10 |
| 230,00 | 18,40 |
| 240,00 | 19,50 |
| 250,00 | 19,30 |
| 260,00 | 21,10 |
| 270,00 | 21,90 |
| 280,00 | 22,20 |
| 290,00 | 25,00 |
| 300,00 | 26,90 |
| 310,00 | 26,20 |
| 320,00 | 27,10 |
| 330,00 | 30,40 |
| 340,00 | 29,60 |
| 350,00 | 23,60 |
| 360,00 | 28,00 |
| 370,00 | 32,30 |
| 380,00 | 34,10 |
| 390,00 | 35,70 |
| 400,00 | 35,70 |

# 12 D : Mathematica code used for curve fitting of Langmuir model

The Following Mathematica Code was used to generate Non-linear fittings of the Langmuir Method to experimental current-Voltage data. The example shown here is applied to the Raw data of Appendix A.

```
Remove /@ Names["Global`*"]; (* Restore and clear all variables*)
S = Import["C:\\Users\\Daniel Cwele\\Documents\\Master
      of Science\\Reports\\Probe Measurements (Tubes).xlsx",
   {"Data", 5, Range[51], {1, 3}}]; (* Extract IV data from Excel File*)
D1 = Dimensions[S][[1]];
ddd = Transpose[S];
V = ddd[[1]];
C1 = ddd[[2]];
max = Max[V];
min = Min[V];
$Assumptions = Vp - min > 0 && Vp - max < 0 ;
(* Restrict Plasma potential Vp to data set*)

(* - Construct a Langmuir piecewise model
   - Perform a Non linear model fitting using
  inertnal Mathematica function with initial fitting parameters
*)
P = NonlinearModelFit[S, Piecewise[
     {{(Ie + Cpe * (x - Vp)) * Exp[b * (x - Vp)], x ≤ Vp}, {Ie + Cpe * (x - Vp), x ≥ Vp}}] +
    Piecewise[{{(Ii + Cpi * (x - Vp)) * Exp[-b2 * (x - Vp)], x ≥ Vp},
      {Ii + Cpi * (x - Vp), x ≤ Vp}}], {{Ie, 12.8067}, {b, 0.233986},
    {Vp, 190}, {Ii, -0.0494717}, {b2, 0}, {Cpi, 0}, {Cpe, 0}}, x];

(*Extract Fitted Parameters*)
Ie = Ie /. P["BestFitParameters"];                          (*El Current*)
b = b /. P["BestFitParameters"] ;
(*Charge/((Boltzman const) (El Temperature))*)
Vp = Vp /. P["BestFitParameters"];                          (*Plasma Potential*)
Ii = Ii /. P["BestFitParameters"];                          (*ion Current*)
b2 = b2 /. P["BestFitParameters"];
(*Charge/((Boltzman const) (ion Temperature))*)
Cpe = Cpe /. P["BestFitParameters"]
(*El coeeficient of sheath expansion (should ideally vannish)...
 Usually larger than Cpi*)
Cpi = Cpi /. P["BestFitParameters"]
(*Ion coeeficient of sheath expansion (should ideally vannish)*)

(*Extract Error Parameters*)
K = P["ParameterConfidenceIntervalTable"];
K2 = P["ParameterConfidenceIntervals", ConfidenceLevel → .9545];

(*Calcilate Uncertainties*)
VpUncert = Abs[(K2[[3]][[2]] - K2[[3]][[1]]) / 2];
(*Plasma Potential Uncertainty*)
IeUncert = Abs[(K2[[1]][[2]] - K2[[1]][[1]]) / 2];
(*El Current Uncertainty*)
IiUncert = Abs[(K2[[4]][[2]] - K2[[4]][[1]]) / 2];
(*Ion Current Uncertainty*)
kTeUncert = Abs[1 / (K2[[2]][[2]]) - 1 / (K2[[2]][[1]])] / 2;
(*El Temperature Uncertainty*)
kTiUncert = Abs[1 / (K2[[5]][[2]]) - 1 / (K2[[5]][[1]])] / 2;
(*El Temperature Uncertainty  ------------- kTiUncert=0 implies nonconvergence*)
CpeUncert = Abs[(K2[[7]][[2]] - K2[[7]][[1]]) / 2];
(*El coeeficient of sheath expansion uncertainty*)
```

```
CpiUncert = Abs[(K2[[6]][[2]] - K2[[6]][[1]]) / 2];
(*Ion coeeficient of sheath expansion Uncertainty*)

(* Extract Coefficient of determination*)
RSqrd = P["AdjustedRSquared"]
(*Adjusted Coefficient of determination*)

(* Plot the Data and the model on the same Axis*)
Show[ListPlot[S, Frame → True, FrameLabel →
   {Style["Probe Bias (V)", FontSize → 20], Style["Current (μA)", FontSize → 20]},
  PlotStyle → Red], Plot[Piecewise[{{(Ie + Cpe * (x - Vp)) * Exp[b * (x - Vp)], x ≤ Vp},
     {Ie + Cpe * (x - Vp), x ≥ Vp}}] + Piecewise[
    {{(Ii + Cpi * (x - Vp)) * Exp[-b2 * (x - Vp)], x ≥ Vp}, {Ii + Cpi * (x - Vp), x ≤ Vp}}],
  {x, min, max}], PlotLabel → Style["Fitted
IV plot of Air", FontSize → 25]]

(* Calculate the Gas Temperatures*)
Kte = 1 / b;                          (*Electron temperature per unit charge *)
Kti = 1 / b2;                          (*Ion temperature per unit charge *)

(*End *)
```

The data, denoted as $S$, in this code is imported from an Excel file. However, the data can also be inserted into the code by means of a mathematica *List*.

# 13 E : LabView codes

The following Labview Block Diagrams were used in the data acquisition, control and analysis protocols of the results presented throughout this document. The following Table summerises the roles and functions of each block Diagram.

Table 12: The roles and functions of Labview Block Diagrams

| Sub-Appendix | Functions |
|---|---|
| D1 | Communicate with THQ Instrument |
| D2 | Connect to THQ instrument<br>Set Desired incremental Voltages<br>Read resulting incremental Currents<br>Plot IV data |
| D3 | Create Excel File For saving Dada<br>Create a File Path for the Excel file<br>Name the path by time,date and Lab. |
| D4 | Graphical user interface |
| D5 | Connect to Arduino Microprocessor<br>Instruct Arduino to :<br>Control Each Motor at given speed<br>Stop at desired coordinates |

## 13.1 E1 : LV code used to serially control power source

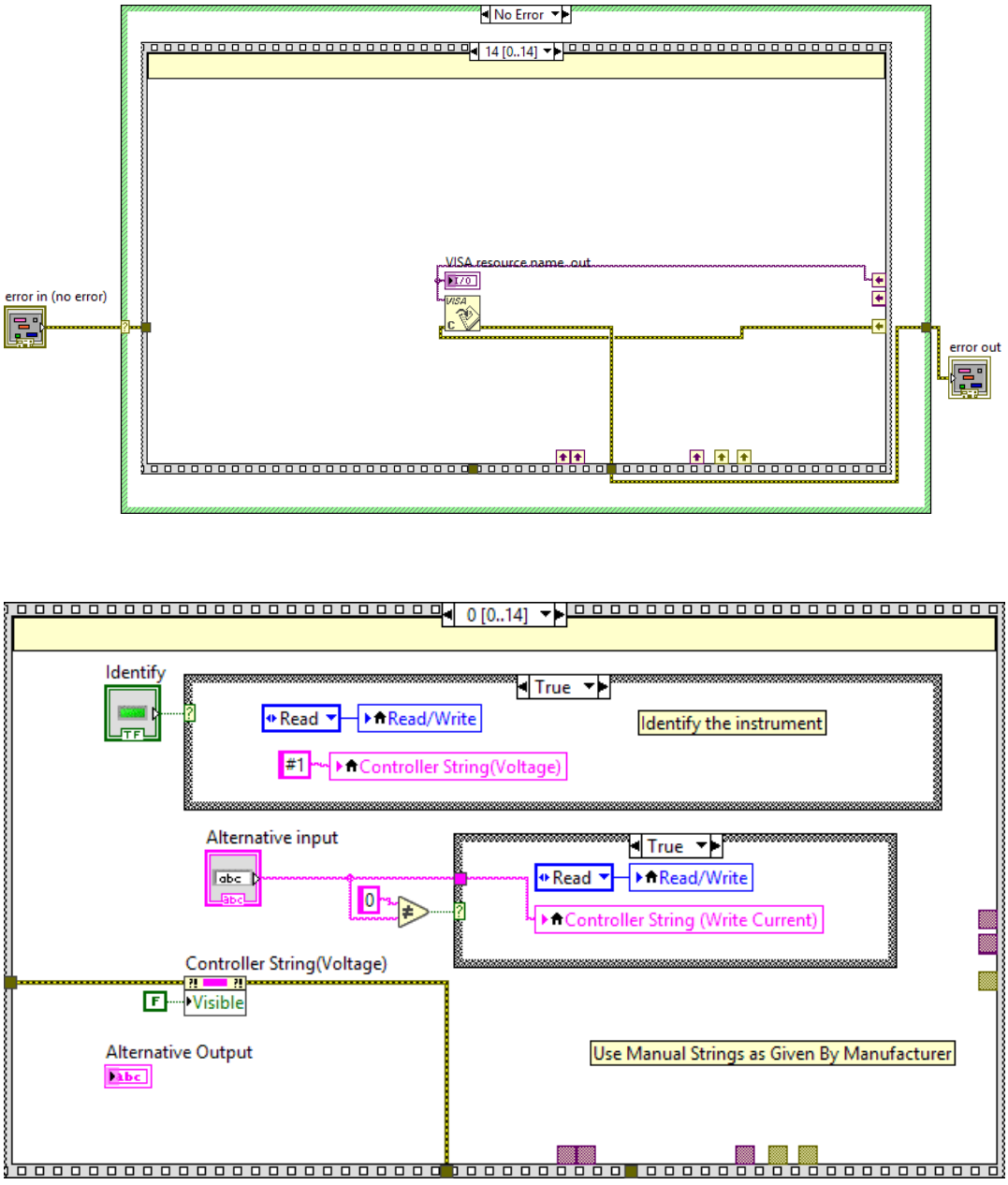

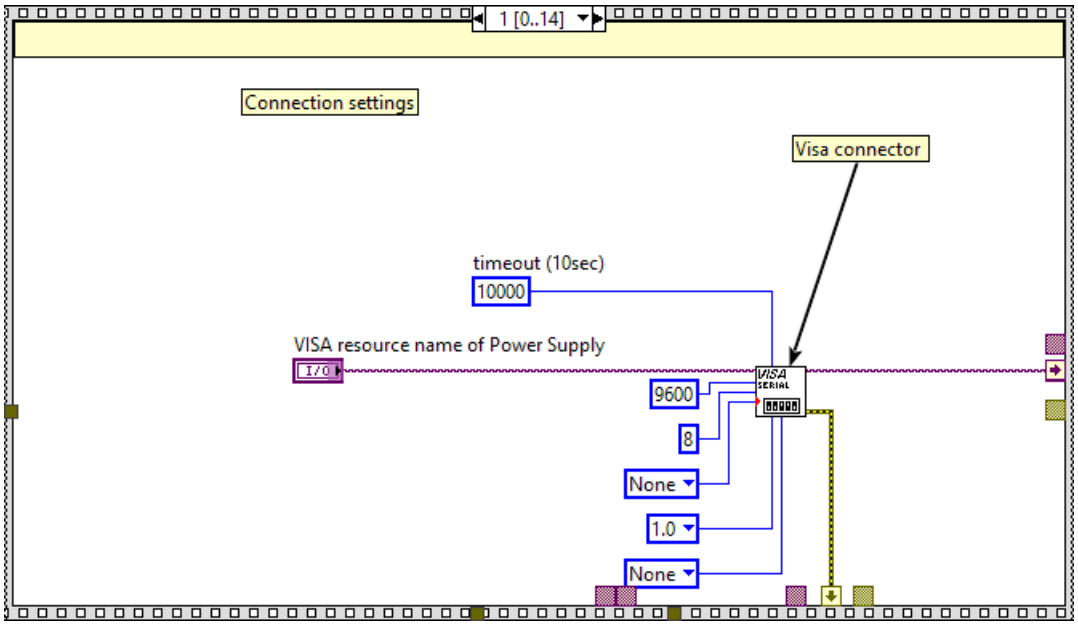
1 [0..14]
Connection settings
Visa connector
timeout (10sec)
10000
VISA resource name of Power Supply
9600
8
None
1.0
None

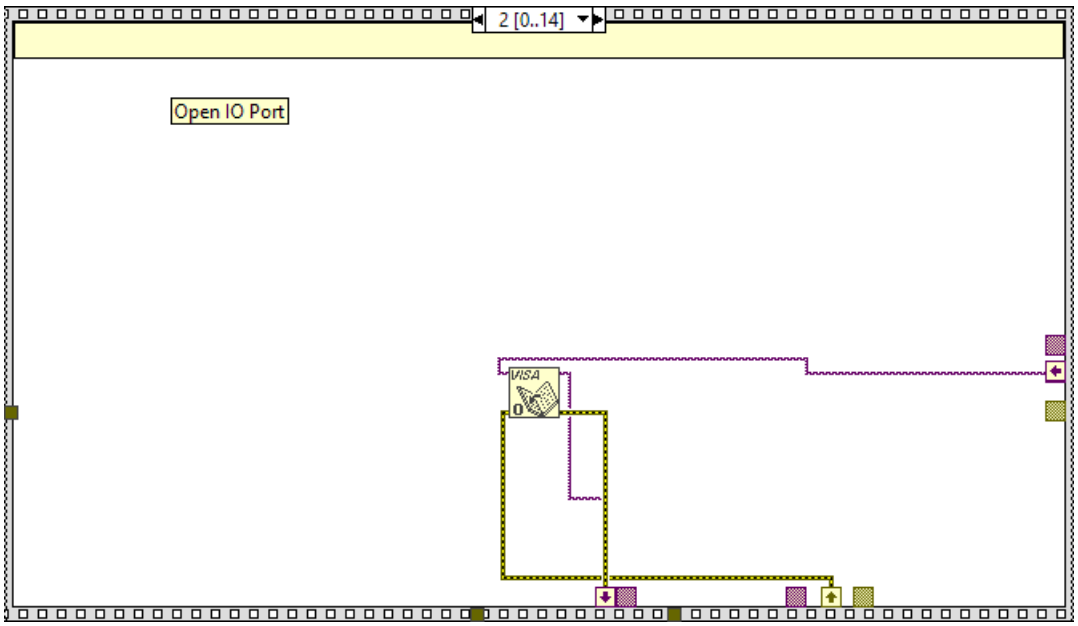
2 [0..14]
Open IO Port

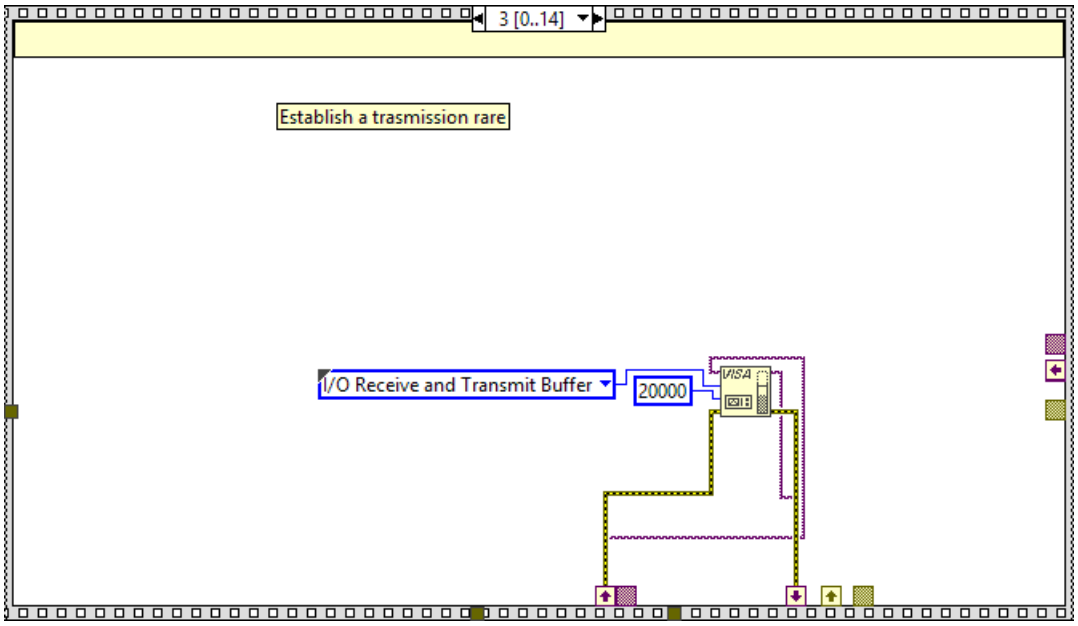
3 [0..14]
Establish a trasmission rare
I/O Receive and Transmit Buffer
20000
VISA

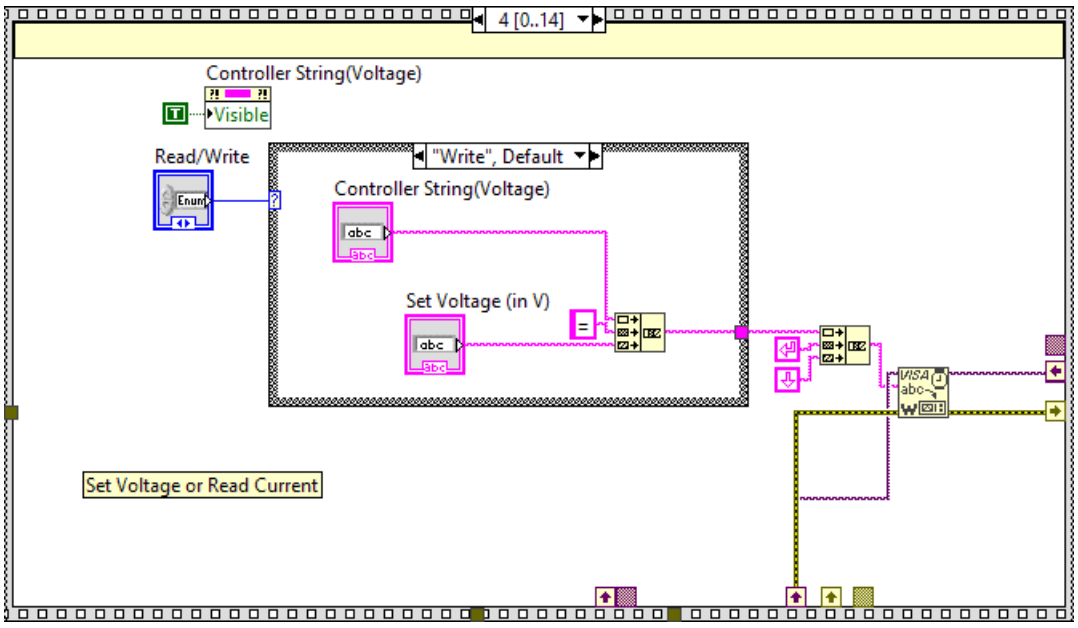
4 [0..14]
Controller String(Voltage)
Visible
Read/Write
Enum
"Write", Default
Controller String(Voltage)
abc
Set Voltage (in V)
=
VISA
Set Voltage or Read Current

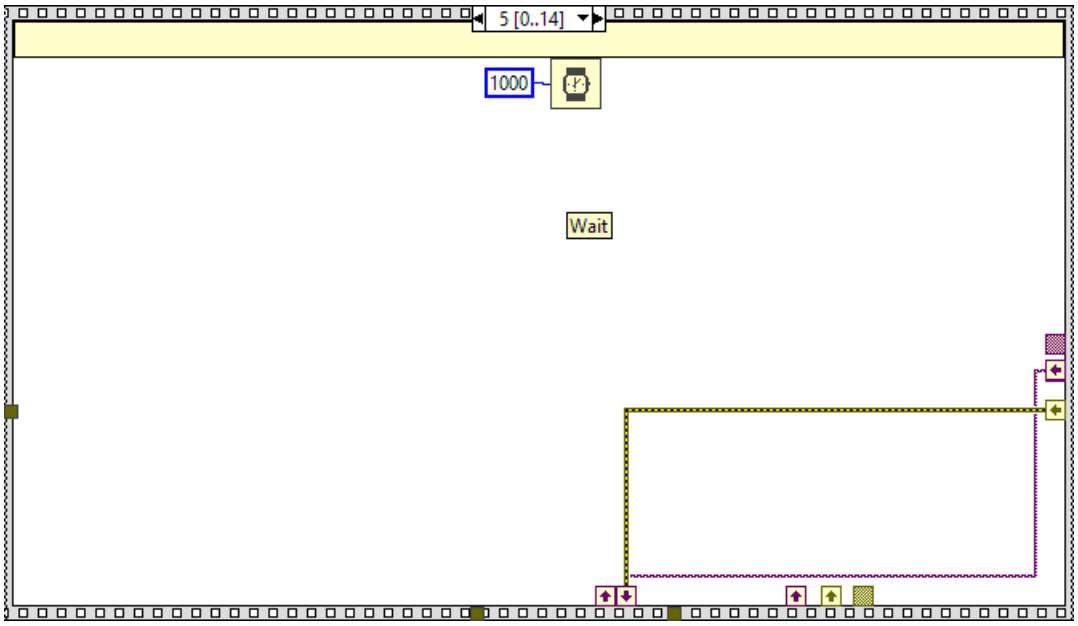
5 [0..14]
1000
Wait

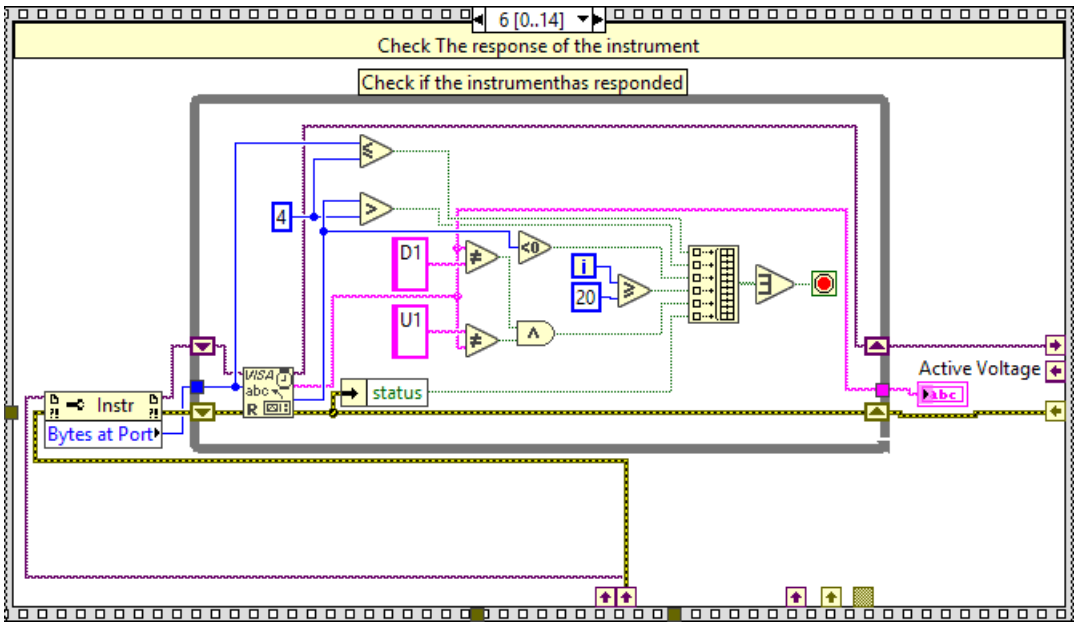
6 [0..14]
Check The response of the instrument
Check if the instrumenthas responded
4
D1
U1
20
Instr
Bytes at Port
status
Active Voltage

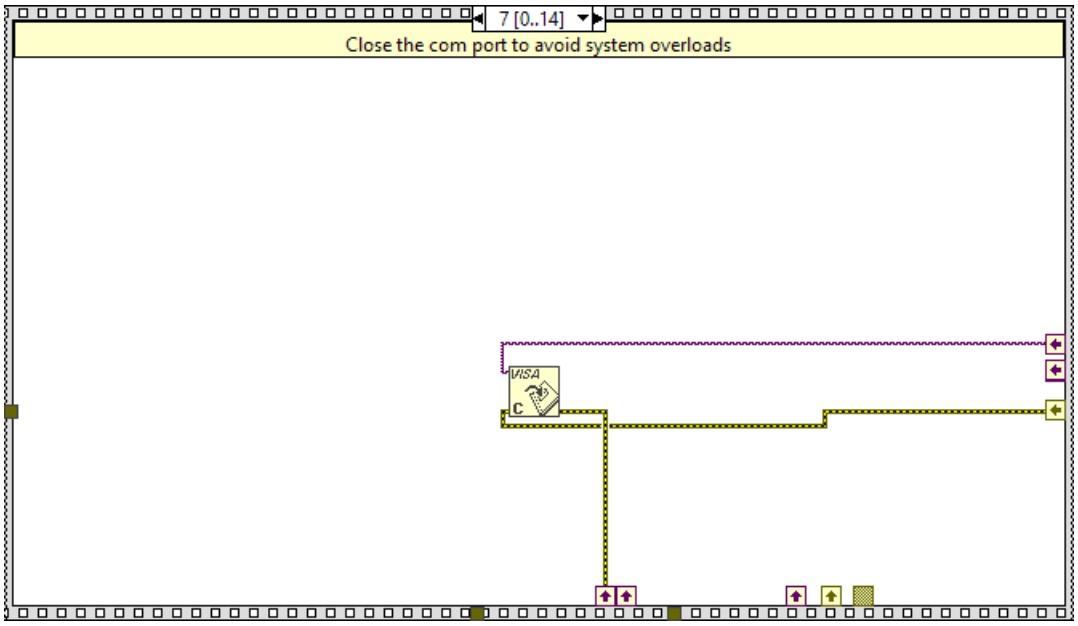
7 [0..14]
Close the com port to avoid system overloads
VISA

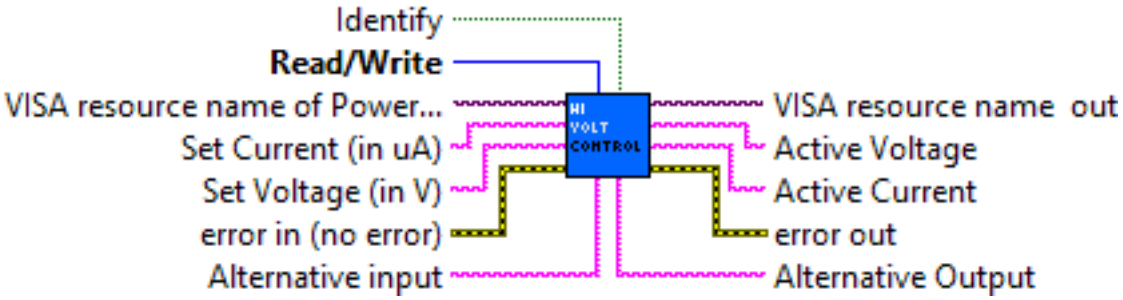
Identify
Read/Write
VISA resource name of Power...
Set Current (in uA)
Set Voltage (in V)
error in (no error)
Alternative input
HI VOLT CONTROL
VISA resource name out
Active Voltage
Active Current
error out
Alternative Output

## 13.2 E2 : LV code used to build IV plots

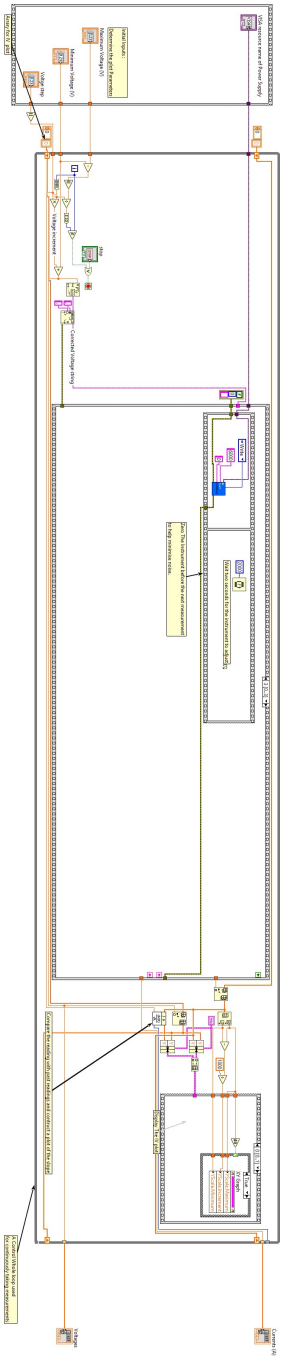

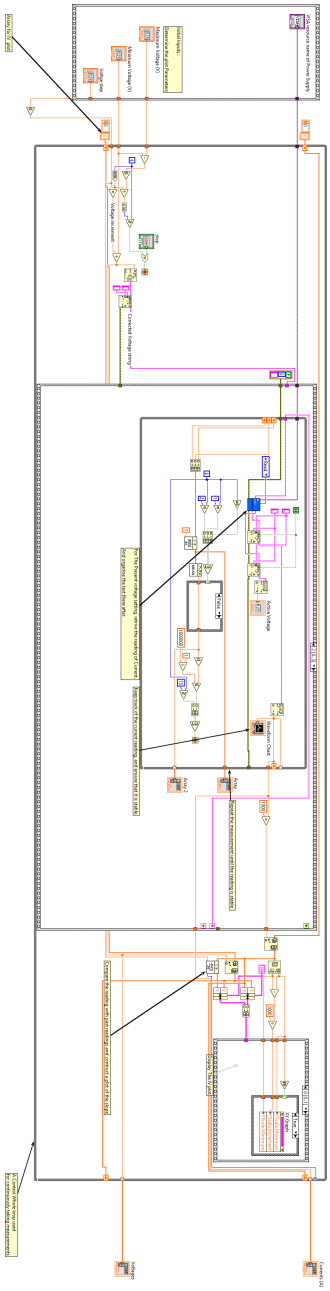

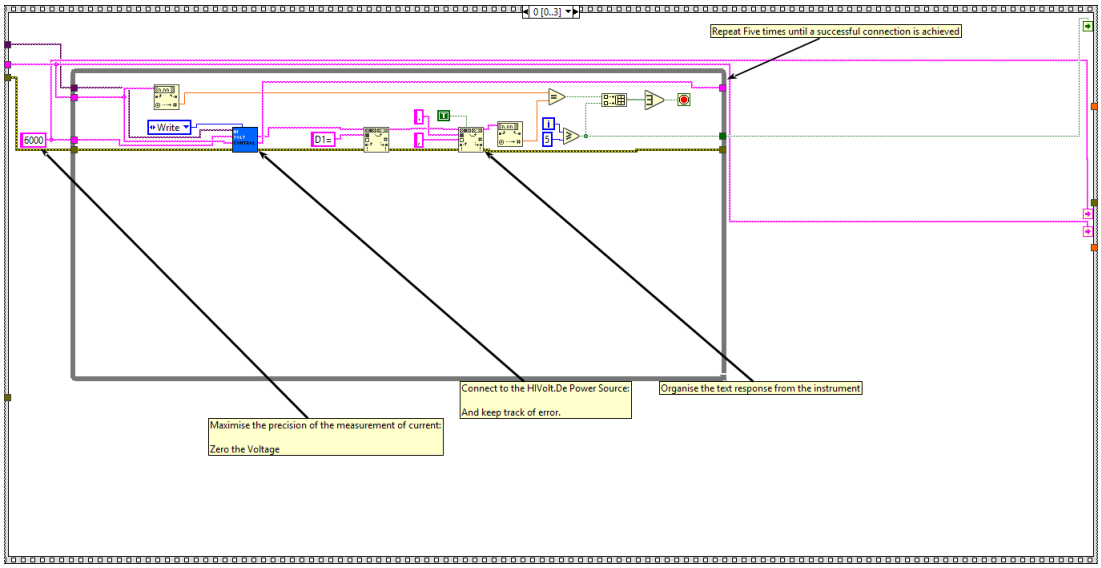
0 [0..3]
Repeat Five times until a successful connection is achieved
Write
6000
D1=
5
Maximise the precision of the measurement of current:
Zero the Voltage
Connect to the HIVolt.De Power Source:
And keep track of error.
Organise the text response from the instrument

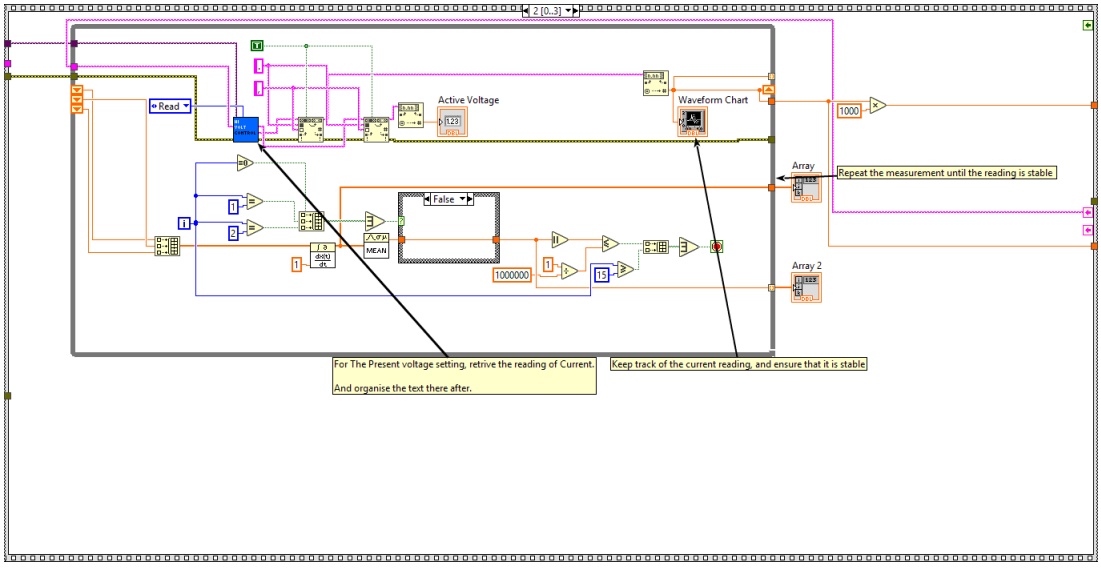
2 [0..3]
Read
Active Voltage
Waveform Chart
1000
Array
Repeat the measurement until the reading is stable
False
MEAN
1000000
15
Array 2
For The Present voltage setting, retrive the reading of Current.
And organise the text there after.
Keep track of the current reading, and ensure that it is stable

## 13.3 E3 : LV code used to build excel reports

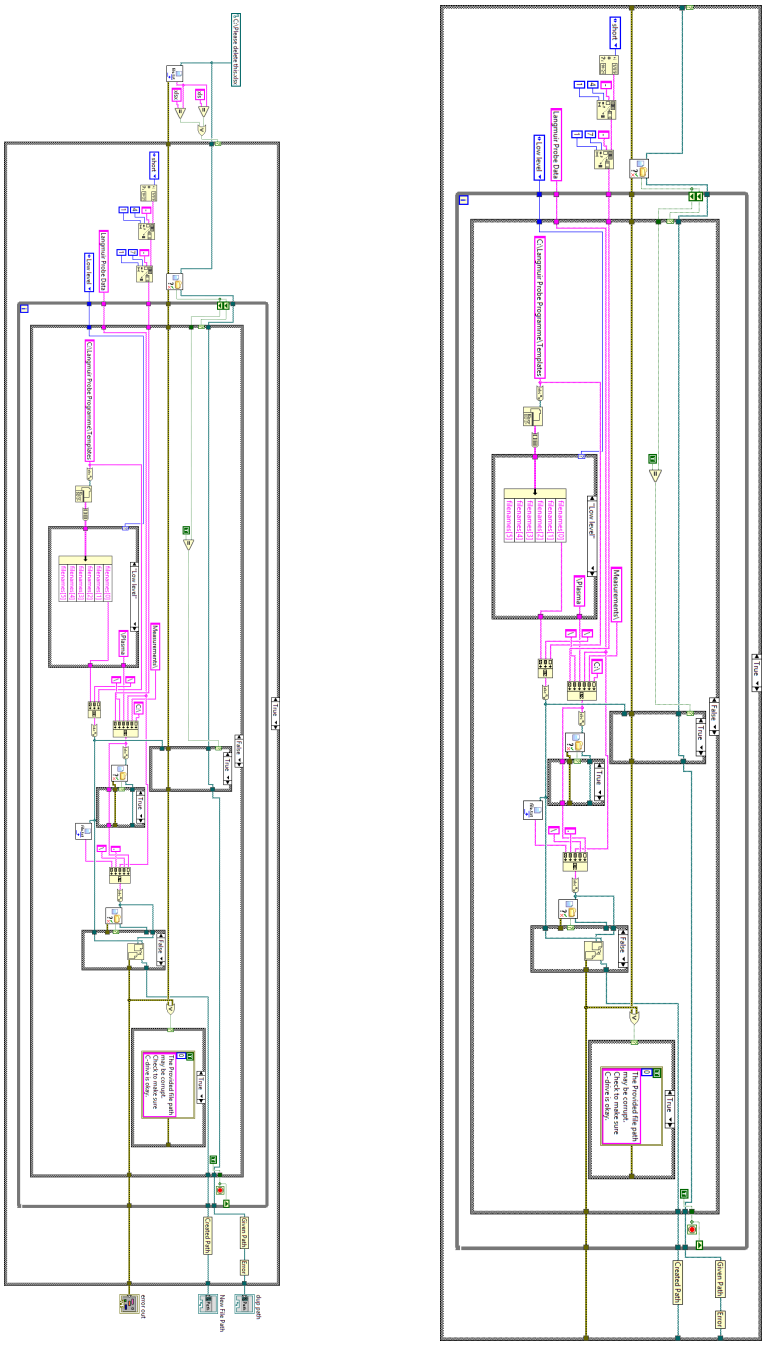

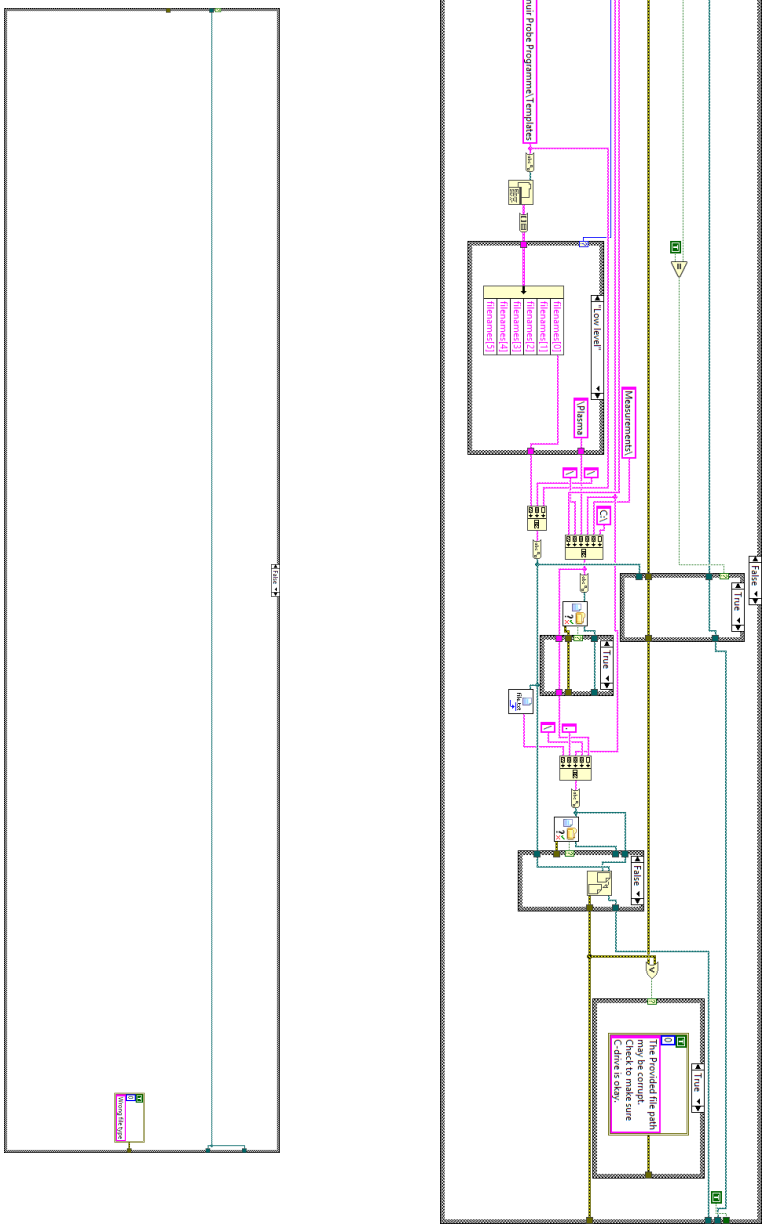
C:\Langmuir Probe Programme\Templates\
filename[0]
filename[1]
filename[2]
filename[3]
filename[4]
filename[5]
Low Res?
Plasma
Measurements
C:\
False
True
True
False
True
The Provided file path
may be corrupt.
Check to make sure
C-drive is okay.
False
Library Handle

## 13.4 E4 : LV front panel for the GUI

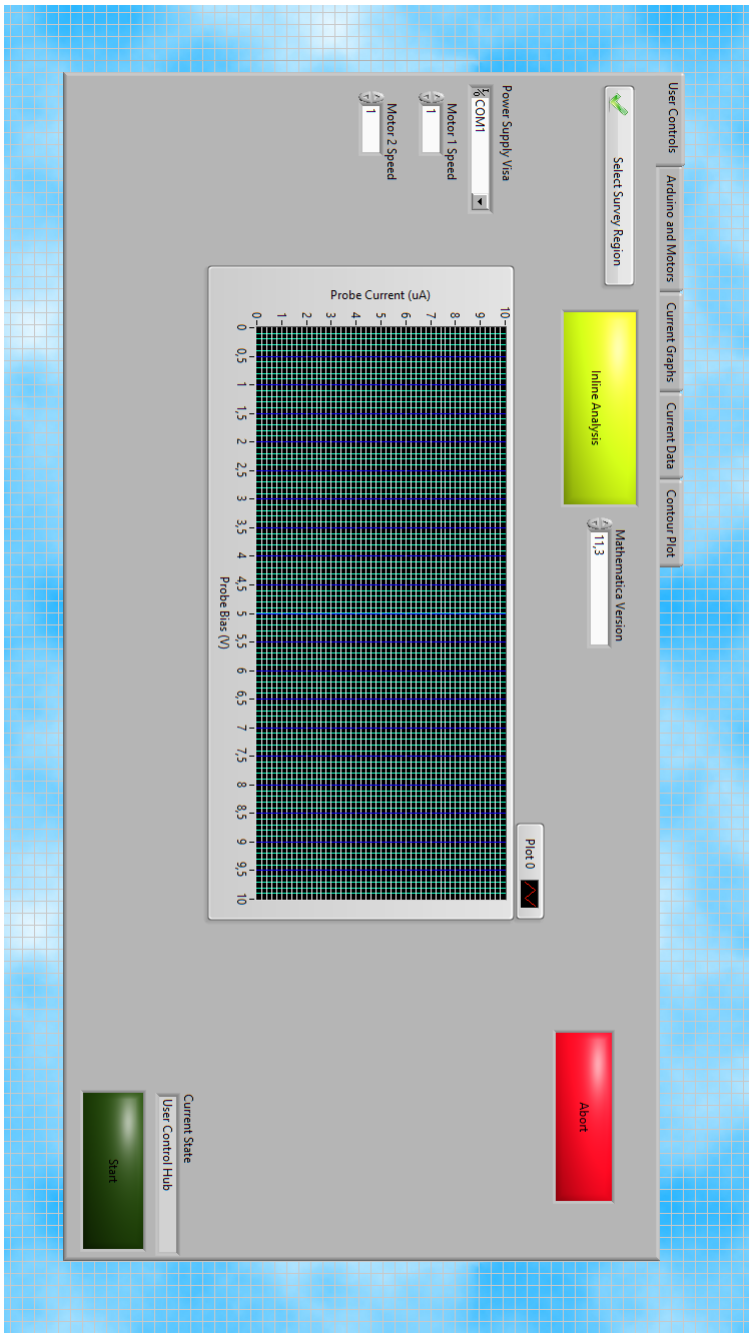

## E5 : LV code used to serially control Arduino

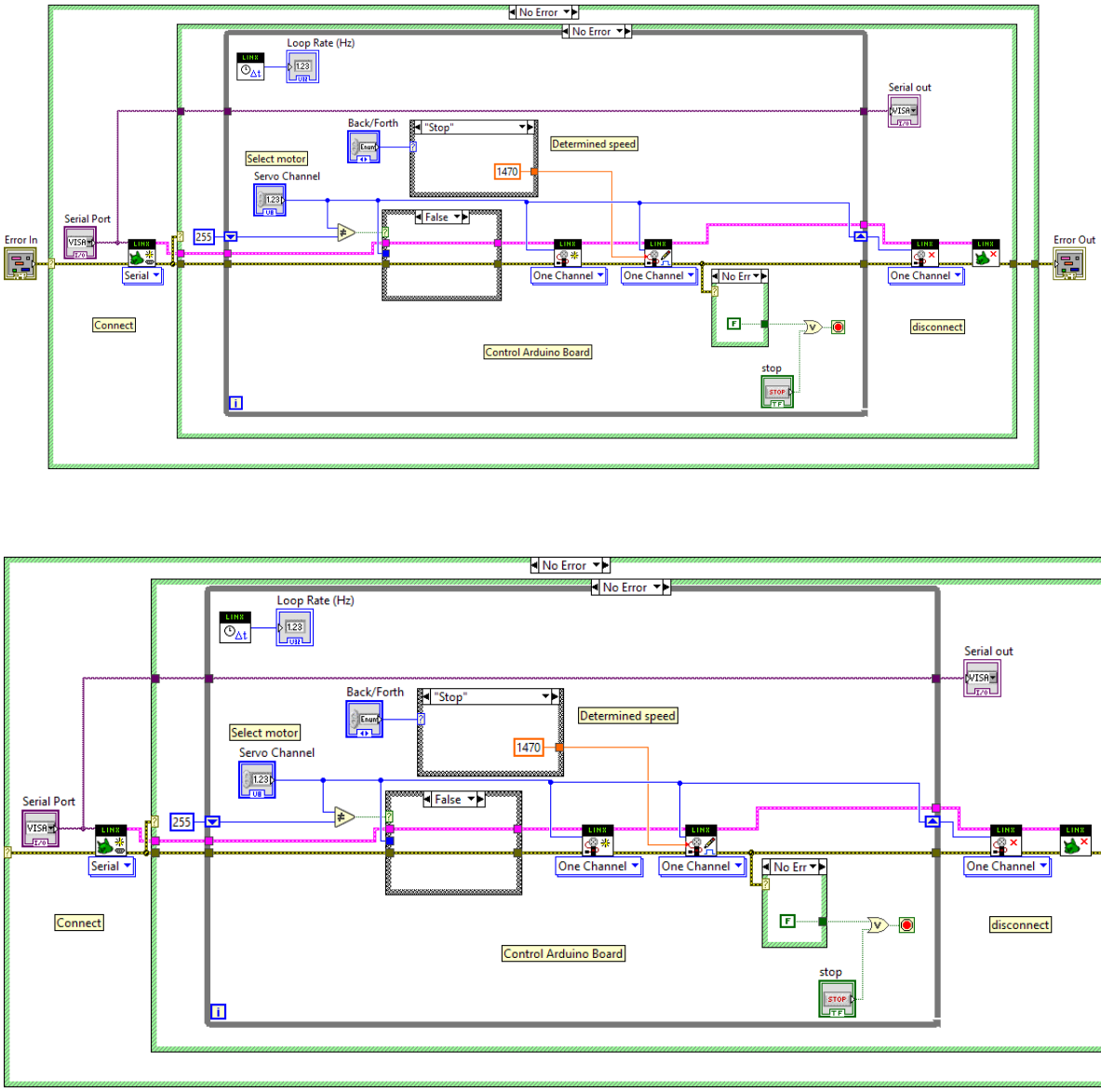


No Error
No Error
Loop Rate (Hz)
Serial out
Back/Forth
"Stop"
Determined speed
Select motor
Servo Channel
1470
False
Serial Port
255
Serial
One Channel
One Channel
No Err
One Channel
Connect
disconnect
Control Arduino Board
stop

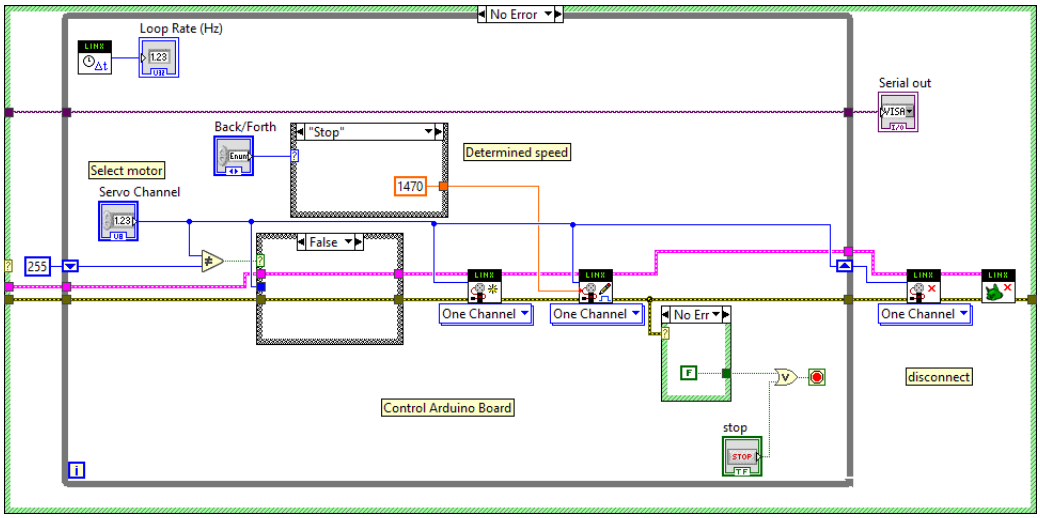
No Error
Loop Rate (Hz)
Serial out
Back/Forth
"Stop"
Determined speed
Select motor
Servo Channel
1470
False
255
One Channel
One Channel
No Err
One Channel
disconnect
Control Arduino Board
stop

# 14 F : Current-Voltage data of Langmuir probe in flowing Argon at 45 to 145 Torr

Table 13: Raw noisy current-Voltage data of Langmuir probe in flowing Argon between 45 and 145 Torr

| probe Bias (V) | probe Current($\mu$A) |
|---|---|
| 100 | 0 |
| 102 | 0 |
| 104 | 0 |
| 106 | 0 |
| 108 | 0 |
| 110 | 0 |
| 112 | 0 |
| 114 | 0 |
| 116 | 0 |
| 118 | 0 |
| 120 | 0 |
| 122 | 0 |
| 124 | 0 |
| 126 | 0 |
| 128 | 0 |
| 130 | 0,1 |
| 132 | 0,7 |
| 134 | 1 |
| 136 | 2,5 |
| 138 | 4,8 |
| 140 | 0 |
| 142 | 2,7 |
| 144 | 9,3 |
| 146 | 6,3 |
| 148 | 5,6 |
| 150 | 0,6 |
| 152 | 8,6 |
| 154 | 8,7 |
| 156 | 7,3 |
| 158 | 12,9 |
| 160 | 7,3 |
| 162 | 11,5 |
| 164 | 12,6 |
| 166 | 14,9 |
| 168 | 11,5 |

# 15 G : High sheath expansion current-Voltage data of Langmuir probe in Argon at 160 Torr

Table 14: Raw high sheath expansion current-Voltage data of Langmuir probe in Argon at 160 Torr

| probe Bias (V) | probe Current($\mu$A) | probe Bias (V) | probe Current($\mu$A) |
|---|---|---|---|
| 0 | 0 | 205 | 19,6 |
| 5 | 0 | 210 | 19,4 |
| 10 | 0 | 215 | 18,1 |
| 15 | 0 | 220 | 18 |
| 20 | 0 | 225 | 18,4 |
| 25 | 0 | 230 | 19,8 |
| 30 | 0 | 235 | 21,9 |
| 35 | 0 | 240 | 22,1 |
| 40 | 0 | 245 | 21,8 |
| 45 | 0 | 250 | 21,7 |
| 50 | 0 | 255 | 21,6 |
| 55 | 0 | 260 | 22,1 |
| 60 | 0 | 265 | 21,6 |
| 65 | 0 | 270 | 23,2 |
| 70 | 0 | 275 | 23,6 |
| 75 | 0 | 280 | 24,2 |
| 80 | 0 | 285 | 24,8 |
| 85 | 0 | 290 | 27,2 |
| 90 | 0 | 295 | 27,2 |
| 95 | 0 | 300 | 27 |
| 100 | 0 | 305 | 28,6 |
| 105 | 0 | 310 | 28,6 |
| 110 | 0,2 | 315 | 31,5 |
| 115 | 0,6 | 320 | 25,1 |
| 120 | 0,8 | 325 | 30,3 |
| 125 | 3,2 | 330 | 32,4 |
| 130 | 2 | 335 | 34,4 |
| 135 | 6,4 | 340 | 36,3 |
| 140 | 6,7 | 345 | 36,4 |
| 145 | 9,4 | 350 | 31,3 |
| 150 | 10,4 | 355 | 40,1 |
| 155 | 13,1 | 360 | 40,4 |
| 160 | 11 | 365 | 40,9 |
| 165 | 0 | 370 | 43,2 |
| 170 | 11,3 | 375 | 44,9 |
| 175 | 14,3 | 380 | 44 |
| 180 | 16,9 | 385 | 47,2 |
| 185 | 17,4 | 390 | 45,1 |
| 190 | 16,8 | 395 | 41,5 |
| 195 | 17,7 | 400 | 49,5 |
| 200 | 17,7 | | |

# 16 H : Current-Voltage data of Langmuir probe in internal flowing Argon at 45 to 145 Torr

Table 15: Raw current-Voltage data of Langmuir probe in Internal Flowing Argon

| probe Bias (V) | probe Current($\mu$A) |
|---|---|
| 0 | 0 |
| 10 | 0 |
| 20 | 0 |
| 30 | 0 |
| 40 | 0 |
| 50 | 0 |
| 60 | 0 |
| 70 | 0 |
| 80 | 0 |
| 90 | 0 |
| 100 | 0 |
| 110 | 0 |
| 120 | 2,5 |
| 130 | 1,5 |
| 140 | 7 |
| 150 | 7,6 |
| 160 | 11,6 |
| 170 | 11,7 |
| 180 | 16,6 |
| 190 | 17 |
| 200 | 18 |
| 210 | 17,2 |
| 220 | 19 |
| 230 | 20,2 |
| 240 | 20,8 |
| 250 | 22,1 |
| 260 | 23,3 |
| 270 | 22,4 |
| 280 | 20,9 |
| 290 | 17,7 |
| 300 | 19,4 |
| 310 | 22,4 |
| 320 | 20,3 |
| 330 | 14,6 |
| 340 | 23,3 |
| 350 | 22 |

# 17 I : Current-Voltage data of Langmuir probe in external flowing Argon at 45 to 145 Torr

Table 16: Raw current-Voltage data of Langmuir probe in external flowing Argon

| probe Bias (V) | probe current($\mu$A) |
|---|---|
| 170 | 0 |
| 171 | 0 |
| 172 | 0 |
| 173 | 0 |
| 174 | 0 |
| 175 | 0 |
| 176 | 0 |
| 177 | 0 |
| 178 | 0 |
| 179 | 0 |
| 180 | 1,3 |
| 181 | 0,9 |
| 182 | 0,4 |
| 183 | 1,1 |
| 184 | 0,2 |
| 185 | 0 |
| 186 | 0 |
| 187 | 0 |
| 188 | 0 |
| 189 | 0 |
| 190 | 0,5 |
| 191 | 2 |
| 192 | 1,8 |
| 193 | 36,5 |
| 194 | 38,9 |
| 195 | 45,8 |
| 196 | 46,5 |
| 197 | 46 |
| 198 | 46,4 |
| 199 | 42,3 |
| 200 | 43,3 |
| 201 | 42,9 |
| 202 | 42,4 |
| 203 | 43,6 |
| 204 | 40,5 |
| 205 | 43,9 |

# 18 J : Voltage source calibration

The following calibration data was used to correct the Voltage setting on the HiVolt.de voltage power source which was used to set the probe bias. This Calibration was done using a Keithley 2100 Series: $6\frac{1}{2}$-Digit USB multimeter, which is used for high accuracy current, charge and Voltage measurements in the Dosimetry laboratories of the National Metrology Institute of South Africa (NMISA).

Table 17: Calibration data for the hivolt.de Voltage Power source

| Set Voltage (V) | (< 20 V) | < 200 V | < 1000 V | Displayed Voltage (kV) |
|---|---|---|---|---|
| 0 | 0,8 | 0,7 | 0 | 0 |
| 1 | 1,7 | 1,7 | 1 | 0 |
| 2 | 2,67 | 2,6 | 2 | 0 |
| 3 | 3,67 | 3,6 | 3 | 0 |
| 4 | 4,44 | 4,5 | 4 | 0 |
| 5 | 5,7 | 5,5 | 5 | 0 |
| 6 | 6,68 | 6,5 | 6 | 0 |
| 7 | 7,6 | 7,6 | 7 | 0 |
| 8 | 8,5 | 8,4 | 8 | 0 |
| 9 | 9,61 | 9,4 | 9 | 0 |
| 10 | 10,65 | 10,4 | 10 | 0 |
| 15 | 15,53 | 15,4 | 15 | 0 |
| 20 | | 20,2 | 20 | 0,02 |
| 25 | | 25,2 | 25 | 0,03 |
| 30 | | 30,1 | 29 | 0,03 |
| 35 | | 35 | 34 | 0,04 |
| 40 | | 40 | 39 | 0,04 |
| 45 | | 44,9 | 44 | 0,05 |
| 50 | | 49,9 | 49 | 0,05 |
| 55 | | 54,8 | 54 | 0,06 |
| 60 | | 59,8 | 59 | 0,06 |
| 65 | | 64,7 | 64 | 0,07 |
| 70 | | 69,8 | 69 | 0,07 |
| 75 | | 74,6 | 74 | 0,08 |
| 80 | | 79,7 | 79 | 0,08 |
| 85 | | 84,6 | 84 | 0,09 |
| 90 | | 89,6 | 89 | 0,09 |
| 95 | | 94,5 | 94 | 0,1 |
| 100 | | 99,5 | 99 | 0,1 |
| 150 | | 149,1 | 148 | 0,15 |
| 200 | | 198,5 | 198 | 0,2 |
| 250 | | | 248 | 0,25 |
| 300 | | | 298 | 0,3 |
| 400 | | | 399 | 0,4 |
| 500 | | | 500 | 0,5 |
| 600 | | | 601 | 0,6 |
| 700 | | | 702 | 0,7 |
| 800 | | | 804 | 0,8 |
| 900 | | | 906 | 0,907 |
| 1000 | | | 1009 | 1,000 |

No calibration certificate was issued for this calibration.

# References


[1] Robert L. Merlino. *Understanding Langmuir probe current-Voltage characteristics.* Am. J. Phys. 75 (12): 2007.

[2] Conde, Luis. "An introduction to Langmuir probe diagnostics of plasmas." Madrid: Dept. Física. ETSI Aeronáut ngenieros Aeronáuticos Universidad Politécnica de Madrid (2011).

[3] D. A. GURNETT and A. BHATTACHARJEE. *INTRODUCTION TO PLASMA PHYSICS With Space and Laboratory Applications.* cambridge university press: 2005.

[4] W.P. Wright and P. Ferrer. *Characterization of Direct Current Discharge Based Electric Microthrusters.* Journal of Applied Physics: 2017, In preparation.

[5] Hartgers, A. (2003). *Modelling of a fluorescent lamp plasma*, Eindhoven: Technische Universiteit Eindhoven DOI: 10.6100/IR565333 https://pure.tue.nl/ws/portalfiles/portal/2345367/200311683.pdf, 07/10/18.

[6] Andy L. Romero Acosta, Stefan G. Lores, *Automated calibration of dosimeters used in radiotherapy* : Laboratorio Secundario de Calibración Dosimétrica del Centro de Protección e Higiene de las Radiaciones (CPHR) Calle 20 No 4113 e/ 41 y 47, Playa. La Habana, Cuba : 2013

[7] Weiner, Lazarus; Chiotti, Premo; and Wilhelm, H. A., *Temperature dependence of electrical resistivity of metals (1952).* Ames Laboratory ISC Technical Reports. 58.

[8] Merlr C. Potter; David C. Wigget; and Bassem, H. Ramadan, *Mechanics of fluids, fourth edition.*Shaligram Tiwari Indian Institute of Technology Madras. PG 381 - 384, PG 418.

[9] ide, *D. CRC Handbook of Chemistry and Physics*, 75 edition. CRC Press, 1995: 12

[10] L. S. Pilling, E. L. Bydder, and D. A. Carnegie, *A computerized Langmuir probe system.*Department of Physics and Electronic Engineering, University of Waikato, Hamilton, New Zealand 2001

[11] L. Sirghi, G. Popa, D. Alexandroaiei and C. Costin *Plasma diagnostics by electrical probes Practicum manual and documentation.*Iaşi, ROMANIA,2011.

[12] F. Mandl,*Statistical Physics : Second edition.*Department of theoretical physics , University of Manchester, John Wiley & Sons Ltd, 1988. P-184 to 204.

[13] W.Bolton,*Mechatronics : Electronic Control Systems in mechanical and electrical engineering, Fifth edition*. Pearson Education Ltd, 2011. P-4 to 24.

[14] R.G. Budynas, J.K. Nisbett,*Shigley's Mechanical Engineering Design, tenth edition*. McGraw-Hill Education Ltd, 2015. P-41 to 83.

[15] R.L. Burden, D.J. Faires, A.M. Burden *Numerical Analysis, tenth edition*. Cengage Learning Ltd, 2005. P-505 to 569.

[16] J.M. Gere, B.J Goono *Mechanics of Materials, eighth edition*. Cengage Learning Ltd, 2009.

[17] Francis F. Chen *Langmuir probe Diagnostics*.Electrical Engineering Department, University of California, Los Angeles,Mini-Course on Plasma Diagnostics, IEEE-ICOPS meeting, Jeju, Korea, June 5, 2003.

[18] F.F. Chen, Electric probes, in "Plasma Diagnostic Techniques", ed. by R.H. Huddlestone and S.L. Leonard (Academic Press, New York), Chap. 4, pp. 113-200 (1965).

[19] N. Hershkowitz, *How Langmuir probes Work, in Plasma Diagnostics*, Vol. 1, ed. by O. Auciello and D.L. Flamm (Academic Press, Boston, 1989), Chap. 3.

[20] M. A. Lieberman, A. J. Lichtenberg, *Principles of Plasma Discharges and Materials Processing, 2nd ed.*Wiley, New York, 2005, CHP. 6.

[21] Pilling, L. S., E. L. Bydder, and Dale A. Carnegie. "A computerized Langmuir probe system." Review of scientific instruments 74.7 (2003): 3341-3346.

[22] I.M. Hutchinson, *Principles of Plasma Diagnostics*, Cambridge University Press, Cambridge, 1987, CHP. 3.

[23] National Laboratory Association of South Africa (NLA), *Uncertainty of Measurement Course, 2017*, Viewed 15 April 2019. `https://www.home.nla.org.za/?page_id=250`

[24] Julien Vaudolon, Stéphane Mazouffre, Carole Hénaux, Dominique Harribey, and Alberto Rossi, *Optimization of a wall-less Hall thruster*, Applied Physics Letters 107, 174103 (2015); doi: 10.1063/1.4932196 `http://dx.doi.org/10.1063/1.4932196`

[25] T1EP 0vv ccc THQ, *High Voltage Desk Top Power Supply Operators Manual*.
`http://www.iseg-hv.com`

[26] National Instruments, *Labview Function and VI Reference Manual*, Viewed 15 April 2019 `http://www.ni.com/pdf/manuals/321526b.pdf`

[27] Diana Adlienė1 and Rūta Adlytė2, *DOSIMETRY PRINCIPLES,DOSE MEASUREMENTS AND RADIATION PROTECTION*, Kaunas University of Technology, Physics Department, Studentu g. 50

[28] G.F. Knoll, *Radiation Detection and Measurement - 3rd edition* , John Wiley & Sons, 1999. CHP 16, CHP17, CHP 18.

[29] J. Langmuir, Proc. Natl Acad. Sci 14, 627 (1928)

[30] D. Bohm, The Characteristics of Electrical Discharges in Magnetic Fields (McGraw-Hill, New York, 1949), p. 77

[31] B.A. Bailey, Experimental studies of the Bohm criterion for plasmas with one or two species of positive ions, BiblioLabsII, ISBN-13: 9781243520340 (2011)

[32] N. Sternberg, V.A. Godyak, IEEE Trans. Plasma Sci. 35, 1341 (2007)

[33] S.D. Baalrud, C.C. Hegna, Plasma Sources Sci. Technol. 20, 025013 (2011)

[34] V.A. Godyak, Phys. Lett. A 89, 80 (1982)

[35] V. Pletnev, J.G. Laframboise, Phys. Plasmas 13, 073503 (2006)

[36] A. Cenian, H. Rachubinski, A. Chernukho, M. Dudeck, Eur. Phys. J. Special Topics 222, 2143–2156 (2013)

[37] James Callen, University of Wisconsin-Madison, Collective Effects, Chapter 1 in "Fundamentals of Plasma Physics",

[38] Ch. 3 [3.1-3.5] in Melissinos

[39] K. R. MacKenzie, R. J. Taylor, D. Cohn, E. Ault, and H. Ikezi, App. Phys. Lett. 18, 529 (1971).

[40] N. St. J. Braithwaite, Plasma Sources Sci. Technol. 9 517 (2000).

[41] Franklin R N 1977 Plasma Phenomena in Gas Discharges

[42] J. Plasma Fusion Res. SERIES, Vol. 8 (2009)

[43] Von Engel A H 1964 Ionised Gases (Oxford: Oxford University Press)

[44] Raizer Y P 1991 Gas Discharge Physics (New York: Springer)

[45] D. Bohm, in The Characteristics of Electrical Discharges in Magnetic Fields, edited by A. Guthrie and R. K. Wakerling (McGraw-Hill, New York, 1949), pp. 77–86

[46] Chung P.M., L. Talbot, K.J. Touryan, Electric probes in flowing and stationary plasmas: Theory and application, Springer-Verlag, New York, 1975.

[47] Tous J., M. Sicha, Z. Hubicka, L. Soukup, L. Jastrabik, M. Cada, M. Tichy, The Radio Frequency Hollow Cathode Discharge Induced by the RF Discharge in the Plasma-Jet Chemical Reactor, Contrib, 2002.

[48] I. Pickova, P. Kudrna, M. Tichy,Langmuir Probe Measurements in the Hollow Cathode Plasma Jet System, Charles University Prague, Faculty of Mathematics and Physics, Prague, Czech Republic. WDS'11 Proceedings of Contributed Papers, Part II, 131–135, 2011.

[49] HAN S.,Eun H.,GUANGSUP C., Properties of high-pressure discharge plasmas,Journal of Plasma Physics 64(03):275 - 285, 2000.

[50] Non Equilibrium Air Plasmas at Atmospheric Pressure, edited by: K. H. Becker, U. Kogelschatz, K. H. Schoenbach, and R. J. Barker, Institute of Physics Publishing/Philadelphia, 2005.

[51] Low Temperature Plasmas: Fundamentals, Technologies, and Techniques, 2nd ed., edited by: R. Hippler, H. Kersten, M. Schmidt, and K. H. Schoenbach, Wiley-VCH/Weinheim, 2008.

[52] M. Dimitrova, Tsv Popov, V.n Tsaneva,N. Stelmashenko,Second derivative Langmuir probe diagnostics of gas discharge plasma at intermediate pressures (review article),Journal of Physics: Conference Series, 2006